1971

The genesis of cellular precipitation in copper rich copper-indium alloys

Raymond Albert Fournelle

THE GENESIS OF CELLULAR PRECIPITATION IN COPPER RICH COPPER-INDIUM ALLOYS

by

RAYMOND ALBERT FOURNELLE, 1941-

A DISSERTATION

Presented to the Faculty of the Graduate School of the

UNIVERSITY OF MISSOURI-ROLLA

In Partial Fulfillment of the Requirements for the Degree

DOCTOR OF PHILOSOPHY

in

METALLURGICAL ENGINEERING

1971

Advisor

ABSTRACT

The morphology of cellular precipitation in a Cu-9.5at.%In alloy has been investigated by light and electron microscopy and x-ray and electron diffraction. Both cellular and general precipitation were observed to occur simultaneously in quenched and aged alloys while only cellular precipitation was observed to occur in isothermally aged alloys. Because of the presence of wide, vacancy depleted precipitate free zones in the vicinity of grain boundaries, general precipitation was observed to have no effect on the early development of cellular precipitation. Hence, the early development of cellular precipitation was found to be identical for both types of heat treatment. By light and electron microscopy of the early stages of precipitation a mechanism for the development of cells from an initially unoccupied grain boundary was developed. According to this mechanism the grain boundary allotriomorphs begin to form, the boundary interacts with them by bowing out between them and trailing precipitate behind to eventually develop a steady state cellular structure. Assuming that the critical step in the development of a cell is the ability of the boundary to bow between initial allotriomorphs, a criterion for the occurrence of cellular precipitation was developed.

ACKNOWLEDGEMENTS

The author wishes to thank Dr. J. B. Clark for suggesting the research topic and for encouragement and help throughout the study.

The author is also indebted to the Department of Metallurgical Engineering for financial assistance of various kinds.

Copper for this study was provided through the courtesy of Mr. Franklin Wilson of Anaconda American Brass Company, Waterbury, Connecticut.

This work was supported by National Science Foundation Grant G. K. 10467.

TABLE OF CONTENTS

Table of Contents (continued) Page

Table of Contents (continued) Page

Table of Contents (continued) Page

LIST OF ILLUSTRATIONS

List of Illustrations (continued) Page

List of Illustrations (continued) Page

List of Illustrations (continued) Page

List of Illustrations (continued) Page

List of Illustrations (continued) Page

LIST OF TABLES

I. INTRODUCTION

In precipitation hardening alloys solute can segregate from supersaturated solid solutions by one of four possible mechanisms. These are general or continuous precipitation, grain boundary precipitation, spinodal decomposition and cellular or discontinuous precipitation. In cellular precipitation, the grain boundary between adjacent supersaturated grains migrates from one grain into the other. As it migrates a lamellar aggregate of depleted solid solution and precipitate phase are formed behind the advancing boundary.

In general, the duplex lamellar structures formed during cellular precipitation are deleterious to the mechanical and stress corrosion properties of age hardening alloys; therefore, it is of interest to determine the cause of the reaction in order to establish a basis for the development of techniques to suppress it. Until now most studies of cellular precipitation have been concerned with either the morphology of the reaction or its growth kinetics. Of these studies only a few have discussed possible causes, and only one has been concerned with the early stages of the development of cellular nodules from an initially unoccupied grain boundary.

Because few studies have considered the early stages of the development of cellular nodules and because such studies may give further insight into the cause of cellular precipitation the present study was undertaken. In this study an attempt is made to establish a mechanism for the genesis or nucleation of cellular structures by an investigation of the early stages of cellular precipitation in an alloy that is

representative of alloy systems exhibiting cellular precipitation and to relate this mechanism to possible causes of the reaction.

II. REVIEW OF LITERATURE

A supersaturated solid solution, such as that formed by quenching an alloy of composition $X\alpha'$ in Figure 1 from temperature T_1 in the α phase field to temperature T_2 in the $\alpha + \beta$ phase field, can decompose to equilibrium α and β or other transitional phases by four different mechanisms during aging at T_2. Three of these four mechanisms are shown schematically in Figure 2. According to this figure, solute segregation can occur by (1) general precipitation, in which an equilibrium or transitional phase nucleates and grows throughout the grain interior gradually depleting the solid solution of excess solute by volume diffusion. It can also occur by (2) grain boundary precipitation, in which the precipitate phase, β, nucleates heterogeneously at grain boundaries, edges or corners and grows, gradually depleting the area near the boundary of solute. Finally, the system can transform by (3) cellular precipitation, in which an originally unoccupied grain boundary migrates from one grain into another leaving behind an aggregate of equilibrium α and β. The fourth mechanism by which the system can decompose, spinodal decomposition, is characterized by a fine periodic coherent composition fluctuation within the alloy. Any one or all of the above methods of segregation may be active in a given alloy system and, in certain cases, two or more of these may compete with one another at a given aging temperature.

Although the above discussion deals with a binary alloy system it is equally applicable to any multicomponent system exhibiting decreasing solid solubility of solute elements with decreasing temperature.

A. Morphology and General Characteristics of Cellular Precipitation

1. General

Smith[54] was the first to describe the general nature of cellular precipitation. Later reviews by Gruhl and Kramer[23] and Bohm[5] confirmed these observations, and since then numerous individual studies have proven them to be correct. According to Smith, in studies of precipitation in Zn-Cu* and Cu-Ag alloys, cellular precipitation occurs when the boundary between two supersaturated grains becomes unstable and migrates from one grain into the other. As the boundary migrates an aggregate of precipitate phase and depleted solid solution is formed behind the advancing interface as shown in Figure 3 for a Zn-Cu alloy. As no visible gradient existed in front of the advancing interface, Smith hypothesized that solute segregated along the advancing boundary, which he described as disordered. In Figure 4 he showed further that the depleted solid solution within the cellular nodule in Figure 3 had the same crystallographic orientation as the grain from which it grew. From these characteristics he compared the reaction with that of recrystallization in that both reactions proceed by the migration of a boundary. The driving force for cellular precipitation was, however, described to be the decrease of chemical free energy accompanying decomposition of the supersaturated solid solution rather than the reduction of the strain energy of cold work for recrystallization. To show the similarity between the two reactions Smith cited the

---

*Throughout this text the first element will represent the major component and the second the minor component.

work of Beck and Sperry[4] on strain induced boundary migration in pure aluminum. Figure 5 shows a migrating boundary in prestrained aluminum for comparison with Figure 3.

2. Structure and Composition of the Cellular Aggregate

Numerous studies, some of which are referenced in Table I, have shown that the aggregate formed behind the advancing interface consists of alternate lamellae of depleted solid solution and precipitate phase; however, aggregates with rod like precipitate morphologies have also been observed[59]. In general, these observations have shown that a constant lamellar spacing is characteristic of a given alloy composition and aging temperature and that this characteristic spacing decreases with increasing supersaturation, whether this supersaturation is achieved by decreasing temperature and constant alloy composition or by increasing solute concentration at constant temperature. Precipitation studies of Pb-Sn,[64,65,66] Fe-Ni-Ti,[55] Cu-Cd,[59] Ni-Cu,[30] Pb-Na,[43] and Zn-Cu[54] alloys have shown that precipitate lamellae can have definite habit planes and crystallographic relationships with the depleted matrix phase. In other studies of Fe-Zn,[56] Cu-In[50,52] and Cu-Co[44] alloys, however, no definite habit plane appears to exist. Branching and gradual changes in direction seem to be characteristic of precipitate lamellae in these systems.

In a theoretical study which will be discussed later, Cahn[12] suggested that for any non-zero growth rate the cellular lamellae cannot attain their equilibrium compositions. X-ray lattice parameter investigations of the depleted matrix phase in Fe-Zn,[56] Cu-In[50,52] and Cu-Cd[59] alloys have shown that this is indeed the case. This

has also been shown to be true for Al-Ag[1] and Pb-Sn[35] alloys by studies of the volume fraction of reaction products formed.

A second kind of cellular aggregate was observed by Sulonen[59] to form in Cu-Cd alloys at temperatures above those where ordinary cellular precipitation occurs. According to Figure 6, the boundary appears to bow out between precipitate particles and then break away to form a new row after advancing a short distance.

3. Rate of Growth of the Cellular Nodule

Like the lamellar spacing, a constant rate of advance of the cellular interface has been found to be characteristic of cellular precipitation at constant temperature in the absence of other competing reactions. In a theory to be disucssed later, Turnbull[67,69] proposed that a relationship between growth rate and lamellar spacing exists once precipitation has achieved a steady state. According to this theory,

$$G = \left(\frac{X_{\alpha'} - X_{\alpha e}}{X_{\alpha'}}\right) \frac{D_V}{S} \quad (1)$$

if solute diffusion in front of the advancing interface is the rate controlling process, or

$$G = \left(\frac{X_{\alpha'} - X_{\alpha e}}{X_{\alpha'}}\right) \frac{\lambda D_B}{S^2} \quad (2)$$

if solute diffusion in the advancing interface between the supersaturated and depleted phases is the rate controlling process.

---

*For consistency all symbols used in this study have been standardized and are listed in Table II.

In almost all investigations listed in Table I in which this theory was tested, solute diffusion in the advancing interface was found to be rate controlling. No alloy system exhibiting cellular precipitation has yet been found in which volume diffusion in front of the advancing interface can be conclusively proven to be the controlling process.

4. Structure of the Advancing Interface

Smith[54] observed that the only orientation relation that needed to be fulfilled by two adjacent grains in order for a cellular reaction to occur was that certain orientations that give rise to ordered boundaries be avoided. In polycrystalline specimens of Cu-Be and Cu-Ni-Mn with [100] fiber axes, Gruhl and Ammann[22] showed that the amount of cellular precipitate at a grain boundary decreased as the tilt orientation of the boundary decreased. They explained this behavior as resulting from decreased nucleation rates at low angle grain boundaries. Cahn[11], however, interpreted the behavior to result from a decreased growth rate resulting from a decrease in grain boundary diffusivity. Watanabe[74] using a special metallographic technique has shown a similar behavior in Zn-Cu alloys, and Liu and Aaronson[35] in kinetic studies of cellular precipitation in Pb-Sn bicrystals have shown that the growth rate of cells decreases with decreasing [001] tilt misorientation. They further observed that precipitation by the cellular mechanism ceases at misorientations of 13° or less. Mäder and Hornbogen[38] have observed a distribution of growth rates in Pb-Na alloys and have described this as resulting from variations in the boundary structure. These variations in boundary structure are

described as being similar to those shown by Gleiter[20,21] to be responsible for the differences in grain boundary migration rates in single phase Al-Cu alloys.

The above observations seem to confirm Smith's hypothesis that the advancing interface has a disordered structure.

5. Effect of the Simultaneous Occurrence of General Precipitation

Cellular precipitation can occur as the only mode of precipitation as in Pb-Sn,[35,68] Cu-Cd[59] and Fe-Zn[31,56]; simultaneously with general precipitation as in Mg-Al,[13] Cu-Mg,[41] Zn-Cu,[23,54] Cu-Be[23,72,73] and Pb-Na[43]; or after general precipitation as in Al-Ag[1]. In those systems in which general precipitation occurs simultaneously with cellular precipitation, cellular precipitation is generally favored at low aging temperatures and high supersaturations while general precipitation is favored at higher temperatures and lower supersaturations. This behavior is generally described as resulting from the increased growth rate of the general precipitate, which results from increased volume diffusion, and the correspondingly decreased driving force for cellular precipitation, which results from low supersaturation at high aging temperatures. At lower aging temperatures the volume diffusivity is lower while the supersaturation is higher, and cellular precipitation is favored.

In some of the systems described above such as Pb-Na, Cu-Mg and Cu-Be the simultaneously forming general precipitate retards and eventually stops the growth of the cellular precipitate by depleting the matrix of solute supersaturation. In other systems, such as Zn-Cu and

Mg-Al, the cellular reaction completely consumes the matrix before general precipitation can completely remove the supersaturation.

6. The Effect of Deformation Prior to Aging

Deformation prior to aging was found to increase the rate of cellular precipitation in both Pb-Sn[68] and Cu-Cd[59] alloys. In Cu-Be[15] and Mg-Al[13] alloys it was found to decrease the growth rate and in Cu-In and Cu-Mg[10] alloys the growth rate was not affected. The increased growth rates are thought to result from an increased driving force resulting from the stored energy of cold work. In those alloys in which the growth rate is retarded, deformation is thought to aid the nucleation of general precipitation which depletes the matrix of solute and retards the growth of cellular precipitate.

7. The Effect of Small Additions of Third Elements

Böhm[7] has studied the behavior of cellular precipitation in Cu-Mg, Cu-Sb, Cu-Be, and Cu-In alloys which had been doped with small amounts of iron, silicon, beryllium, indium, magnesium and antimony. Cellular precipitation was found to be favored when the third element differed only slightly from the solute element in atomic size, and it was found to be suppressed when the atomic size differed markedly. According to Böhm[8] this behavior is best explained by considering the effect of the third element on the grain boundary diffusivity of the solute. That is, the doping elements either retard or enhance the interface diffusivity and, thereby, cause corresponding changes in the growth rate.

In a Pb-Na alloy Mäder and Hornbogen[38] found that small additions of silver retarded the rate of cell growth by a factor of 10. An attempt was made to describe this observation by the Gleiter[20,21] theory of grain boundary migration.

The effect of small additions of indium, thallium, lead and gallium on cellular precipitation in a Ag-Cu alloy has been studied by Predel and Ruge[46] who found that the growth rate of cells was accelerated by additions of gallium and retarded by additions of the other elements. Böhm's theory, described above, accounts well for these observations.

8. Miscellaneous Observations on Cellular Precipitation

Studies by Speich[55] on an Fe-Ni-Ti alloy and by Petermann and Hornbogen[43] on Pb-Na alloys show that two discontinuous precipitation reactions can occur simultaneously, with one growing much faster than the other. In both cases the slower reaction, which has a much larger lamellar spacing, eventually grows into the area transformed by the first reaction and decomposes it. The driving force for the reaction apparently is associated with a decrease in the lamellar surface energy.

Spencer and Mack[57] have shown that a eutectoid Cu-Ga alloy, transformed massively to the supersaturated, metastable ζ_S phase, can subsequently decompose by a cellular reaction to equilibrium ζ and γ. Mack[37] has observed a similar decomposition of a martensite formed by quenching and aging a eutectoid Cu-Al alloy.

In undercooled Ni-Sn alloys Jones[32] has observed cells to initiate at γdendrite-eutectic boundaries and to grow into the nickel rich γdendrite.

B. Growth Theories

In Section I.A. cellular precipitation was described as a reaction that has a constant growth rate and a constant lamellar spacing at a given reaction temperature for a given alloy composition. In other words cellular precipitation is one of several phenomena, such as eutectoid decomposition and eutectic solidification, which are classified as steady state cooperative growth phenomena. Such phenomena are amenable to analytical interpretation, and a brief review of the present theories of cellular growth is given in this section. For consistency and simplicity all theories are discussed with reference to the alloy of composition X_α, in Figure 1 at the aging temperature T_2 and with reference to Figure 7, a schematic diagram of an advancing cellular interface which shows all pertinent quantities. For simplicity most symbols used in this study are given in Table II.

1. Turnbull's Boundary Diffusion Control Theory

Turnbull[67,68,69], after observing that precipitation in Pb-Sn occurred at a rate much faster than could be predicted by volume diffusion alone and that the reaction product appeared similar to that of pearlite, suggested that transformation occurs in a manner similar to that described by Zener[76] for pearlite formation; however, Turnbull suggested that solute segregation occurred within the advancing interface by boundary diffusion rather than in front of it by volume

diffusion. Using dimensional arguments and Fisher's[16] modification (Equation 1) of Zener's relation between growth rate and lamellar spacing, Turnbull obtained the relation shown in Equation 2 for the case of interface diffusion control.

$$G = \left(\frac{X_{\alpha'} - X_{\alpha}}{X_{\alpha'}}\right) \frac{D_V}{S} \tag{1}$$

$$G = \left(\frac{X_{\alpha'} - X_{\alpha}}{X_{\alpha'}}\right) \frac{D_B \lambda}{S^2} \tag{2}$$

Comparing Equations 1 and 2 he further stated that interface diffusion becomes the controlling mechanism when

$$\left(\frac{D_B}{D_V}\right) > \left(\frac{S}{\lambda}\right) . \tag{3}$$

Noting that the concentration term in Fisher's equation was unduly approximate Aaronson and Liu[2] derived a modified version of Equation 2 using a flux balance between solute precipitated at the β lamellae and solute flux in the cell interface. This relation is given in Equation 4.

$$G = 4 \left(\frac{X_{\beta} - X_{\alpha}}{X_{\beta} - X_{\alpha'}}\right) \frac{D_B \lambda}{S^2} \tag{4}$$

As mentioned previously, numerous studies have shown that cellular reactions in most systems are controlled by diffusion in the advancing interface.

2. Cahn's Boundary Diffusion and Reaction Control Theory

After noting that incomplete partitioning of solute resulted from cellular precipitation Cahn[12] suggested that, if diffusion is limited

to the advancing cell boundary, the lamellar product phases cannot attain equilibrium composition for any non-zero growth rate and that diffusion rates alone cannot account for the growth rate of the cells. He indicates that at least two controlling kinetic parameters are required to describe the reaction and suggested that these could be grain boundary diffusivity and grain boundary mobility, where growth rate is proportional to the net free energy change for the reaction.

Accordingly, assuming mobility control, Cahn writes for the cell growth rate,

$$G = -M\Delta F \ . \tag{5}$$

where, considering the incompleteness of the reaction, the net free energy change, ΔF, is given by

$$\Delta F = P\Delta F_o + \frac{2\sigma_{\alpha/\beta}V}{S} \ . \tag{6}$$

Here the chemical free energy change ΔF_o is given by

$$\Delta F_o = RT\left[X_{\alpha'} \ln \frac{X_{\alpha e}}{X_{\alpha'}} + (1-x_{\alpha'}) \ln \frac{(1-X_{\alpha e})}{(1-X_{\alpha'})}\right] \ . \tag{7}$$

Assuming a flat interface, uniform boundary thickness and diffusivity, and a steady state, diffusion in the interface is described by

$$D_B\lambda \frac{d^2X_B}{d\bar{Z}^2} + G(X_{\alpha'} - X_\alpha) = 0 \ . \tag{8}$$

Assuming that the composition of the α lamellae is related to the boundary composition by $k = X_\alpha/X_B$, Equation 8 has the following solution.

$$X_\alpha = X_{\alpha'} + A \cosh\sqrt{\theta}\,\frac{\bar{Z}}{S} \ , \tag{9}$$

where A is a constant and $\theta = kGS^2/D_B\lambda$. Integrating $(X_\alpha - X_{\alpha'})/(X_{\alpha e} - X_{\alpha'})$ over the entire α lamellae gives the following expression for the fraction of solute precipitated.

$$Q = \frac{2}{\sqrt{\theta}} \tanh \frac{\sqrt{\theta}}{2} \tag{10}$$

Assuming that the free energy of the α phase is a quadratic function of the solute concentration, the fraction of chemical free energy released is obtained by integration to be

$$P = \frac{3}{\sqrt{\theta}} \tanh \frac{\sqrt{\theta}}{2} - \frac{1}{2} \operatorname{sech}^2 \frac{\sqrt{\theta}}{2} \tag{11}$$

Substituting this expression into Equation 6 and maximizing ΔF with respect to θ, Cahn, finally obtains a parameter, β, in terms of basic quantities associated with the precipitation reaction.

$$\beta = - \frac{k M \sigma_{\alpha/\beta}^2 V^2}{D_B \lambda \Delta F_o} \tag{12}$$

Figure 8 shows the values of P, Q and R plotted as functions of β. Using values of β determined from fundamental quantities associated with the reaction, Figure 8 can be used to determine P, Q and R and thereby establish the completeness of precipitation.

Kinetic studies of precipitation in Pb-Sn[35] and Al-Ag[1] have shown that the theory correctly predicts solute segregation by interface diffusion. In Cu-In alloys[50,52] determinations of M from Equation 5 and from Figure 8 have shown the theory to be internally consistent although the values of M were much lower than those for other mobility controlled reactions.

In the only study in which ΔF_o was calculated from measured activities, Speich[56] has shown that, in Fe-Zn alloys, the growth rate

is proportional to $(\Delta F)^3$ rather than ΔF. However, an analysis similar to Cahn's using this third power dependence correctly describes the behavior of the reaction.

3. Shapiro and Kirkaldy's Metastable Monotectoid Theory

Noting the morphological similarity between cellular precipitation and eutectoid decomposition, Shapiro and Kirkaldy[50] suggested that cellular precipitation might be the result of the existence of a metastable monotectoid. Such a situation is shown graphically in Figure 9. Assuming the existence of this condition the authors further suggested that the precipitation behavior could be described by their theory of eutectoid decomposition,[51] which assumes local equilibrium across and boundary diffusion along the advancing interface. Using these assumptions and entropy optimization the following relation was obtained.

$$GS^3 = \frac{48 \lambda D_B V \left(\frac{S\Delta F_o}{2\sigma_{\alpha/\beta} V} - 1 \right)}{q \left(\frac{1}{2} - a \right)^2} , \qquad (13)$$

where $q = \frac{1}{2} \frac{\partial^2 F_\alpha}{\partial X_\alpha^2}$ and $\underline{a}$ is a concentration term dependent on the relative locations of the α and β phase boundaries. As the details of the development of Equation 13 are lengthy they will not be presented here.

A kinetic study of precipitation in Cu-In alloys by Shapiro and Kirkaldy[50,52] has shown that the theory predicts a reasonable activation energy for interface diffusion. No other investigations have yet evaluated this theory.

4. Hillert's Interface Control Theory

Noting that previous theories failed to describe the mechanism by which the net free energy change, ΔF, available for the cellular reaction dissipated itself, and hence, the mechanism by which part of this energy is converted to a driving force for boundary migration, Hillert[26] suggested that a model that considers the thermodynamic, mechanical and diffusional properties of the advancing interface might describe the partitioning of this free energy. Accordingly, he proposed that the advancing interface could be treated as a thin film of material of constant composition, X_B, and uniform thickness λ. He further proposed that this layer of boundary phase could have a characteristic free energy curve just as do the α and β phases as shown in Figure 10, a free energy composition diagram for the system shown in Figure 1 at temperature T_2. In addition to the free energy-composition diagram, composition profiles of the advancing interface for both the α and β lamellae are given. According to diagrams such as this, Hillert shows that only a portion of the free energy, ΔF, available for precipitation is converted to a driving force on the boundary. In this particular case, in which no volume diffusion occurs in front of the advancing interface, the driving force is given by ΔF_p for α lamellae and ΔF_B for β lamellae.

To convert these free energies into driving forces Hillert introduces a force balance for a curved migrating α/α' interface.

$$\frac{\sigma_{\alpha/\alpha'}}{r} = \frac{\Delta F_p}{V} - \frac{G}{VM} \tag{14}$$

The y component of the force, $\sigma_{\alpha/\alpha'}/r$, is then integrated over the entire interface and equated to that fraction, L, of the α/β interfacial energy, $\sigma_{\alpha/\beta}$, balanced by $\sigma_{\alpha/\alpha'}$ to give

$$2L\sigma_{\alpha/\beta} = \int_{-\frac{S_\alpha}{2}}^{+\frac{S_\alpha}{2}} \left(\frac{\Delta F_p}{V} - \frac{G}{VM}\right) d\bar{Z} \ . \tag{15}$$

A similar equation results for the α'/β interface.

$$2(1-L)\sigma_{\alpha/\beta} = \int_{-\frac{S_\beta}{2}}^{+\frac{S_\beta}{2}} \left(\frac{\Delta F_\beta}{V} - \frac{G}{VM}\right) d\bar{Z} \tag{16}$$

For the case of solute segregation in the advancing interface, Hillert solved Cahn's diffusion equation (Equation 8) for α lamellae assuming, as did Cahn, that $X_\alpha = kX_\beta$. However, for the β lamellae he assumed that the composition, X_β, was constant. The solutions for the α and β lamellae are respectively

$$\frac{X_B - X_{\alpha'}}{X_{B_3} - X_{\alpha'}} = \frac{\cosh \sqrt{\frac{VS_\alpha^2}{k\ D_B\ \lambda}}\ \frac{\bar{Z}}{S_\alpha}}{\cosh \sqrt{\frac{VS_\alpha^2}{4k\ D_B\ \lambda}}} \tag{17}$$

and

$$\frac{X_B - X_{B_3}}{X_{\alpha'} - X_\beta} = \frac{GS_\beta^2}{8k\ D_B\ \lambda} \left[1 - \left(\frac{2\bar{Z}}{S_\beta}\right)^2\right] , \tag{18}$$

where X_{B_3} is the boundary composition at the intersection of the α/α', α/β and α'/β interfaces.

Substituting compositional expressions based on Henry's and Raoult's laws into Equations 15 and 16 for ΔF_p and ΔF_p and using the two solutions of the diffusion equation (Equations 17 and 18), Hillert obtains the following expressions for S_α and S_β.

$$\frac{S_\alpha}{S_{\alpha o}} = L \cdot \frac{\sqrt{\theta}}{\tanh\sqrt{\theta}/2} \cdot \frac{1 + \frac{H}{4}\left(1 + \frac{\sqrt{\theta}}{\sinh\sqrt{\theta}}\right)}{1 + \frac{\sqrt{\theta}}{\sinh\sqrt{\theta}}} \tag{19}$$

$$\frac{S_\beta}{S_{\beta o}} = 2L \cdot \frac{1 + \frac{H}{4}\left(1 + \frac{\sqrt{\theta}}{\sinh\sqrt{\theta}}\right)}{1 + \frac{\sqrt{\theta}}{\sinh\sqrt{\theta}}}, \tag{20}$$

where $\theta = (VS_\alpha)/(kD_B\lambda)$, $S_{\alpha o}$ and $S_{\beta o}$ are the minimum values of S_α and S_β, and H is a constant for a given alloy and aging temperatures. The term G/VM in Equations 15 and 16 was neglected in these calculations.

As yet no experimental investigations have been performed to test the theory.

5. Petermann and Hornbogen's Mobility Control Theory

To explain time dependent cellular growth rates in Pb-Na alloys Petermann and Hornbogen[43], using a dimensional argument similar to that used by Turnbull, adapted Lücke's mobility control theory for grain growth and recrystallization[36] to the cellular reaction. According to Lücke the rate of grain boundary migration in single phase alloys is given by

$$G = \frac{\lambda\Delta F}{\tau RT}, \tag{21}$$

where τ is the time required for every atom in a grain boundary to jump into just one of the adjacent grains and λ is the distance through which they jump. Petermann and Hornbogen suggested that τ could be associated with the time required to drain the solute from an advancing α/α' interface and that λ could be associated with the distance of advance of the β lamellae as the result of the addition of these drained solute atoms. Thus,

$$\tau = \frac{S^2}{8D_B} \tag{22}$$

and

$$G = \frac{8D_B\lambda\Delta F}{S^2RT} . \tag{23}$$

Comparison of this equation with Equation 5 shows that the above development relates M and D_B by the equation,

$$M = \frac{8D_B\lambda}{S^2RT} . \tag{24}$$

Until now insufficient investigations have been performed to truly evaluate this theory but it is interesting to note that if the growth rate, B, is maximized with respect to the lamellar spacing, S, the growth rate becomes

$$G = \frac{8\lambda D_B(\Delta F_o)^3}{27\sigma_{\alpha/\beta}{}^2V^2RT} \tag{25}$$

This agrees well with Speich's observation[56] in Fe-Zn that $G = C(\Delta F_o)^3$, where $C = C_o \exp(-Q/RT)$.

In summary, all of the above described growth theories have been applied but have had only limited success in predicting cellular

growth. Lack of specific thermodynamic and diffusion data have precluded direct testing of the theories without general assumptions.

C. The Cause of Cellular Precipitation

Most previous theories of cellular precipitation have been concerned with the growth of the cellular nodules rather than with the fundamental cause of the reaction. A few observations have, however, been made on this subject and these are presented here.

Geisler[19] in his review of precipitation phenomena suggested that cellular precipitation occurred by the same mechanism as recrystallization and that the driving force for the migration of the cell boundary was supplied by the strain energy of the matrix phase resulting from prior coherent general precipitation within the grains. This concept, however, cannot account for the precipitation behavior of those systems, such as Pb-Sn and Fe-Zn, in which only cellular precipitation is observed.

Gruhl and Kramer[23] have suggested that cellular precipitation will not occur unless the driving force for the reaction, as given by

$$\Delta F = \Delta F_o + \frac{2\sigma_{\alpha/\beta} V}{S} + \frac{\sigma_{\alpha/\alpha'} V}{r_n} , \qquad (26)$$

where r_n is the radius of the cellular nodule, is negative. Although this may explain the fact that cellular precipitation occurs in some systems only after a certain amount of undercooling it does not explain the total absence of the reaction in other systems.

After studying the effect of uniaxial tension on the precipitation behavior in Cu-Cd, Ag-Cu, Pb-Sn, Zn-Cu, Cu-Ag and Cu-Mg, Sulonen[57,58] suggested that the driving force for the migration of the advancing

cell interface results in the formation of a solute impoverished zone in front of the advancing cell interface. Within this impoverished zone stresses are said to develop as the result of a change in the lattice parameter of the supersaturated solid solution. These stresses are believed to supply the driving force for the advance of the interface in the same way that a deformed matrix supplies energy for recrystallization.

In his experiments Sulonen showed a dependence of cell growth rate in the above mentioned alloys on the direction and magnitude of an applied uniaxial load. This dependence was described as being caused by the superposition of the applied stresses on those already existing in the impoverished zone. It must be noted, however, that this dependence was readily apparent only in the case of Cu-Cd alloys and that the effect appeared most prominent in those alloys in which creep was occurring simultaneously with precipitation. It must also be pointed out that this theory would limit cellular precipitation to those alloys whose lattice parameter exhibits a large dependence on composition and, hence, whose solute and solvent atoms show a large difference in atomic size. This agrees well with the results of Böhm[7,8] who showed that cellular precipitation in copper base alloys occurs only in those systems in which solute and solvent atomic radii differ by at least 11%; however, it does not explain the cellular precipitation in other alloys such as Al-Ag and Cu-Co where the atomic mismatch is very slight. In addition, the theory is in direct conflict with Hillert's interface theory[26] which predicts that cellular precipitation can occur only when boundary segregation is sufficiently rapid to prevent

the formation of a solute depleted zone in front of the advancing interface.

In conclusion it should be noted that of the above theories, only that of Gruhl and Kramer[23] attempts to describe the cause of the reaction in terms of the basic thermodynamic quantities associated with it and that none of the theories attempts to establish a criterion for the occurrence of cellular precipitation in terms of these quantities.

D. The Tu-Turnbull Theory for the Genesis of Cellular Lamellae in Lead Rich Lead-Tin Solid Solutions

As mentioned in the introduction only one previous investigation of the initiation of a cellular reaction and the nucleation of precipitate lamellae had been performed prior to this study. In this investigation Tu and Turnbull[64,65,66] studied the morphology of the early stages of precipitation in lead rich lead-tin solid solutions by light and electron microscopy and x-ray diffraction. A review of the results of the investigation is given in reference 70.

According to this and other studies[35,68] tin, β, has been shown to precipitate from supersaturated lead rich solid solutions only by cellular precipitation, and that segregation of solute occurring during this reaction is incomplete. It has also been shown that the β lamellae have a rigid habit in and a strong orientation relationship with the depleted lead rich α lamellae with which they form. {111} planes in the α lamellae form the habit for the β, and the orientation between α and β is given by $(010)_{Sn} \,||(111)_{Pb}$ and $[001]_{Sn}||[110]_{Pb}$. This habit and orientation relationship represents the matching of close packed planes in both α and β and should result in a

semi-coherent, low energy interface. Electron microscopy of the β lamellae has shown that they are not interconnected and, hence, that branching does not occur. Laue back reflection x-ray techniques have shown that parallel lamellae within the same cell have the same orientation.

To determine how such lamellae could nucleate and multiply from an initially unoccupied grain boundary, Tu and Turnbull[63,64] studied the morphology of the early stages of precipitation in lead-tin bicrystals misoriented about a [001] tilt axis. Figure 11 shows schematically the mechanism resulting from this study. According to this diagram a cell develops from an initially unoccupied grain boundary (a) between two supersaturated α grains, α_1 and α_2, in the following manner. With time a β platelet forms at the initially unoccupied boundary (b) in such a way that it has a semi-coherent, low energy interface, characterized by the rigid habit and orientation relationship described above, with one grain (in this case α_1) and an incoherent, high energy interface with the other grain, α_2. After the platelet attains a certain critical size the grain boundary originally attached to the platelet at x in (b) migrates around the incoherent interface as shown in (c) eventually imbedding the platelet in α_1 with semicoherent, low energy interfaces on both sides of the platelet. The driving force for this motion is proposed to be the decrease in interfacial surface energy resulting from the replacement of the high energy interface with one of lower energy. Once the platelet is imbedded in α_1 it reportedly grows, carrying the grain boundary along as it advances. Eventually the grain boundary is brought into a position favorable for the nucleation of another β platelet of the same orientation

as shown in (d). "Replacive" motion of the grain boundary again occurs (e) and eventually, by this process, the number of platelets multiply and form a cell (f). Once the cell is formed it grows into α_2 with the boundary being carried forward by the advancing β lamellae.

It must be noted that this theory implies that the crystallographic orientation of the initial grain boundary precipitate establishes the growth direction and morphology of the final cellular structure and that growth of the cell results from the α/α' interface being dragged along by advancing β lamellae.

E. Precipitation in Copper Rich Copper-Indium Alloys

1. Phases

According to Figure 12, the copper-indium phase diagram from Hansen and Anderko[24], indium has a maximum solid solubility of 11.0 at.% (18.2 wt.%) in the copper rich f.c.c. α phase at 574°C. This decreases to 1.2 at.% (2.15 wt.%) at 300°C. The δ phase which segregates from supersaturated α solid solutions during aging has a nominal composition of Cu_9In_4 and actual composition limits of 29.9 at.% In and 30.6 at.% In. Weibke and Eggers[75] described the δ phase as having a γ brass type structure while the work of Hellner and Laves[25] indicates that it is a superlattice based on the NiAs type of structure. More recently, however, Reynolds, Wiseman and Hume-Rothery[48] have shown that it can best be described as a tetragonal distortion of the complex cubic γ brass structure with a = 8.99Å, c = 9.16Å and c/a = 1.020.

2. Morphology and Kinetics

Precipitation phenomena in quenched and aged copper rich copper-indium alloys have recently been investigated by Böhm,[6,7,8,9,10] Corderoy and Honeycomb,[14] and Shapiro and Kirkaldy[50,52]. The results of these investigations are reviewed below.

In a kinetic study of precipitation in Cu-In alloys ranging from 4 wt.% In to 15 wt.% In, Böhm,[6] using light microscopy, observed a transition zone in the vicinity of 0.8 T_s, where T_s is the absolute solvus temperature, above which only general precipitation occurred and below which only cellular occurred. Corderoy and Honeycomb[14], using transmission electron microscopy, observed, however, that in 8.5 and 10.0 at.% In alloys general precipitation competed with and eventually stopped cellular precipitation at all temperatures at which cellular precipitation was observed. Shapiro and Kirkaldy[50,52] observed, on the other hand, that the reciprocal of the lamellar spacing extrapolated to a temperature below the absolute solvus, indicating that cellular precipitation does indeed require a certain amount of undercooling for its occurrence.

Using transmission electron microscopy Shapiro and Kirkaldy[50,52] observed that cellular nodules developed from original grain boundary allotriomorphs whose "spacing" was larger than that of the lamellae of the nodule. Regular lamellar spacing was observed to obtain only after a steady state of co-operative growth was attained. Additional observations by these authors of cell morphology include (1) an identical orientation of the α lamellae to the α' of the grain from which they grew, (2) the existence of twins in the α lamellae, (3) high dislocation density in the vicinity of the original grain boundary and (4) a

concave forward α/α' interface. Finally, using x-ray diffraction, the depleted α lamellae were found to contain a slight excess of solute above that which would be expected at equilibrium.

Corderoy and Honeycomb[14], studying general precipitation of δ in the temperature range of 250°C to 400°C by transmission electron microscopy observed that δ was the only phase precipitated at all aging temperatures and at all aging times and that all precipitates eventually attained a length of about 1μ. Selected area diffraction patterns from thin foils and carbon extracted precipitate platelets were interpreted to give the following habit plane relationship.

$$\{111\}_{\delta} \,||\, \{100\}_{\alpha}$$

After prolonged aging of a 10.1 at.% In alloy at 330°C Shapiro and Kirkaldy[50,52] observed an additional fine precipitate which they called δ'.

Analyses of cell growth rate and lamellar spacing by Böhm[6] and by Shapiro and Kirkaldy[50,52] show that cell growth, as analyzed by Turnbull's theory, is controlled by interface diffusion. As mentioned previously Shapiro and Kirkaldy's results show the consistent behavior of the Cahn theory.[12]

As discussed earlier, Böhm[7] has observed that additions of magnesium and antimony increase the growth rate while additions of iron, silicon and beryllium decrease it. He also observed that the growth rate was not affected by prior deformation.

TABLE I

Systems Exhibiting Cellular Precipitation

Ag-Cu (46,60)
Al-Ag (1,18,73)
Al-Zn (47,73)
Au-Pt (62)
Co-Nb (45)
Co-Ni-Nb (45)
Co-Ta (33)
Co-Ti (17)
Cr-Ni (30,53)
Cu-Ag (39,49,54,60)
Cu-Be (15,22,72)
Cu-Cd (59,61)
Cu-Co (44)
Cu-In (6,9,10,14,50,52)
Cu-Mg (7,10,41,60)
Cu-Ni-Mn (22)
Cu-Sb (7)
Cu-Sn (7)
Fe-Ni-Ti (55)
Fe-Zn (31,56)
Mg-Al (13,73)
Nb-Cr (29)
Ni-Sn (32)
Ni-Ti (40)
Pb-Na (38,43)
Pb-Sn (35,60,64-68)
Zn-Ag (73)
Zn-Cu (54,60,73,74)

TABLE II

List of Symbols

G	velocity of cell growth
S	lamellar spacing
S_α	width of α lamellae
S_β	width of β lamellae
D_V	volume diffusion coefficient
D_B	boundary diffusion coefficient
R	universal gas constant
T	absolute temperature
V	molar volume
$X_{\alpha'}$	mole fraction of solute in the supersaturated α' solid solution
X_α	mole fraction of solute in the depleted α lamellae
$X_{\alpha e}$	equilibrium mole fraction of solute in the α solid solution
X_β	mole fraction of solute in the β phase
X_B	mole fraction of solute in the α/α' boundary
λ	width of the α/α' boundary
$\sigma_{\alpha/\alpha'}$	surface energy of the α/α' boundary
$\sigma_{\alpha/\beta}$	surface energy of the α/β boundary
$\sigma_{\alpha'/\beta}$	surface energy of the α'/β boundary
r	radius of curvature of the α/α' boundary
ΔF_o	chemical free energy change for the formation of one mole of reaction products
ΔF	net free energy change for the formation of one mole of reaction products
P	fraction of chemical free energy released during reaction

TABLE II - List of Symbols - (continued)

Q	fraction of minor component precipitated during reaction
R	fraction of ΔF_o converted to $\sigma_{\alpha/\beta}$ during reaction
M	interface mobility

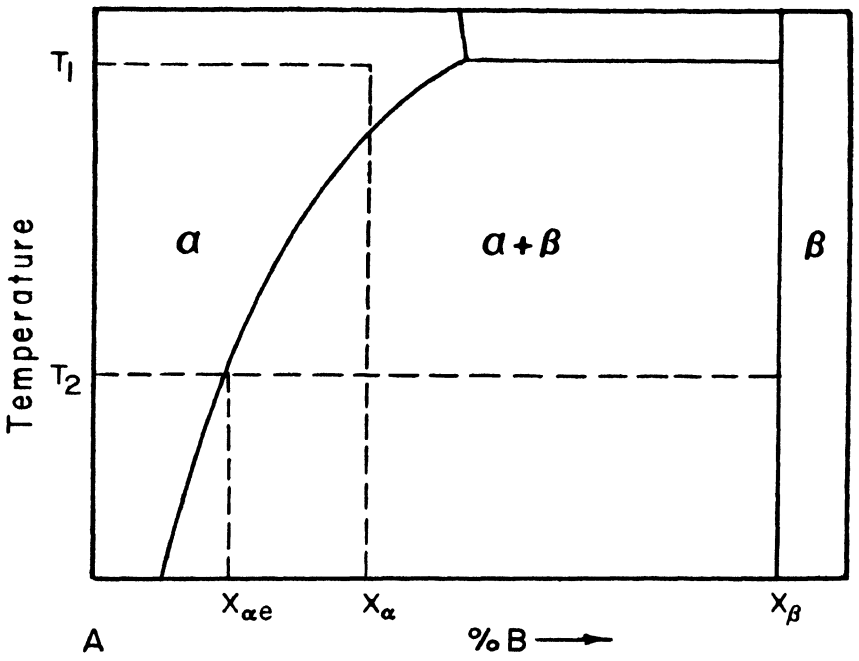

Figure 1. Schematic diagram of a portion of a binary phase diagram showing limited solid solubility of B in A.

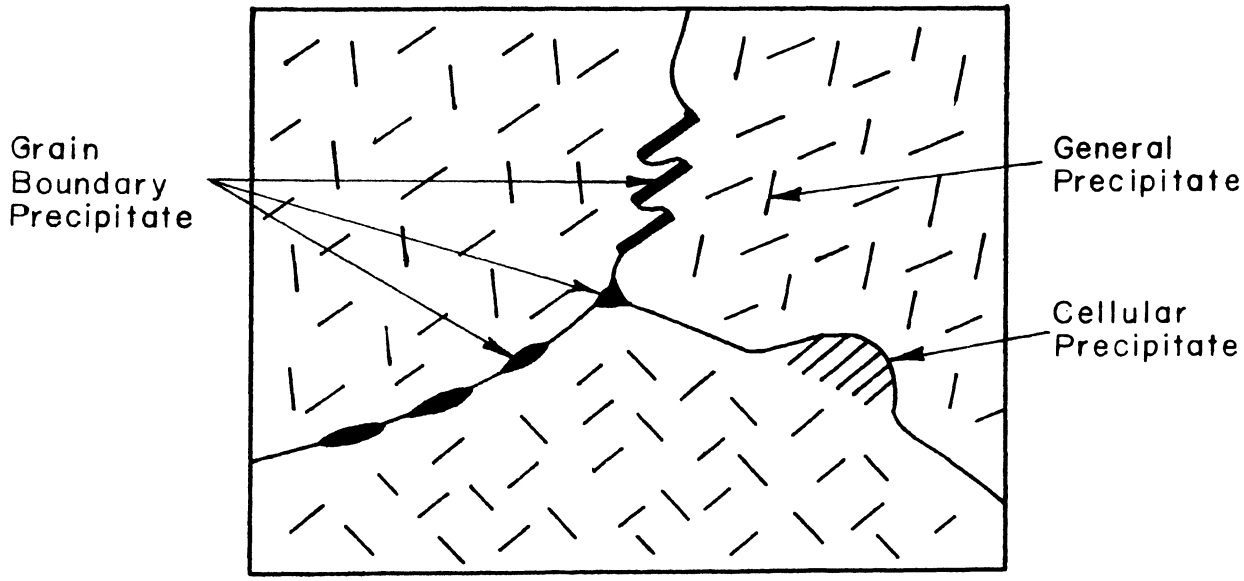

Figure 2. Schematic diagram of a possible microstructure of an alloy of composition X_α, aged at T_2.

Figure 3. Zn-2at.%Cu, solution treated 12 hours at 400°C, aged 36 hours at 200°C. X200(54)

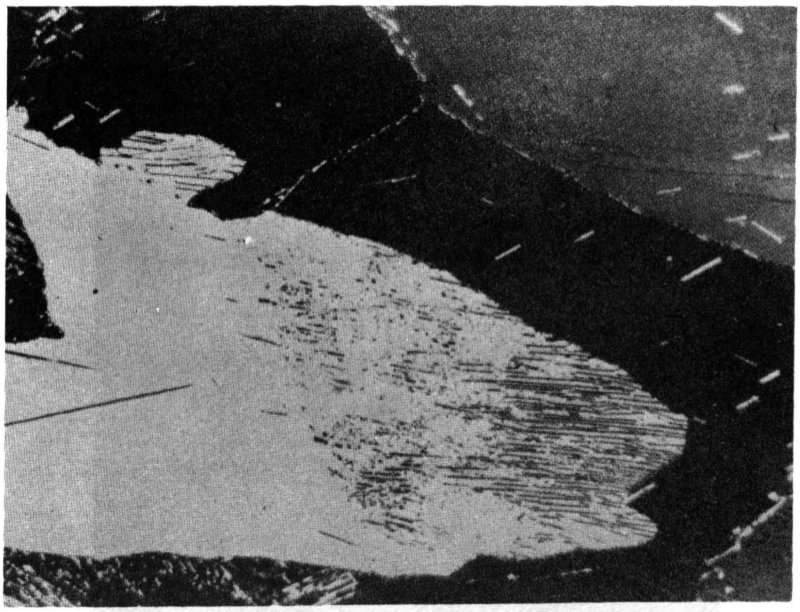

Figure 4. Same area as in Figure 3 under polarized light.(54)

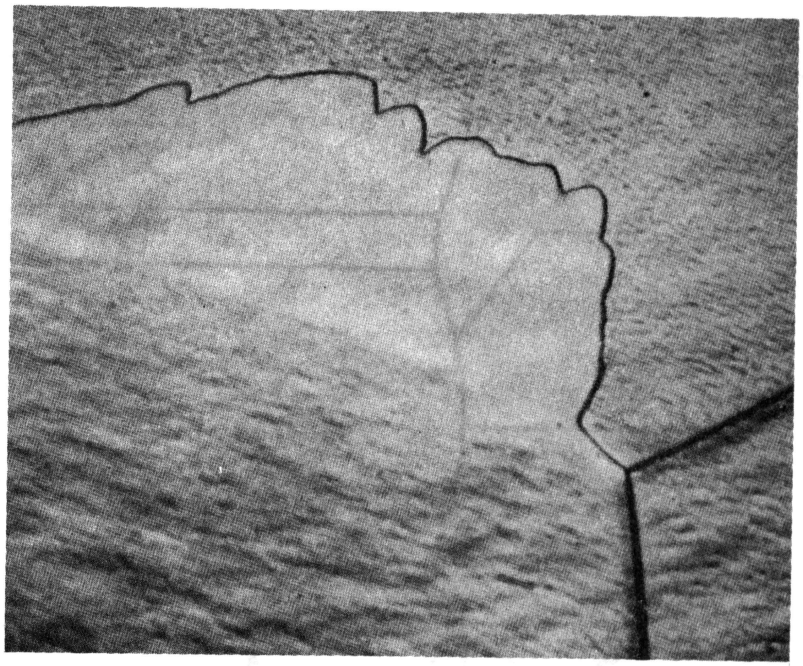

Figure 5. Pure aluminum. Cold rolled 14%, annealed 5 minutes at 400°C. X75(4)

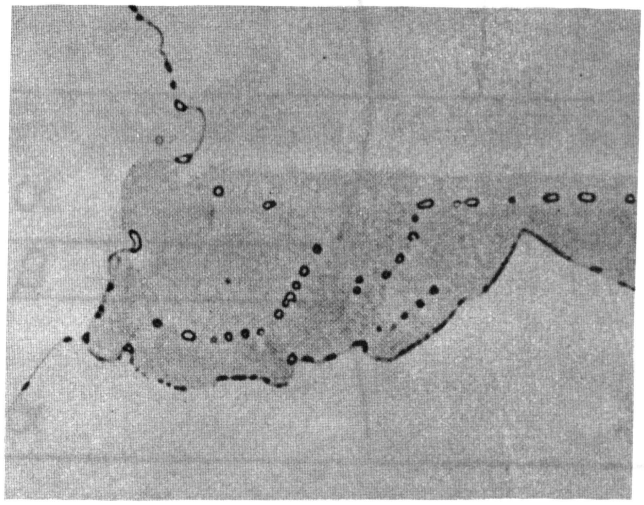

Figure 6. Cu-3.81wt.%Cd, aged 4 minutes at 530°C. X1,000(59)

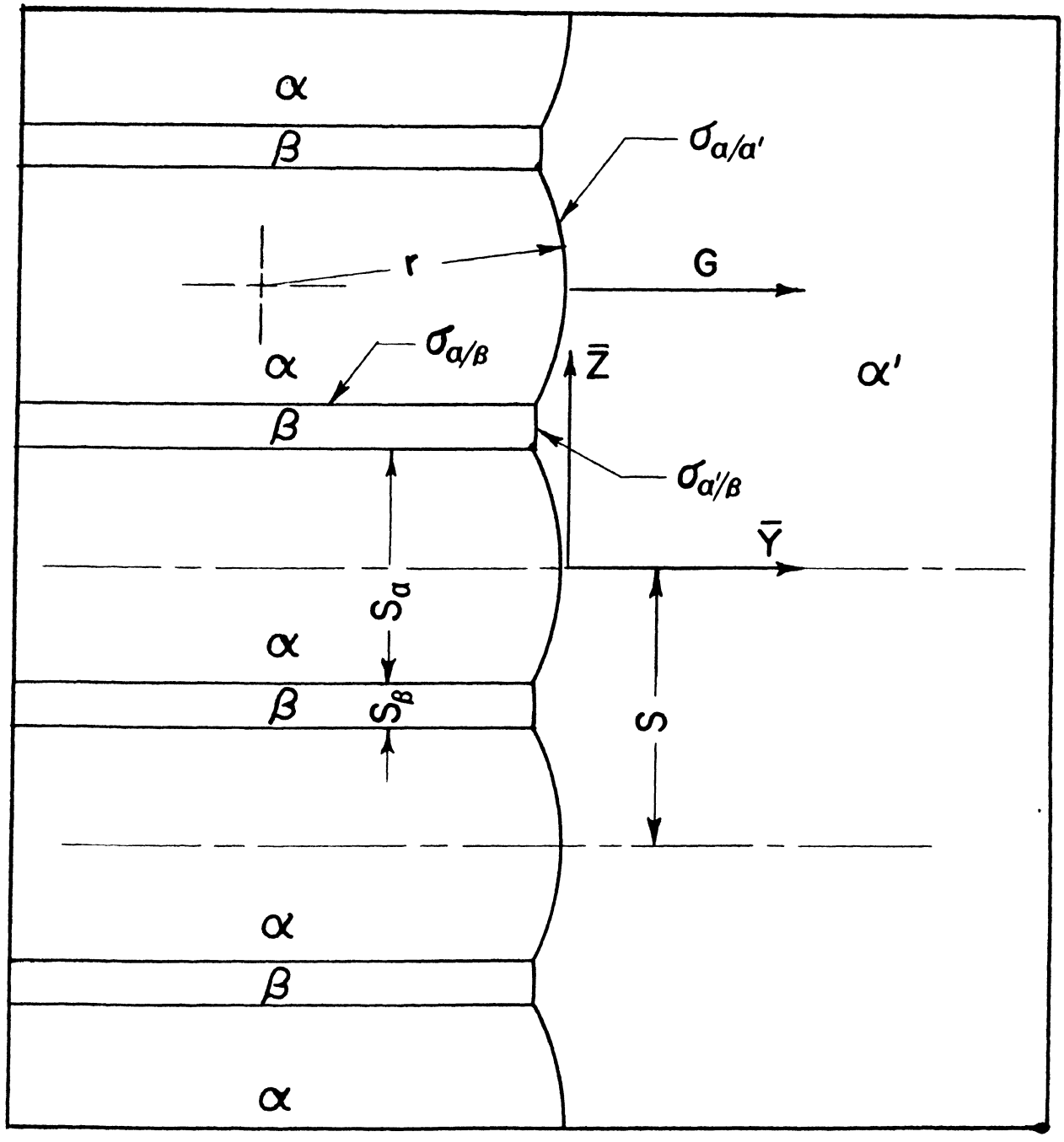

Figure 7. Schematic diagram of the advancing interface of a cellular nodule growing into and decomposing a supersaturated solid solution according to the reaction, $\alpha' \rightarrow \alpha+\beta$.

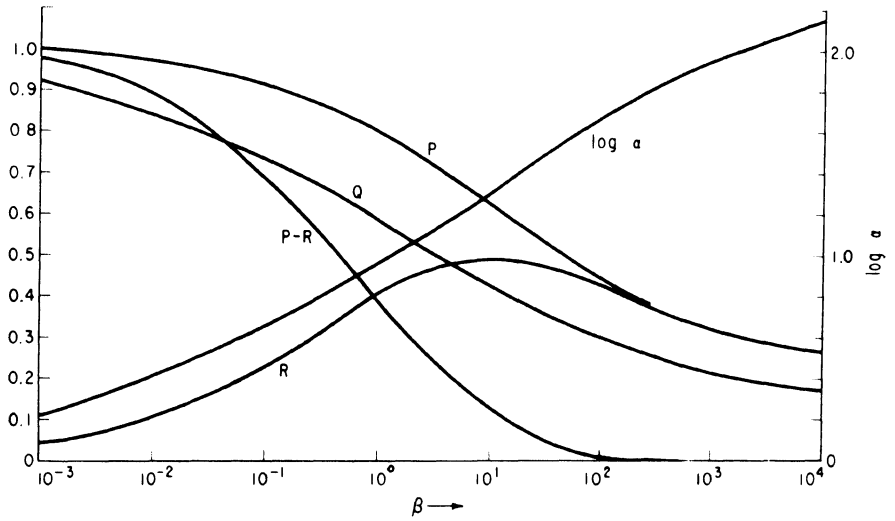

FIG. 2. Precipitation from dilute solution as a function of the parameter $\beta = -MV^2\sigma^2/D_B\delta\Delta F_0$
P the fraction of ΔF_0 realized.
Q the fraction of material precipitated.
R the fraction of ΔF_0 expended on surface energy.
$P - R$ the fraction of ΔF_0 exerting a pressure on the cell boundary $\beta = kGS^2/D_B\delta$

Figure 8. P, Q and R as functions of the β parameter from Cahn's analysis.(12)

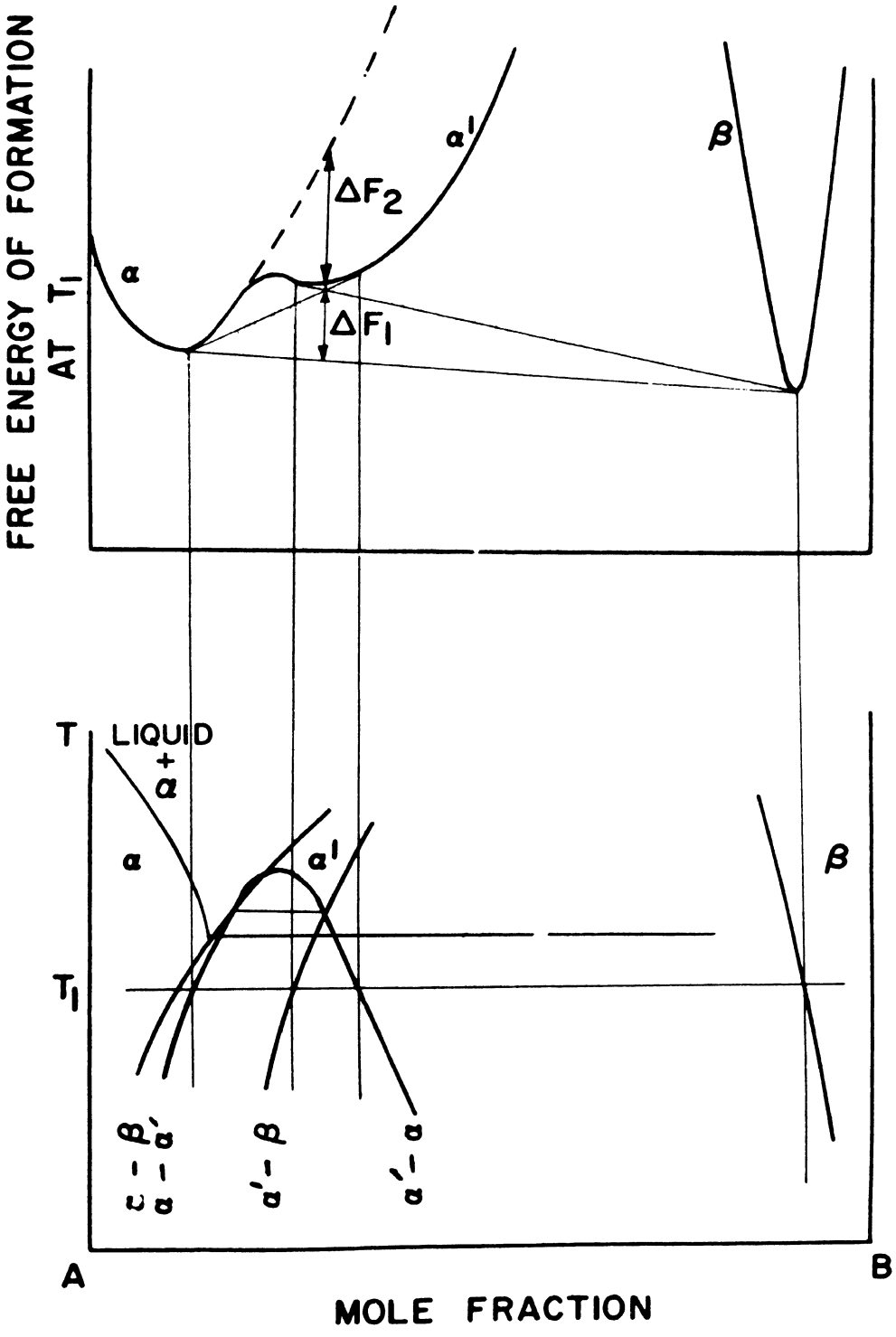

Figure 9. Free energy curves and phase diagram for a metastable monotectoid reaction according to Shapiro and Kirkaldy.[50,52]

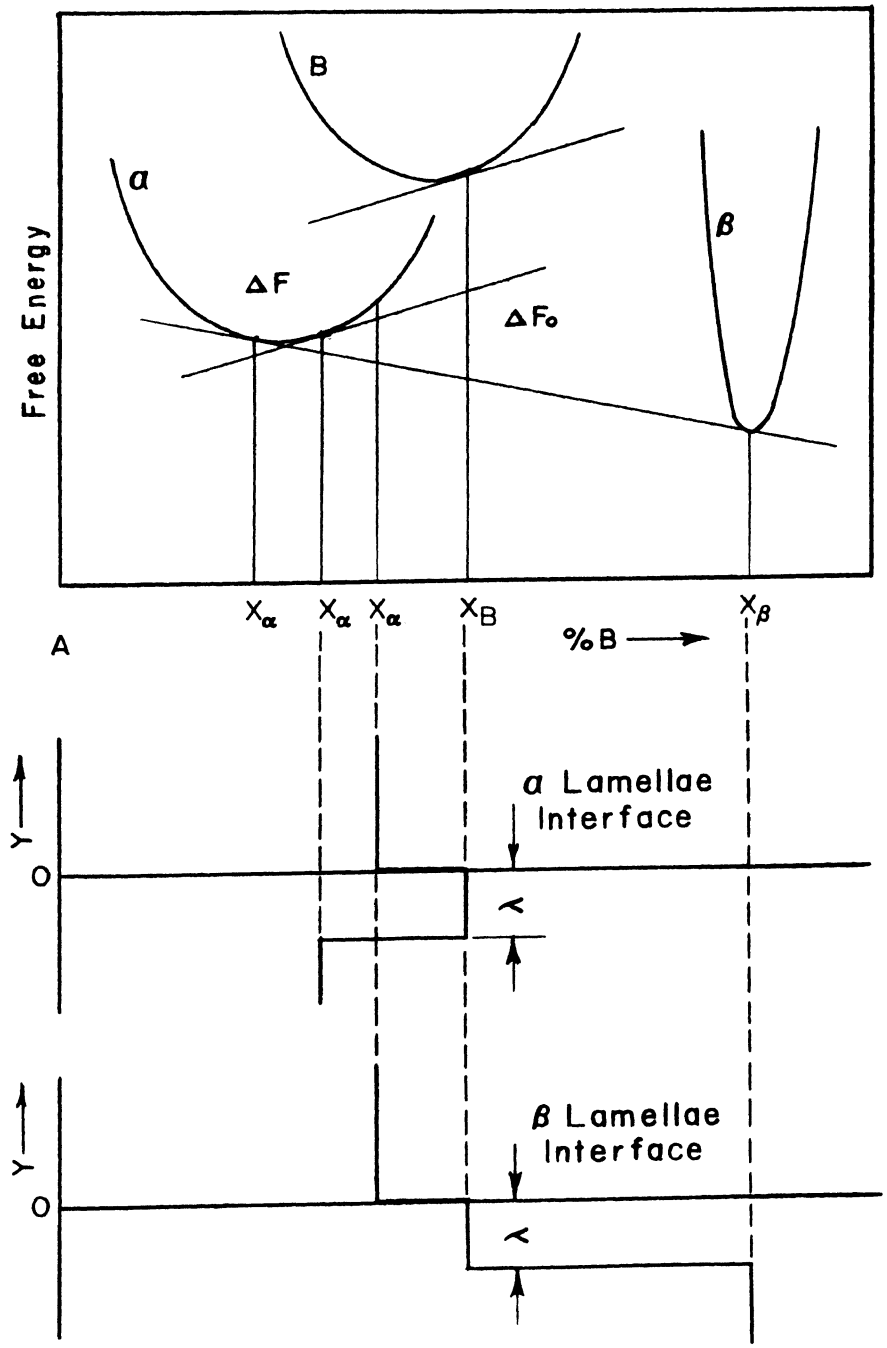

Figure 10. Free energy-composition diagram for the system illustrated in Figure 1 at T_2 showing Hillert's thermodynamic concept of the α/α' interface. Composition profiles of the α/α' and α/β interfaces are also shown.

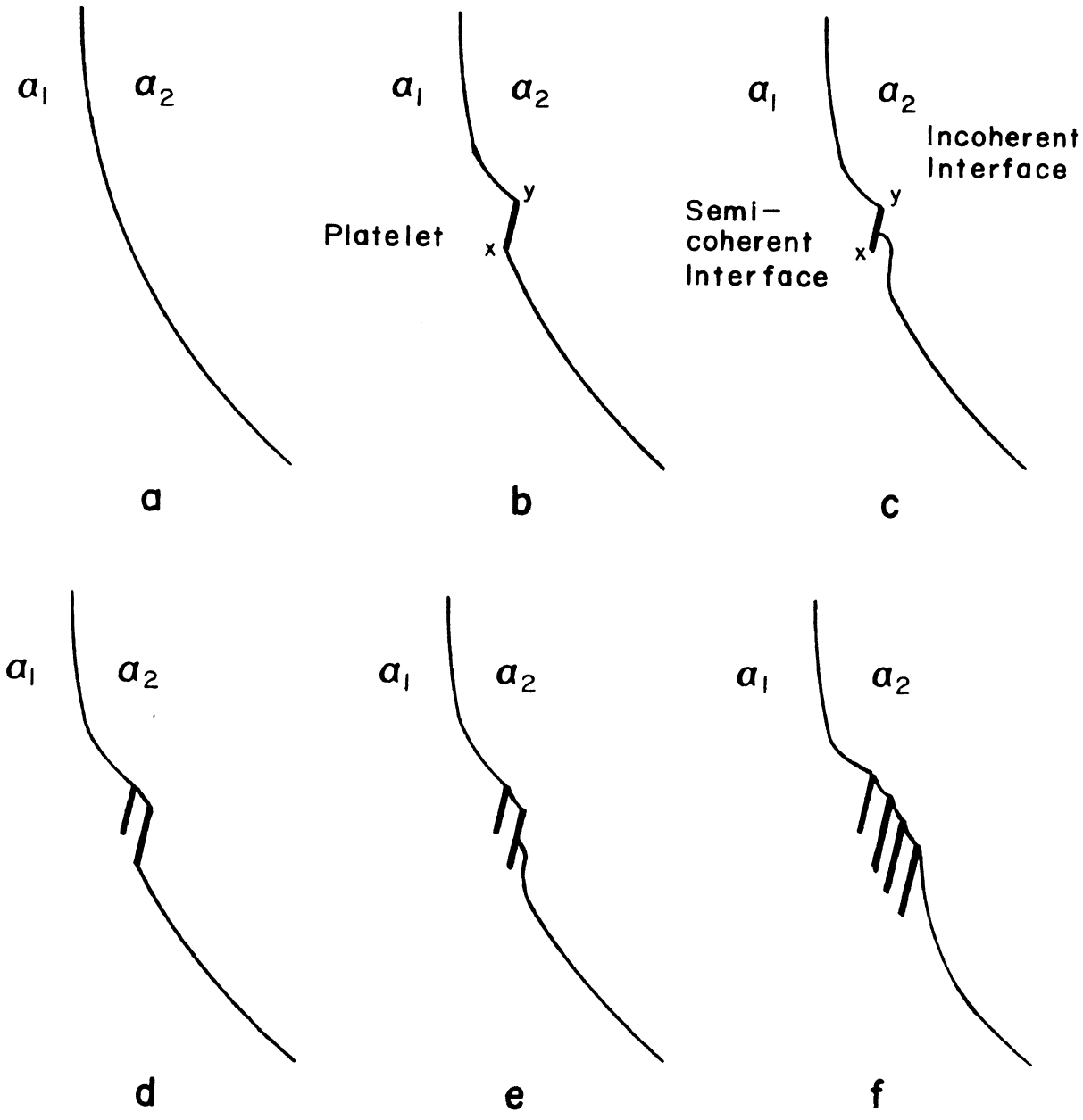

Figure 11. Schematic diagram showing the nucleation of β lamellae in a lead rich lead-tin solid solution.

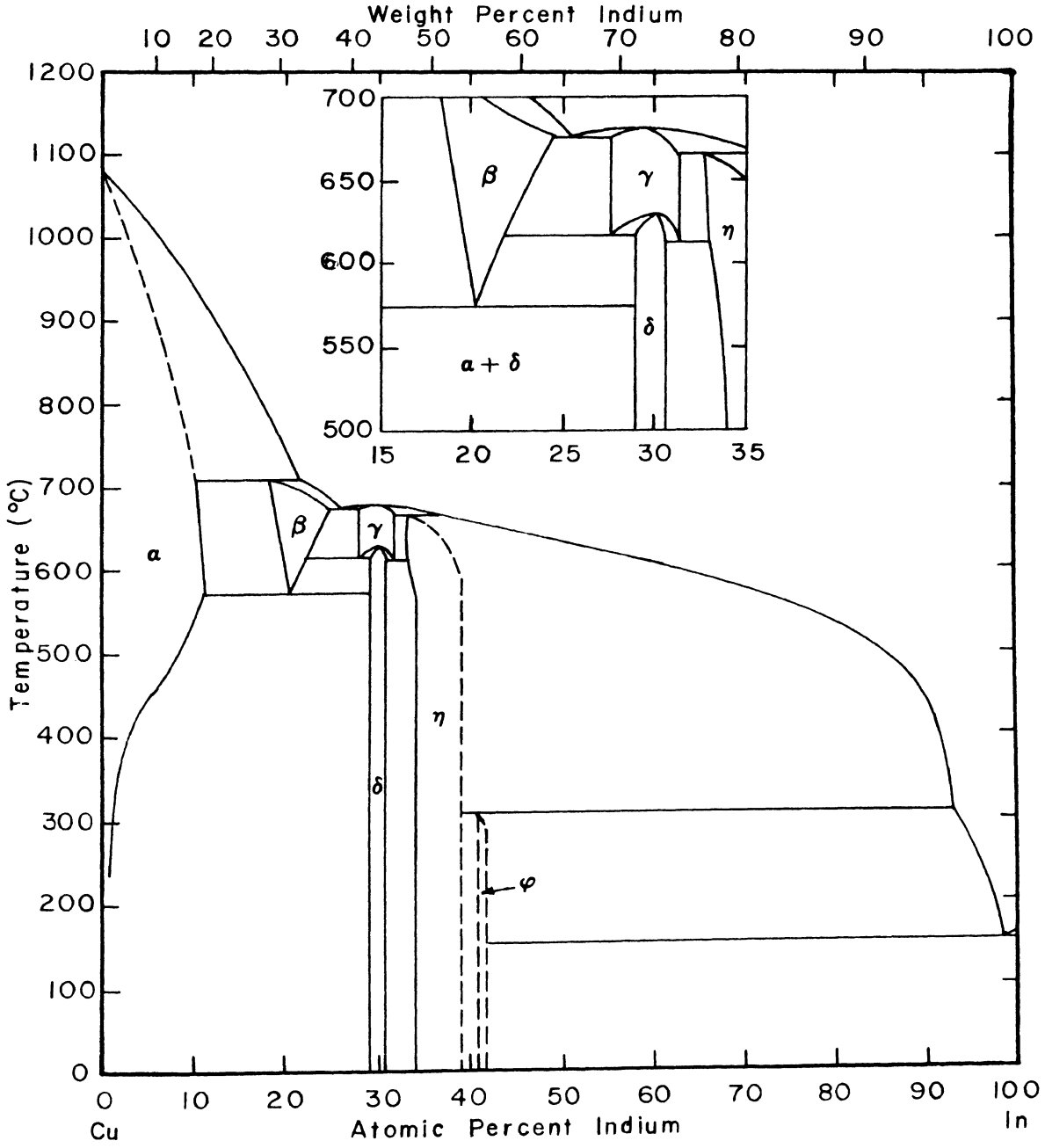

Figure 12. Copper-Indium Phase Diagram[24]

III. EXPERIMENTAL OBJECTIVES

As mentioned in the introduction, this investigation seeks to determine a mechanism for the genesis of cellular nodules from an initially unoccupied grain boundary and to establish a cause for the reaction based on this mechanism.

Consistent with this overall objective the following experimental objectives were set forth for a systematic investigation of the morphology of cellular precipitation. A preliminary study was performed to select an alloy system exhibiting appropriate precipitation phenomena and desirable properties for experimental examination. After the alloy was selected the major characteristics of both cellular and general precipitation were established for both quench and age and isothermal aging heat treatments. These characteristics included the habit plane and orientation relationship for both the general precipitate and the cellular lamellae, the growth kinetics of the cellular nodules and any extraordinary morphological features that require an explanation.

Once the general characteristics of general and cellular precipitation had been established, the time-temperature-transformation curves for the start of general and cellular precipitation were determined for both types of heat treatment using light microscopy. Using these curves and other background information as a basis, light and electron microscopy studies of the early stage morphologies at all aging temperatures where cellular occurs were performed to establish a mechanism for cell formation. After a mechanism for the genesis of

cellular precipitation had been established an attempt was made to relate this mechanism to a possible cause of the reaction.

IV. EXPERIMENTAL PROCEDURE

A. Preliminary Study for the Selection of an Alloy System

In accordance with Section III a preliminary investigation was performed to select an alloy system for study. The criteria for the selection of a system required not only that characteristic cellular precipitation occur during aging but also that the system be amenable to the various metallographic techniques. Some of these criteria are listed below.

From a metallographic standpoint the cellular aggregate should have a lamellar rather than a rod like or degenerate morphology, the lamellar structure of the cells and the initial grain boundary structure formed in the alloy during aging should be coarse enough to be resolved by light microscopy, a sufficient amount of cellular precipitate should be formed at all aging temperatures and the alloy should be amenable to standard specimen preparation techniques for light and electron microscopy. From an experimental standpoint the alloy must be capable of being melted, cast and formed to rod and foil specimens by standard metallurgical techniques. These rod and foil specimens must then be adaptable to heat treatment in commercial salt baths and, in conjunction with this, the precipitation reaction should occur at reasonable aging temperatures and times. Finally, the transformation should be amenable to observation by hot stage metallographic techniques. These techniques may be either those of light microscopy or those of transmission electron microscopy.

Considering the above criteria a review was made of the available literature, some of which is referenced in Table I, in order to select

systems for the preliminary investigation. A survey of the systems listed in Table I shows that cellular precipitation is characteristic of many copper base alloy systems and that the morphology and growth kinetics of cellular nodules in these systems are characteristic of the cellular reaction as described in Section II. In addition, many of these copper base systems were found to be adaptable to the various experimental techniques. Therefore, on the basis of this review, three copper base systems, Cu-In, Cu-Mg and Cu-Sb, were selected for the preliminary investigation. Other copper base systems were excluded from this study either on the basis of the morphology of the cellular aggregate or the nature of the alloy element; e.g., beryllium was excluded because of its toxicity.

For the experimental evaluation of the above alloy systems cylindrical alloy ingots of Cu-7at.%In, Cu-5at.%Mg and Cu-5at.%Sb were prepared by melting and casting in a manner similar to that described in Section IV. A. 2. Following casting, during which no difficulty was encountered, an attempt was made to swage the ingots to 0.3 inch diameter rods. Here the Cu-5at.%Sb alloy proved to be too brittle to be cold or hot swaged and was eliminated from the investigation. Both the Cu-In and Cu-Mg alloys were ductile enough to be swaged and rolled to rod and foil form although the Cu-In alloy could only be hot swaged.

After being solution treated, water quenched and aged for various times at various temperatures samples from both alloys exhibited cellular nodules with easily resolvable lamellar structures when observed by light microscopy; however, attempts to prepare thin foils of the Cu-Mg alloy for transmission electron microscopy by standard electrolytic techniques failed to retain the Cu_2Mg precipitate phase

and this alloy was eliminated from study. Thus, only the Cu-7at.%In alloy satisfied the criteria for selection, and, subsequently, a Cu-9.5at.%In alloy was selected for study. This higher indium content alloy was selected because the range of temperatures at which cellular precipitation occurs is larger for this alloy than for the 7at.%In alloy.

B. Preparation of the Cu-9.5at.%In Alloy Specimens

1. Alloy Elements

The Cu-9.5at.%In alloy used in this study was prepared from electrolytic copper of 99.997% purity donated by Anaconda American Brass Company and indium shot of 99.99% purity purchased from Atomergic Chemetals.

2. Alloy Preparation

About 820 grams of Cu-9.5at.%In alloy in the form of three ingots, 0.65 inch in diameter, were obtained by melting appropriate quantities of the above components in a graphite crucible and chill casting the melt in graphite molds, 0.65 inch in diameter. Prior to melting, the alloy elements were cleaned in dilute nitric acid, water and methanol after which they were degassed in a vacuum. Following a final weighing, the copper was melted in the graphite crucible under a charcoal top by induction heating. The indium shot was then added, wrapped in copper foil, and the resultant solution was stirred with a carbon rod to insure homogeneity. Then, after superheating the melt 200°C to 1,150°C the alloy was chill cast as described above.

Measurement of the weight of the ingots showed the loss of 1.1 grams, or < 0.2% of the total weight of the alloy elements, during melting. As with the alloys of the preliminary study little difficulty was encountered in melting and casting.

3. Alloy Specimen Preparation

The alloy ingots described above were annealed, swaged and rolled to form rod stock for light microscopy specimens and foil stock for transmission electron microscopy specimens. A solution anneal at 650°C was performed prior to swaging to remove any solute segregation resulting from the cooling of the ingots through the wide α + liquid phase field, shown in the copper-indium phase diagram, during solidification. The ingots were cleaned by belt sanding, encapsulated under argon, annealed for 200 hours at 650°C and water quenched. Prior experience in the preliminary study showed that such an anneal would remove all of the dendritic segregation.

After annealing, the ingots were reduced by hot swaging to rods having a 0.316 inch diameter. Some of these rods were cut to form 1/4 inch thick discs for light microscopy specimens while other rods were hot and then cold rolled to form 0.007 inch thick foil for electron microscopy specimens. The metallographic disc specimens were subsequently annealed under argon for 96 hours at 650°C to give a grain size adequate for light microscopy studies. This grain size was found by the intercept method to be about 0.5 millimeter. Later it was found that aged light microscopy specimens could be recycled by solution treating them at 650°C for 2 hours without significantly affecting the above grain size.

Two samples, which represented what had been the center and the top of an ingot, were cut from a swaged rod and analyzed chemically and spectrographically by Industrial Testing Laboratory, St. Louis, Missouri, for copper and indium content and for impurity level respectively. The results of these analyses, given in Table III, show that vertical segregation of copper and indium is negligible, that the minimum purity of the alloy is 99.9% and that the impurities present are within their solubility limits in copper.

C. Specimen Heat Treatment

As mentioned in Section III two different aging heat treatments are used in this investigation. These are (1) quench and age heat treatments in which the alloy is quenched from the solution treatment temperature into water and then heated to and held at the aging temperature and (2) isothermal aging heat treatments in which the alloy is transfered directly from the solution treatment temperature to the aging temperature.

Schedules for both of the above heat treatments and for both light and electron microscopy specimens were standardized to eliminate any time dependent annealing effects. Light microscopy specimens were all solution treated for two hours at 625°C prior to aging while those for electron microscopy were held only five minutes at 625°C. All quenched and aged samples were held five minutes at room temperature prior to aging. All samples were quenched in water after aging.

Except for the solution treatment of the specimens used for the determination of the time-temperature-transformation diagram for quenched and aged alloys, all solution and aging heat treatments were

performed in salt baths whose temperatures were controlled to ± 1°C. Houghton Liquid Heat 300 was used for solution treatments while Houghton Draw Temp 275 and 430 were used for aging treatments. The solution treatment of the quenched and aged specimens used to establish the TTT curve was performed in a muffle furnace after encapsulation under argon.

D. Metallographic Techniques

1. Light Microscopy

Aged specimens were prepared for metallographic examination by cold mounting, belt sanding and wet grinding through 600 grit paper after which they were polished, using first 9μ and then 1μ diamond paste. Final surface preparation consisted of alternate polishing with 0.05μ alumina and etching with a potassium dichromate etch whose composition is given below.

$K_2Cr_2O_7$ ..... 2 grams
NaCl ..... 1.5 grams
H_2SO_4 ..... 8 milliliters
H_2O ..... 100 milliliters

In all cases etching was performed by swabbing. All light microscopy was performed on a Bausch and Lomb Research Metallograph.

2. Electron Microscopy

Thin foil transmission electron microscopy specimens were prepared electrolytically by the "window" method[28] using a nitric acid-methanol electrolyte containing 33% nitric acid by volume cooled to

below -40°C. A copper screen was used for the cathode and 6 to 7 volts was found to be best for uniform specimen thinning. Appropriately thinned specimens were rinsed twice in methanol, cooled to less than -40°C, and then dried in air after excess methanol had been removed by absorption onto a paper towel. Specimens were cut from the thin foil with a scalpel using a rolling motion rather than a cutting motion. All electron microscopy observations, including hot stage observations, were obtained with a Hitachi HU-11B electron microscope equipped with an HK-2BM heating and rotating tilt stage.

E. Sequential Heat Treatment Technique

Because the grain boundary and cellular morphologies were too fine at most aging temperatures to be studied at low magnifications (<X1,000) and because surface precipitation occurred at all aging temperatures, light microscopy hot stage techniques could not be utilized for the study of precipitation behavior in this alloy. Therefore, a technique was developed that would allow the observation of the complete development of cellular nodules at a single grain boundary. As this technique is sufficiently different from standard metallographic techniques, it is briefly outlined here.

The special metallographic specimen developed for this technique consists of one of the 0.316 inch diameter light microscopy disc specimens imbedded in a mount of pure aluminum as shown schematically in Figure 13a. The specimen was fabricated by casting pure aluminum around a light microscopy disc specimen centered in a graphite mold as shown in Figure 13b. Before casting, grooves were filed in the Cu-In sample to provide an anchor for the aluminum, after which it was held

at 400°C in air to form a thick oxide film to prevent reaction with the molten aluminum. After casting, the resultant aluminum mounted metallographic specimen was used to study the development of cellular structures as described below.

The specimen was first given one of the standard aging treatments described in Section IV. C. with the aging time being just long enough to start some of the boundaries migrating but not long enough to form steady state cellular structures. Following this heat treatment, the specimen was ground, polished and etched using the procedure described for ordinary specimens in Section IV. D. 1. After placing a Knoop microhardness indentation in the center of the Cu-In sample and scribing a reference mark on the back of the aluminum mount, the specimen was examined by light microscopy using the oil immersion lens with the largest numerical aperture, and photomicrographs of boundaries whose initial behavior appeared interesting were obtained. The locations of these boundaries with respect to the Knoop indentation were established using the micrometer adjustments on the microscope stage.

Following examination the specimen was cleaned of immersion oil, wrapped tightly in aluminum foil to prevent contact of the polished surface with the molten salt, given an additional short aging treatment and quenched in liquid nitrogen until just cool. After polishing lightly with 1μ diamond and 0.05μ alumina to remove a surface precipitate layer that had formed, the alloy was reetched, and the boundaries observed initially were reexamined and photographed. The above process was then repeated several times to obtain a sequence of photomicrographs showing the development of cellular precipitate and grain

boundary morphologies.

It should be mentioned that the light polishing step described above was required to remove a surface precipitate that formed even at short aging times and low aging temperatures, and, although no measurement of the thickness of the layer of material removed was made, it was sufficiently thin that distinguishing details of cellular development could be traced through the sequence of photomicrographs.

F. X-ray Diffraction Techniques

Debye-Scherrer x-ray techniques were used to study the crystal structure of the δ precipitate phase while compositional changes in the copper rich α phase were followed by changes in the α lattice parameter obtained from diffractometer measurements. The former techniques are described in Appendix A while the latter are given below.

Diffractometer measurements were obtained from light microscopy disc specimens which had been mounted in such a way as to minimize the effects of textures resulting from swaging. However, these effects could not always be removed, and, in most cases, the lattice parameters had to be determined from (222), (311) or (220) reflections. All measurements were made using nickel filtered copper radiation and all lattice parameters were calculated directly from Equation 27; and, as no extrapolation techniques were used,

$$a = d_{hkl}(h^2+k^2+l^2)^{\frac{1}{2}} \tag{27}$$

accuracy was limited to three significant figures. The α phase composition was then obtained from the lattice parameter using a

relationship established by Straumanis and Yu,[58]

$$a = 3.6149 + 0.0091x \tag{28}$$

where $\underline{x}$ is the α phase composition in weight percent and $\underline{a}$ is the lattice parameter in angstroms.

TABLE III

Analysis of the Cu-9.5at.%In Alloy

	Center of Ingot	Top of Ingot
1. Chemical Analysis in Weight Percent		
Copper	84.01	84.14
Indium	15.90	15.83
2. Semiquantitative Spectrographic Analysis in Weight Percent		
Silver	0.001-0.01	0.01-0.1
Calcium	<0.01	<0.01
Aluminum	<0.001	0.001-0.01
Iron	<0.003	0.003-0.03
Silcon	<0.001	0.001-0.01
Lead	0.01-0.1	0.01-0.1
Magnesium	<0.005	0.01-0.1

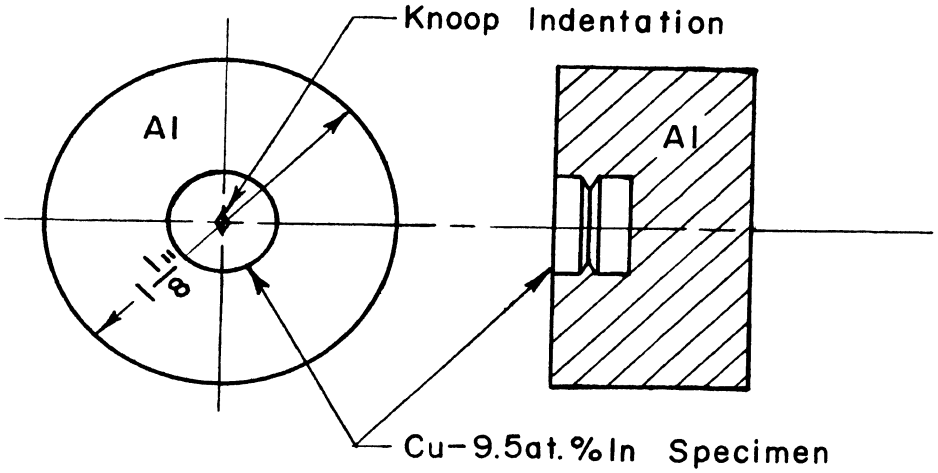

a. Specimen

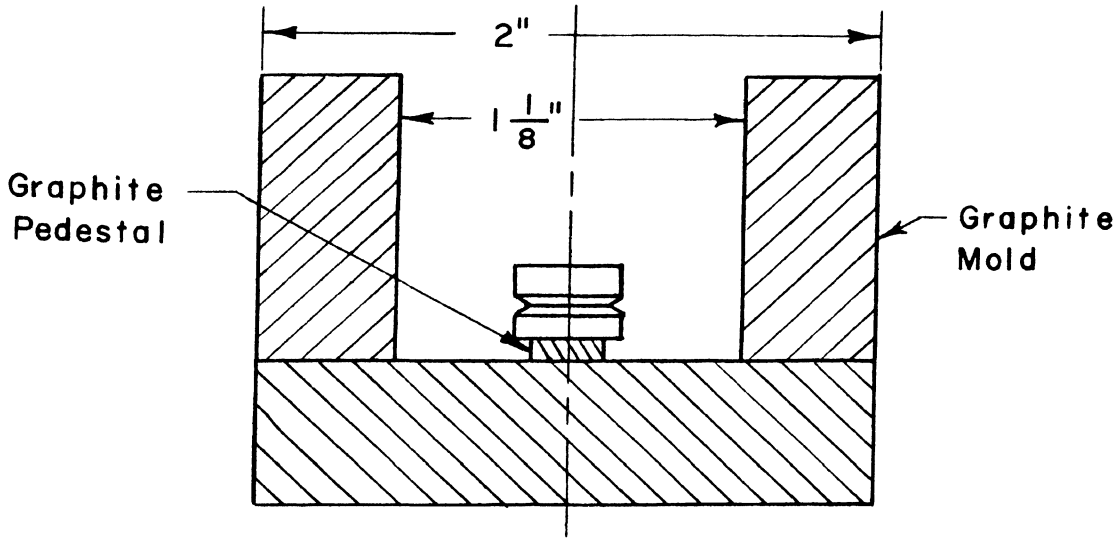

b. Mold

Figure 13. Sequential heat treatment specimen and mold.

V. EXPERIMENTAL RESULTS AND DISCUSSION

A. Morphology and General Characteristics

1. General

In accordance with the experimental objectives set forth in Section III, the major characteristics of cellular and general precipitation in Cu-9.5at.%In were established for both quench and age and isothermal aging heat treatments. Figures 14 and 15 show the morphology of precipitation in alloys aged at 420°C by both heat treatments. These morphologies are characteristic for all aging temperatures studied (250-500°C) with variations in morphology being of degree rather than type. In agreement with previous studies, Figure 14 shows Widmanstätten general precipitate occurring simultaneously with cellular precipitation in the quenched and aged alloy. The precipitate free zone in the vicinity of grain boundaries where cellular nodules have not formed appears to result from a lack of nucleation sites for general precipitate caused by the depletion of vacancies in this region by their migration to the boundary. Moisio and Mannerkoski[41] have observed similar zones in Cu-Mg alloys and Unwin, Lorimer and Nicholson[71] have recently discussed the origin of such zones in Al-Mg-Zn alloys.

Figure 16 shows the solute depletion of the α' resulting from general precipitation and Figure 29 shows the sequential development of precipitation in a quenched and aged alloy. These results show that solute depletion resulting from general precipitation gradually slows and finally stops the growth of cellular precipitation. Additional

studies have shown that cellular precipitation is essentially stopped after about 2 hours of aging at 422°C. This corresponds to about a 2 at.% decrease in indium content. In general, above this temperature the effect of general precipitation becomes greater while below it cellular precipitation becomes more prominent.

In contrast to quenched and aged alloys, in which cellular and general precipitation compete, isothermally aged alloys exhibit only cellular precipitation, as shown in Figure 15; and, as seen in Figure 52, the cellular reaction eventually consumes the entire α' matrix. Apparently the isothermal aging heat treatment suppresses the formation of nucleation sites for the general precipitate. It is interesting to note that Moisio and Mannerkoski[41] did not observe a complete suppression of general precipitation during isothermal aging of Cu-Mg alloys but only a coarsening of precipitation and a substantial widening of precipitate free zones.

2. General Precipitation

As seen in Figure 17 the general precipitate occurs as Widmanstätten platelets about 1μ in length with dislocation tangles surrounding each platelet. This observation at 420°C is in agreement with those of Corderoy and Honeycomb[14] at 250, 300 and 400°C; however, an analysis of the habit plane of the platelets results in a set of planes other than the {100} set proposed by these authors. Figure 19 shows the traces of the poles of the habit planes of the platelets shown in Figure 17 on a standard (110) projection whose orientation was established from Figure 18, a selected area diffraction pattern of Figure 17. Analyses of the traces in Figure 19 and in other stereographic

projections obtained from other specimens have shown that the traces consistently pass through only {113} poles, indicating that {113} planes of the face-centered cubic α matrix are the habit planes of the δ platelets. Trace analyses of Figures 12, 13, 14 and 15 in Corderoy and Honeycomb's paper, which show general precipitate formed at 300 and 400°C, result in this same habit and, indeed, these authors observed the {100} habit only for relatively short aging times at 250°C as shown in their Figure 10. In addition a {100} habit would limit the number of distinguishable habits to three, which is clearly inconsistent with the observation of up to six platelet orientations within one α grain as seen both in their electron micrographs and in Figure 17.

Considering the densities of the α and δ phases and their crystal structures, the dislocation tangles associated with the precipitate platelets appear to result from a distortion of the α' caused by the tetragonally distorted cubic structure of the δ precipitate phase rather than volume strain resulting from a density difference between the α and δ phases. Densities of the α calculated from lattice parameters determined by Straumanis[58] range from 8.93 gms/cm^3 for pure copper to 8.97 gms/cm^3 for a 10 at.%In alloy while the density of a 29.5at.%In alloy (δ phase) has been determined by this author to be 8.93 gms/cm^3. (See Appendix A). Clearly, little volume strain can be expected solely on the basis of this density difference between the α and δ no matter what the composition of the α phase is. On the other hand, considerable shear strain should result from the formation of a tetragonal structure with c/a = 1.02 in a cubic matrix; however, the establishment of a mechanism for the generation of the dislocations is

precluded by the lack of knowledge of the orientation relationship between the α and the δ. Finally, it is of interest to note that similar dislocation tangles are associated with initial grain boundary allotriomorphs as shown in Figure 36.

The previous observation of precipitate free zones in quenched and aged alloys suggests that loops or voids, formed during aging by condensation of excess vacancies, are the nucleation sites for general precipitate. This vacancy excess apparently results from the retention of vacancies, initially at equilibrium at the solution treatment temperature, during the quench to room temperature. Apparently, an insufficient excess of vacancies results from the direct transfer from solution treatment temperature to aging temperature, which is characteristic of isothermally aged alloys, for loops or voids to form. Attempts to observe the defects at aging temperatures above 250°C failed because precipitation had already started after only a few seconds of aging. No defects were observed in water quenched alloys. At 250°C, however, nucleation kinetics were sufficiently slow that the development of precipitate nuclei from the initially defect free as quenched state required about 1 minute. Accordingly, after aging about 30 seconds at 250°C defects had formed and had a density similar to that of the fine precipitate shown in Figure 20. The structure of the defects could not be established because of their small size, and they could only be distinguished from the initial precipitates by their disappearance in areas of poor diffraction contrast; i.e., away from extinction contours. A study of their behavior near grain boundaries shows that, like the fine precipitate in Figure 20, their density gradually decreases and finally becomes zero as the boundary is

approached. It should be noted that the initial precipitates appear similar to the δ' observed by Shapiro.[50,52]

Finally, Figure 21 shows that, in addition to nucleating on the defects described above, general precipitate can also nucleate on dislocations. Still other observations have shown that platelets can nucleate on twin boundaries. These two results hold true for both quenched and aged and isothermally aged alloys.

3. Cellular Precipitation

The major morphological features of cellular precipitation in Cu-In alloys are illustrated in Figures 15, 22, 23 and 39 while specific crystallographic details are given in Figures 54 through 59. As can be seen in Figure 39, cellular nodules appear to form from grain boundary allotriomorphs, such as the one at A, whose "spacing" is larger than the resulting steady state lamellar spacing near the advancing cell boundary. Figures 15 and 22 show that the δ lamellae can achieve this steady state spacing by branching, while the newly formed precipitate phase at B in Figure 39 shows that they can also multiply by nucleation in the advancing interface. This is in agreement with the results of down quench experiments by both Shapiro[50,52] and Böhm[5] which showed that new lamellae were nucleated at the advancing interface when a sample was quenched from one aging temperature to a lower one.

Twins in the depleted α lamellae, shown best in Figure 22, are another morphological feature worthy of comment. An analysis of crystallographic details of early stage cellular morphologies described in Appendix B shows that the twins are {111} growth twins and that they

apparently form by accidents of growth. The formation of these twins at an advancing α/α' interface can also be seen at A in Figure 38.

As shown in both Figures 15 and 23, the δ lamellae have the ability to change direction as well as to branch in the continuous, depleted α phase. Such behavior suggests that no habit plane of orientation relationship exists for the δ in the α; however, analyses of selected area diffraction patterns from areas of parallel lamellae such as seen at A in Figure 23 were performed to establish if any relationship existed. Accordingly, trace analyses of such areas have shown that the lamellae have habits like those observed for general precipitate platelets in only about half of the cases studied. Analyses of the composite diffraction patterns from these areas, such as those shown in Figures 54 and 55 in Appendix A, show that the parallel δ lamellae all have the same crystallographic orientation; however, no definite crystallographic relation could be established between them and the α. This apparent lack of a rigid habit suggests that the crystallography of the transformed α and δ phases is of secondary importance to the development of cellular structures in this alloy. This is in agreement with Hillert's observation on the growth of pearlite in steel.[27] Identical orientations of parallel δ lamellae can be explained by branching from a single source.

As in the selected area diffraction studies of general precipitate platelets performed by Corderoy and Honeycomb,[14] the above selected area diffraction patterns of the δ lamellae show the presence of superlattice spots with interplanar spacings ("d" values) that are too large to be accounted for by the tetragonal unit cell proposed by Reynolds, Wiseman and Hume-Rothery.[48] An analysis of these electron

diffraction patterns and x-ray diffraction patterns described in Appendix A has shown that the δ precipitate structure can be described as a superlattice based on the original tetragonal structure and having lattice parameters of a = 35.95 Å and c = 36.63 Å.

Two final morphological features of the cellular structure which should be noted are (1) the shape of the advancing α/α' interface and (2) the dislocation structure at the original grain boundary. First, in agreement with the observations of Shapiro,[50] the advancing α/α' interface is generally concave forward as shown in Figure 22. Considering the second feature, this same figure shows the existence of dislocations in the α' on the unreacted side of the original grain boundary. These are thought to arise from the same crystallographic distortion that causes the dislocation tangles around general precipitate platelets.

B. Time-Temperature-Transformation Diagrams

In order to establish a basis for light and electron microscopy investigations of the early stages of cellular precipitation in the Cu-9.5at.%In alloy, the time-temperature-transformation curves for the start of both cellular and general precipitation were determined. The curves, shown in Figures 24 and 25, were determined by light microscopy using an 80X oil immersion lens with a numerical aperture of 1.40. The start of both the cellular and the general reactions at a given temperature was established by bracketing the start of the particular reaction between two times. At the shorter of the two aging times no precipitate had yet appeared, while after aging for the longer period the reaction product had just become visible. When the interval

between the two aging times became small with respect to the total aging time, it was taken to describe the start of the reaction.

For quenched and aged alloys Figure 24 shows that the curve for the start of general precipitation lies at higher temperatures and longer aging times than that for cellular precipitation. This indicates that the initial development of cells will not be affected by general precipitation. The observation of precipitate free zones in quenched and aged alloys confirms this conclusion. It must be noted, however, that electron microscopy observations have shown that general precipitate nucleates after only a few seconds at aging temperatures above 250°C rather than after the times shown in Figure 24. Nevertheless, the effect of these precipitates on cellular precipitation does not seem to be appreciable until they have grown to a size visible by light microscopy. This conclusion is confirmed by comparing the general precipitate curve in Figure 24 with the solute depletion curve shown in Figure 16.

A comparison of Figures 24 and 25 shows that the curves for the start of cellular precipitation are similar, indicating that the mode of heat treatment does not affect the early stages of the cellular reaction and that both types of heat treatment can be used for the study of the early stage cellular morphologies. Light microscopy observations of grain boundary morphologies formed during both types of heat treatments confirm this conclusion.

In the course of the determination of these curves, the following observations concerning the subsequent early stage morphological studies were made. Light microscopy observations must be limited to above 400°C because grain boundary and lamellar structures become

unresolvable below this temperature. Hot stage light microscopy is precluded because these observations are limited to low magnification objectives with low resolving power.

Finally, it should be noted from both diagrams that cellular precipitation ceases to occur at temperatures above 0.9 of the absolute solvus temperature in agreement with the observations of Böhm.[5]

C. The Genesis of Cellular Precipitation

1. Light Microscopy

Because morphological studies by light microscopy were limited to aging temperatures above 400°C and because cellular precipitation ceased above about 450°C, investigations of the development of grain boundary and cellular morphologies by the sequential heat treatment technique described in Section IV. E. were performed at about 420°C. Figures 26 and 29 show the development of cellular and grain boundary structures revealed by this technique in quenched and aged alloys, whereas Figures 27 and 28 show the development in isothermally aged alloys.

The sequence in Figure 26 shows that the final cellular structure initiates from the grain boundary allotriomorphs shown in a, which appear to have a crystallographic relationship and habit with one of the two grains. This habit could be the (113) habit found for a grain boundary allotriomorph by trace analysis in Appendix B; however, no direct evidence of this could be obtained for these photomicrographs. With time the boundary between these allotriomorphs is seen to migrate

downward between the allotriomorphs as shown in b. As it migrates new precipitate appears to nucleate independently of the original allotriomorphs in the advancing interface as seen at A. At c the boundary has migrated to the tips of the original allotriomorphs. From here it continues to migrate into the lower grain to eventually form the structure in e. This sequence of events seems to give some credence to the crystallographic approach of Tu and Turnbull described in Section II. D.; however, it must be noted that the final structure in e seems to degenerate from the initial crystallographic habit of a.

In contrast to these observations, Figure 27 shows the relative unimportance of the initial allotriomorph crystallography in determining the final cellular structure. As seen in a of this figure the initial precipitate morphology consists of allotriomorphs at A apparently having a habit in one of the grains and an irregular precipitate structure at B interacting with a boundary migrating into the top grain. As seen in the remaining photomicrographs of this sequence, cells never develop from the allotriomorphs at A while at B the grain boundary continues to migrate, interacting locally with the precipitate phase to eventually form the steady state structure shown in e.

Both Figures 28 and 29 again show cellular structures developing by the original grain boundary migrating and interacting locally with allotriomorphs to form the final cellular structure. In addition, at A in Figure 28, the interaction of the original boundary with the allotriomorphs at this early stage of precipitation shows that the boundary appears to bow out between the allotriomorphs toward the top grain. Indeed, as shown in the latter stages of the sequence, this area develops into a cell growing into the top grain. Similar but not

so dramatic observations of this bowing phenomena are seen at B in Figure 28 and along the entire boundary in Figure 29. Considering these and numerous other observations, the morphological developments shown in Figure 26 appears to result from a fortuitous sequence of events rather than from the direct influence of the crystallographic habit of the initial allotriomorphs.

From the above discussion of Figures 26 through 29 it can be concluded that cells in this alloy develop from an initially unoccupied grain boundary by the migration of this boundary from one grain into the other. As it migrates it interacts locally with grain boundary allotriomorphs, that have formed, to eventually form a steady state lamellar structure. The exact nature of this grain boundary-grain boundary allotriomorph interaction cannot be ascertained from the above observations; however, it can be said that the crystallographic nature of the initial allotriomorphs has little influence on the morphology of the final cellular structure in this alloy, in contrast to cellular precipitation in lead-tin alloys where a strong precipitate habit exists.

2. Electron Microscopy

After having established by light microscopy that cells develop by the local interaction of a migrating grain boundary with simultaneously forming grain boundary allotriomorphs, transmission electron microscopy of the early stages of cellular precipitation was utilized to study the details of the morphology of the grain boundary-grain boundary allotriomorph interaction and cell development.

Initially, the early stage grain boundary morphologies of alloys aged for times and temperatures in the vicinity of the cellular start curves of the time-temperature-transformation diagrams were examined. From this study a mechanism was established for the development of cellular structure from an initially unoccupied grain boundary by an interaction between the original grain boundary and simultaneously forming grain boundary allotriomorphs. This mechanism was found to be valid at all aging temperatures studied (300 to 440°C) with variations of behavior with temperature being of degree rather than type; i.e., the morphological details only changed in size with aging temperature. Once this mechanism for cell development had been established an attempt was made to observe the development of the cellular structure by hot stage microscopy.

Figures 30 through 39 show results representative of the early stage morphology study and Figures 40 and 41 show two possibilities for the development of cells from two different grain boundary allotriomorph structures. These two possibilities are presented to show that cells can develop from various initial grain boundary allotriomorph structures by the same general mechanism.

The development of the mechanism shown in Figures 40 and 41 can best be described by comparing the various steps in cell development shown in these figures with the early stage morphologies shown in Figures 30 through 39. Accordingly, both Figures 40 and 41 show that cell development from an initially unoccupied grain boundary at (1) begins by the formation of grain boundary allotriomorphs at (2). In Figure 40 these have no crystallographic relation with either grain while in Figure 41 a habit is established between the precipitate and

the left grain. As precipitation continues the grain boundary begins to bow out between the allotriomorphs. This is shown clearly in Figures 30 and 31 where the boundary has just started to bow between the allotriomorphs at A in the direction shown by the arrow. The flat facets on the precipitates in Figure 31 indicate that they may have a habit in the left grain.

With time these boundaries continue to bow, as shown in Figures 32 and 33, depleting the area behind them of solute by boundary segregation of solute to the allotriomorphs, whose size consequently increases. This corresponds roughly to step (3) in Figures 40 and 41.

Now, having developed a driving force from the depletion of solute behind it, the bowing boundary continues to migrate, forming a trail of precipitate which acts as sink for the solute segregating in the advancing interface. The development of the trailing precipitate is clearly seen at A in Figure 34, and the characteristic "U" and "L" shaped morphologies resulting from the migration of the bowing boundary are shown in Figures 35 through 37. Step (4) in both Figures 40 and 41 corresponds to this stage of cellular development.

As the boundary continues to migrate the trailing precipitate can branch or new precipitate can nucleate at the advancing interface, as described in Section V. A. 3. and as shown at B in Figure 39, to eventually develop a steady state lamellar structure. This is depicted in step (5) of Figure 40.

To understand how the "U" shaped allotriomorph morphologies, shown best at A in Figure 36, can develop into cellular lamellae, the migration of the advancing interface must be considered in three dimensions as shown in step (5) of Figure 41. Accordingly, the boundary

migration required to transform the solid solution within the "U" shaped allotriomorph results from that portion of the boundary above or below the plane of observation. That such morphologies can develop is clearly shown at B in Figure 39.

Additional morphological features observed in the early stages of precipitation are shown in Figure 38. Here, precipitate having a (113) habit in the left grain is seen to form at the advancing α/α' interface giving rise to "U" shaped structures within the cell as depicted in steps (5) and (6) in Figure 41. (111) twins are also observed to form at the advancing interface as shown at A in Figure 38 and depicted in steps (5) and (6) in Figure 41. Presumably, these twins are formed as accidents of growth.

Having established the mechanism described in Figures 40 and 41 for the development of cellular structure, an attempt was made to observe the development of cells by hot stage transmission electron microscopy in order to confirm the above observations. Hot stage observations were limited to boundaries that were partially precipitated rather than those free of precipitate because the chance of picking a potentially active boundary from among the unreacted boundaries in the solution treated condition was small.

Figure 42 shows the development of cellular structure from such a partially precipitated boundary while the specimen was held at about 350°C in the electron microscope hot stage. At A in Figure 42a an early stage of cellular structure has developed during conventional aging at 366°C while at B the original boundary remains unoccupied.

After aging for 14 minutes at about 350°C in the hot stage,* the advancing interface at A in 42b is seen to have migrated forward about 0.2μ leaving a trail of precipitate to the initial lamellae. At B in Figure 42b the initially unoccupied grain boundary is seen to have migrated forward by bowing between faintly visible, simultaneously forming grain boundary allotriomorphs at C. With increasing aging time the interfaces at A and B continue to migrate, as shown in 42c; however, the structure behind the advancing interface becomes cloudy; and with further aging these cloudy areas, which appear to be surface precipitate, migrate over the surface, depleting the thin foil sample of solute and stopping the cellular reaction. These surface precipitates formed during all hot stage studies and, thus, precluded the observation of the development of a complete cell by this technique; however, the results shown in Figure 42 seem to confirm the earlier random observations.

From the above discussion of the morphological development of cellular structures it can be concluded that cells form from initially unoccupied grain boundaries by the boundary bowing out between simultaneously forming grain boundary allotriomorphs. As the boundary bows it depletes the region behind it of solute by solute partitioning in the advancing α/α' interface. The solute segregating in the advancing interface accumulates on the initial allotriomorphs to eventually form trailing precipitates behind the advancing α/α'

---

*This 14 minutes includes a heating time of about 10 minutes that was required for the specimen to attain the aging temperature from room temperature.

boundary. These trailing precipitates then branch or new precipitates nucleate in the advancing interface to form the final steady state lamellar structure. Crystallographic relationships between initial allotriomorphs and adjacent grains seem to have a minimal influence on the final cell structure.

D. The Cause of Cellular Precipitation

Having established that cellular precipitation occurs by a boundary bowing out between simultaneously forming grain boundary allotriomorphs and trailing precipitate behind as it migrates, the problem of establishing a cause for the reaction becomes one of determining why the boundary bows and, further, why it bows in a particular direction.

1. The Influence of Grain Boundary Migration Reactions Occurring Simultaneously With Cellular Precipitation

At the aging temperatures used in this investigation, grain boundary migration resulting in grain growth would be expected to occur in this alloy in the absence of precipitation. In addition, in the absence of precipitation, strain induced boundary migration would also be expected to occur in a deformed alloy at these temperatures. However, as precipitation at the grain boundaries does occur, these phenomena are not observed. Nevertheless, they should be expected to have an influence on boundary migration prior to the formation of the first grain boundary allotriomorphs. Therefore, a study of the direction of cellular growth from boundaries whose direction of migration in the absence of precipitation could be predicted by

existing grain boundary migration theories was undertaken.

Initially, the direction of cellular growth was followed in undeformed alloys at those boundaries whose direction of migration could be predicted by grain growth theories. This limited the observations to highly curved boundaries where growth would be expected toward the center of curvature. Figure 43 shows the development of cellular precipitation at such a curved boundary on a small appendage of a large grain. As can be seen the cellular growth direction is the same as the expected direction of boundary migration shown by the arrows.

Similar cell growth behavior is shown in Figure 44. Here a small triangular grain is apparently being consumed by the much larger grains surrounding it in accordance with grain coalescence theory.[42] Cell growth is again in the same direction as the expected direction of grain boundary migration as shown by the arrows. This behavior was found to be characteristic of most of the highly curved boundaries and small triangular grains observed; however, precipitation at the more gently curved large grain boundaries was found to be erratic.

To study the direction of cellular growth at a boundary initially migrating into a deformed matrix, thermo-mechanical treatments such as that described in the caption of Figure 45 were developed to produce partially recrystallized and aged structures such as that shown in this figure. The structure of this partially recrystallized and aged alloy is seen to consist of areas of recrystallized grains (A), partially recovered original grains (B), and occasionally, an individual recrystallized grain growing in one of the original grains (C).

To study cellular growth at a boundary migrating into a deformed matrix the precipitation behavior at the individual recrystallized grains was examined. Accordingly, Figure 46 shows a small recrystallized grain (A), that had initially formed in a deformed grain (B) during the 10 second solution treatment at 625°C, after aging for 15 minutes at 420°C. As can be seen the cellular structures formed during aging are growing outward into the deformed grain in the same direction as the initial grain boundary would be expected to be migrating. Figure 47 shows cellular precipitation occurring at a boundary initially migrating by strain induced boundary migration. Again the cellular growth is away from the newly recrystallized region (A) into the deformed region (B). The similarity between this structure, resulting from strain induced boundary migration and cellular precipitation, and the combined observations of Smith,[54] and Beck and Sperry[4] in Figures 3 and 5, respectively, should be noted. Examination of precipitation behavior at numerous individual recrystallized grains have shown this behavior to be consistent; however, it must be noted that, after long recrystallization anneals at the solution treatment temperature, the initially deformed grains may recover sufficiently to stop the growth of the new grains and make the above observations erratic.

The above observations of the effect of simultaneously occurring grain boundary migration reactions on the development of cellular structures can be explained as follows with reference to Figure 48, a schematic diagram of the development of cellular structure from an initially unoccupied grain boundary. Initially, the grain boundary at (1) in Figure 48 will be subject to the ordinary forces of boundary

migration associated with a single phase alloy and will start to migrate accordingly, in this case to the right. However, after moving a short distance, Δ, as shown at (2), allotriomorphs begin to form, pinning the boundary. Assuming that the narrow region, Δ, behind the migrating boundary was depleted of solute by boundary diffusion of solute to the newly forming allotriomorphs, the boundary now has a thermodynamic incentive to continue moving to the right and; thus, it bows out between the pinning precipitates, continuing to deplete the area behind it of solute. The cellular structure then develops as described in Section V. C. 2. and illustrated in Figures 40 and 41.

2. The Driving Force for Cell Initiation

Having established the influence of initial grain boundary migration behavior on the direction of cellular growth, a driving force for the genesis of cellular precipitation at an initially unoccupied grain boundary, consistent with this influence, can now be described in terms of accepted grain growth and recrystallization theories; and a general relationship between this initial driving force and the final steady state driving force for cellular precipitation can be discussed in terms of the individual contributions of chemical free energy, α/α' surface energy, α/β surface energy and matrix strain energy to the net free energy change accompanying the reaction.

In general, the net free energy change, ΔF, for the transformation of one mole of supersaturated solid solution by cellular precipitation to depleted solid solution and precipitate phase can be given by

$$\Delta F = a\Delta F_o + b\sigma_{\alpha/\beta}V + \frac{\sigma_{\alpha/\alpha'}V}{r} + Z(t), \qquad (29)$$

where ΔF_o, $\sigma_{\alpha/\beta}$, $\sigma_{\alpha/\alpha'}$, V and r are defined in Table II and Figure 7. The first term in this equation, $a\Delta F_o$, is the chemical free energy released during the reaction, where a is the fraction of the total free energy, ΔF_o, available for the reaction. The second term, $b\sigma_{\alpha/\beta}V$, is that portion of the chemical free energy converted to α/β surface energy during precipitation, where b is a dimensional term that is dependent on the size and shape of the precipitate phase. $\sigma_{\alpha/\alpha'}V/r$, the third term, is that portion of ΔF associated with the curvature of the α/α' interface, and the last term, Z(t), is any strain energy (stored energy of cold work) associated with the α' matrix phase. The contribution of the curvature of the α'/β interface has been neglected here. For the case of cellular growth into an undeformed matrix, Z(t)=0, and Equation 29 becomes

$$\Delta F = a\Delta F_o + b\sigma_{\alpha/\alpha'}V + \frac{\sigma_{\alpha/\alpha'}V}{r} . \qquad (30)$$

With reference to step (1) in Figure 48 and the conclusions of Section V. D. 1., the driving force for boundary migration at the start of aging in an undeformed alloy results solely from the curvature of the α'/α' grain boundary in accordance with the theory of grain growth. If the surface energy of the original grain boundary is assumed to be identical with that of the advancing α/α' interface of a cell, this driving force can be given by

$$\Delta F = \frac{\sigma_{\alpha/\alpha'}V}{r} . \qquad (31)$$

As the boundary migrates it depletes the area behind it of solute, and allotriomorphs begin to form along it as shown in step (2) in Figure 48. During this stage of cell development the first two terms of

Equation 30 increase from zero to some finite value depending on the extent of solute depletion behind the boundary and the shape of the initial precipitate allotriomorphs. As aging continues, the boundary bows out between the allotriomorphs, continuing to deplete the area behind it of solute, and a cell develops as described previously. Once a steady state of growth is attained, a = P and b = 2/S according to Cahn's growth theory,[12] and ΔF assumes its steady state value of

$$\Delta F = P\Delta F_o + \frac{2\sigma_{\alpha/\beta}V}{S} + \frac{\sigma_{\alpha/\alpha'}V}{r} . \qquad (32)$$

In general, the transition of the driving force from the grain boundary migration force acting on the boundary at t = 0 to the steady state driving force for cellular precipitation can be shown schematically as in Figure 49. Here the individual terms of Equation 30 and the resultant ΔF are shown developing as functions of aging time. The transition of the terms from their initial values to their steady state values is shown by broken lines as no attempt was made to describe their behavior in this region.

The initial and final values of the individual terms in Figure 49 were determined for precipitation in the Cu-9.5at.%In alloy aged at 420°C. The product, $P\Delta F_o$, was calculated from Equation 7 in Section II. B. 2. using X_α in place of $X_{\alpha e}$ rather than be determining P and ΔF_o separately. The values of X_α, $\sigma_{\alpha/\beta}$ and S were obtained from the work of Shapiro[50] to be 0.042, 400 ergs/cm.^{2} and 0.21μ respectively, while $\sigma_{\alpha/\alpha'}$ was assumed to be 650 ergs/cm.^{2}, the same as that for pure copper.[18] The molar volume, V, was found to be 7.36 cm.^{3}/mole for both the α' and the cellular aggregate. The steady state radius of curvature of the α/α' interface, r, was obtained from the α/α'

interface in Figure 22, while the initial radius of curvature of the original grain boundary was obtained from Figure 43a. The values of the individual terms calculated from these quantities are shown in Figure 49 along with the resultant value of ΔF.

From this figure it can be seen that ΔF transforms from an initial value of -0.02 cal./mole, resulting from the curvature of the original boundary, to a final value of -25.3 cal./mole, after a steady state is attained. Clearly, the contribution of the original boundary curvature is small but it does provide a driving force that starts the reaction in a particular direction.

For the case of cellular precipitation in a deformed matrix, as shown in Figures 46 and 47, the influence of the stored energy of deformation, Z(t), must be considered in the expression for ΔF. In general, Z(t) is a function of time, as recovery processes are occurring in the deformed matrix simultaneously with precipitation. According to Li[34] the release of stored energy during recovery can be described by

$$1/Z(t) = 1/Z_o + k_R t, \tag{33}$$

where Z_o is the stored energy of cold work at the start of aging and k_R is a function of temperature.

Assuming that the values of the other terms are not affected by growth into a deformed matrix a quasi steady state expression for ΔF is obtained from Equation 29 to be

$$\Delta F = P\Delta F_o + \frac{2\sigma_{\alpha/\beta}V}{S} + \frac{\sigma_{\alpha/\alpha'}V}{r} + Z(t) , \tag{34}$$

where Z(t) is given by Equation 33; while, at the start of aging, the driving force acting on the boundary between an undeformed and a

deformed region is given by

$$\Delta F = \frac{\sigma_{\alpha/\alpha'} V}{r} + Z_o \quad . \tag{35}$$

Assuming an initial value of 4 cal./mole for Z_o[3] and the same values of the other terms obtained previously for precipitation in Cu-9.5at.%In at 420°C, the transition of ΔF from its value at the start or aging to its value at the quasi steady state is shown schematically in Figure 50. According to this diagram, ΔF increases to a maximum from its initial value given by Equation 35 and then declines asymptotically to the steady state value of ΔF given in Figure 49 as Z(t) decreases monotonically to zero. Clearly, a strong initial driving force exists here for the start of cellular growth into a cold worked matrix.

From the above discussion it can be concluded that a driving force for boundary migration does exist at the original grain boundary at the start of aging and that this driving force aids in starting cellular growth. As the cell develops, the free energy change accompanying the development of the cell transforms from a value characteristic of the original boundary to a value characteristic of a steady state reaction. The exact nature of this transformation is not known but will probably vary from one boundary to another because of the various initial grain boundary allotriomorph morphologies.

3. The Criterion for the Occurrence of Cellular Precipitation

In previous sections, a mechanism for the development of cellular structure from original, unreacted grain boundaries was established; the influence of simultaneously occurring boundary migration reactions

on the initiation of cellular precipitation was determined; and a driving force for cell initiation consistent with these observations, was identified. In this section, a criterion for the occurrence of cellular precipitation, based on these previously described concepts, is developed. A study of the sequence of events in the development of cellular structure, shown schematically in Figure 48, indicates that a critical requirement for the formation of a cell is that the boundary must be able to bow between two pinning allotriomorphs to a sufficient size to supply them with enough solute for them to grow and eventually develop a steady state growth structure. From this observation, it seems that the problem of determining a criterion for the occurrence of cellular precipitation reduces to establishing the necessary conditions for the boundary to bow to some "critical" size. From Figure 48 it can be seen that the quantities involved in this problem are (1) the initial allotriomorph spacing, 2L; (2) the α/α' surface energy, $\sigma_{\alpha/\alpha'}$; (3) the fraction of chemical free energy released by the depletion of the area behind the bowing interface of solute, $P\Delta F_o$; and (4) the α/β surface energy, $\sigma_{\alpha/\beta}$.

Neglecting the contribution of $\sigma_{\alpha/\beta}$ to the net free energy change accompanying the formation of a bow and using an analysis similar to that used by Bailey[3] in his development of the "bulge" nucleation mechanism for recrystallization, a criterion for the boundary to bow beyond a certain "critical" size, can be established as follows. The net free energy change resulting from a small increase in the size of a bowing boundary is given by

$$\Delta F \cdot \delta V = P\Delta F_o \cdot \delta V + \sigma_{\alpha/\alpha'} V \cdot \delta A \ , \qquad (36)$$

where δA is a small increase in the surface area of the bow associated with a small increase in volume, δV. Clearly, for the boundary to continue bowing $\Delta F \cdot \delta V$ must be negative, and

$$P\Delta F_o \cdot \delta V + \sigma_{\alpha/\alpha'} V \cdot \delta A < 0 \quad \text{or} \quad \frac{P\Delta F_o}{\sigma_{\alpha/\alpha'} V} < - \frac{\delta A}{\delta V} . \tag{37}$$

Assuming, as shown at (3) in Figure 48, that the bow is a cylindrical cap of unit depth and radius $\underline{r}$, and that the initial allotriomorph spacing is $2L$, $\delta A/\delta V$ is given by

$$\frac{\delta A}{\delta V} = \frac{2 \sin \Theta}{L} . \tag{38}$$

Substituting this into (37), the requirement for the further development of the bow becomes

$$- \frac{P\Delta F_o}{\sigma_{\alpha/\alpha'} V} > \frac{2 \sin \Theta}{L} ; \tag{39}$$

or, noting that $r = L/\sin \Theta$,

$$- \frac{P\Delta F_o}{\sigma_{\alpha/\alpha'} V} > \frac{2}{r} . \tag{40}$$

Here we have the requirement for a bow to develop beyond a certain size in terms of its radius of curvature.

The maximum value of the right terms in (39) and (40) is set by the initial allotriomorph spacing to be $2/L$. Assuming that the bow must grow to a "critical" size corresponding to this maximum value for cellular precipitation to occur, the inequalities (39) and (40) become

$$- \frac{P\Delta F_o L}{\sigma_{\alpha/\alpha'} V} > 2 . \tag{41}$$

Here, based on the mechanism for the genesis of cellular precipitation developed in this investigation, a criterion for the occurrence of cellular precipitation has been determined in terms of four of the quantities associated with the early stages of grain boundary precipitation; namely, $P\Delta F_o$, $\sigma_{\alpha/\alpha'}$, V, and 2L. Unfortunately, insufficient experimental information on these quantities, principally interfacial energies, is available to test this criteria for its ability to predict the occurrence of cellular precipitation in various alloy systems. It should be noted, however, that the criterion correctly predicts the occurrence of cellular precipitation in Cu-9.5at.%In at 420°C, as a value of 14.1 was calculated for the left term in (41) using the same values for $\sigma_{\alpha/\alpha'}$, $P\Delta F_o$ and V used in Section V. D. 2. and a value of 1μ for 2L.

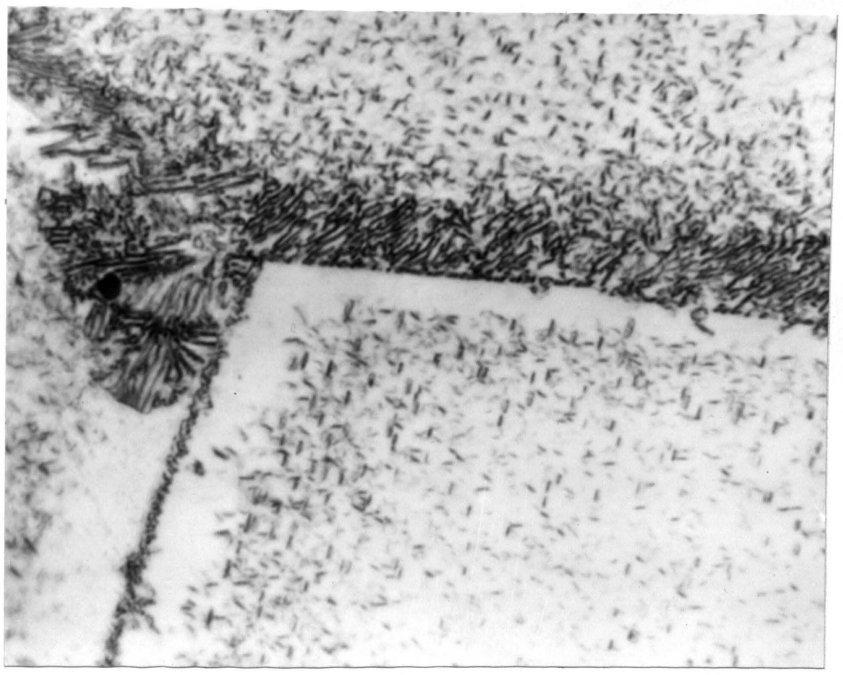

Figure 14. Cu-9.5at.%In, solution treated 2 hours at 625°C, water quenched and aged 60 minutes at 420°C. X1,900

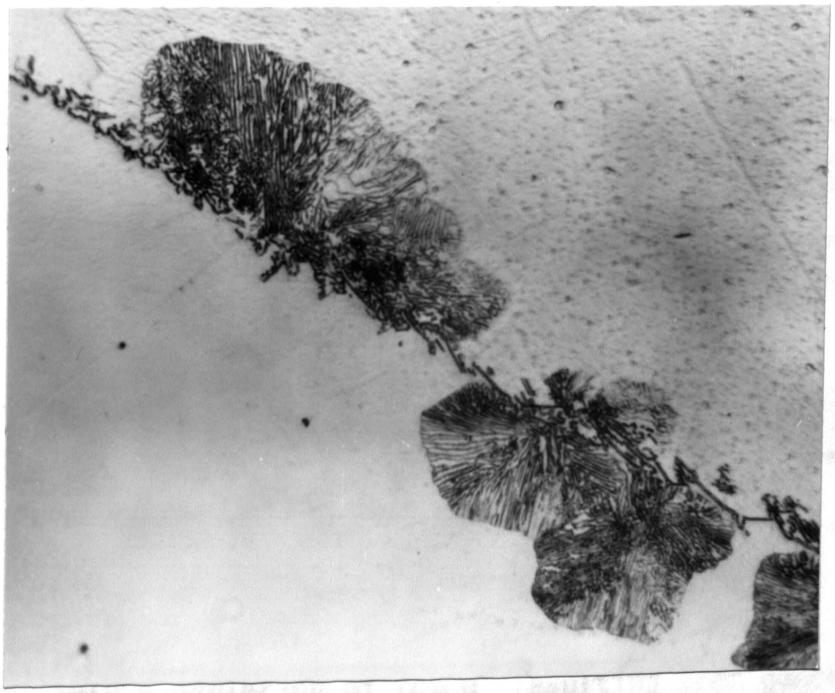

Figure 15. Cu-9.5at.%In, solution treated 2 hours at 625°C, isothermally aged 60 minutes at 420°C. X1,000

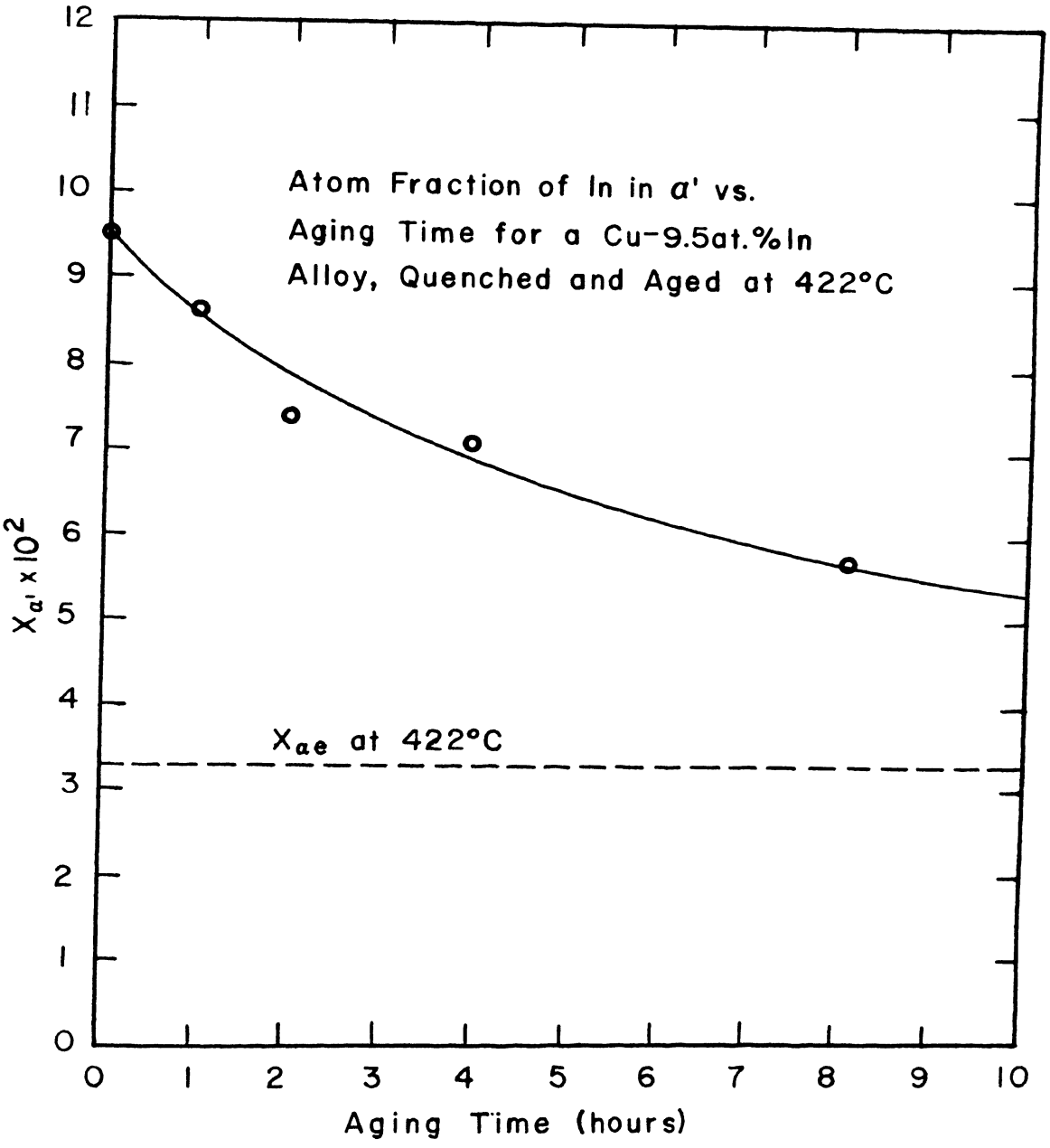

Figure 16. Solute depletion of the α' resulting from general precipitation during a quench and age heat treatment.

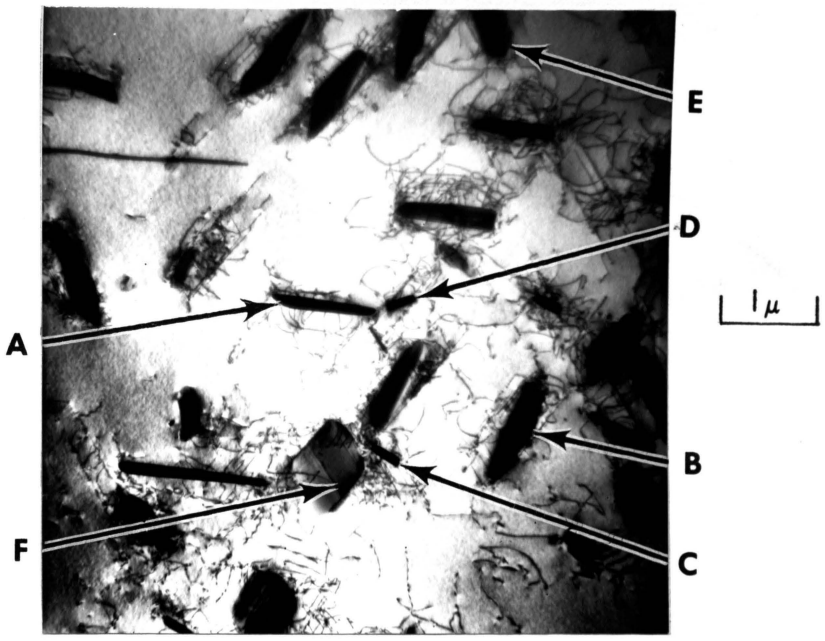

Figure 17. Cu-9.5at.%In, solution treated 5 minutes at 625°C, water quenched and aged 1 hour at 420°C. General precipitate. X12,500

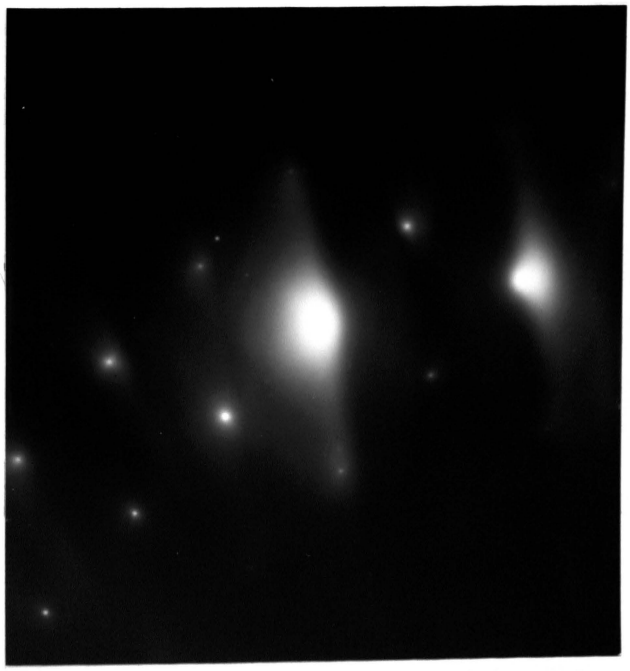

Figure 18. Selected area diffraction pattern of Figure 17. [110] zone of α'. ₀Rotated 15.5° counterclockwise from Figure 17. λl=3.45Acm.

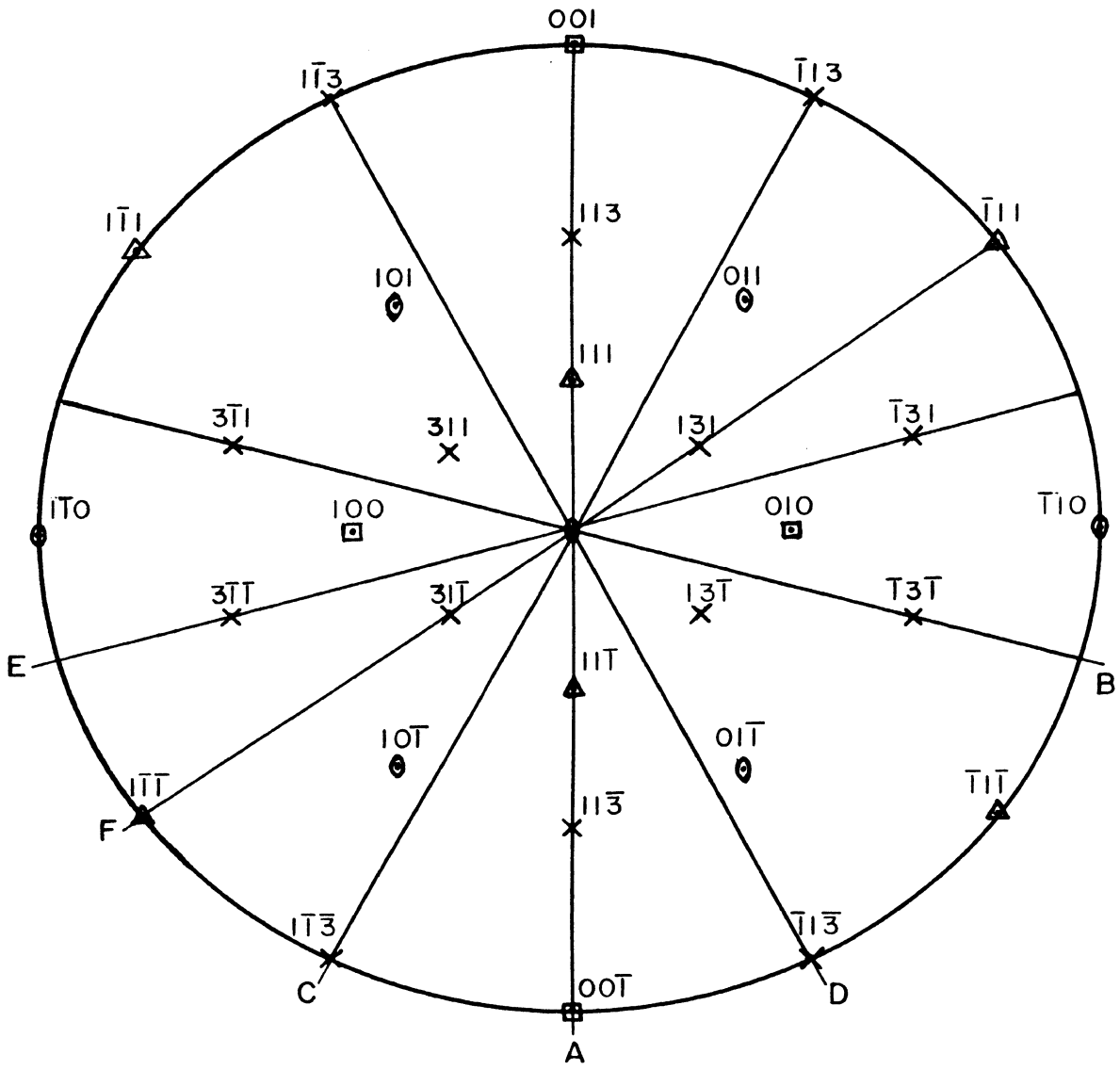

Figure 19. Stereographic projection of the [110] zone shown in Figure 18 showing the traces of the poles of the habit planes of the general precipitate in Figure 17.

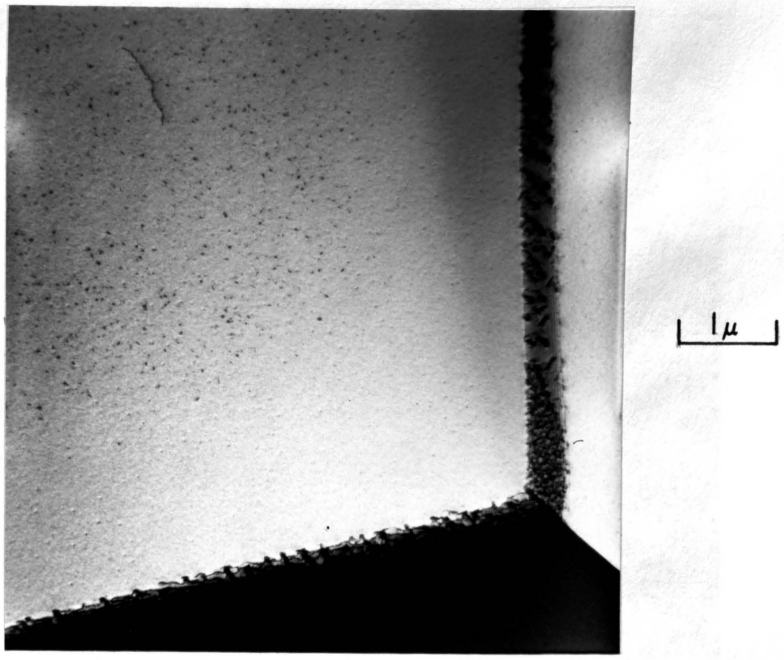

Figure 20. Cu-9.5at.%In, solution treated 5 minutes at 625°C, water quenched and aged 2 hours at 250°C. General precipitation near a grain boundary showing a precipitate free zone. X12,500

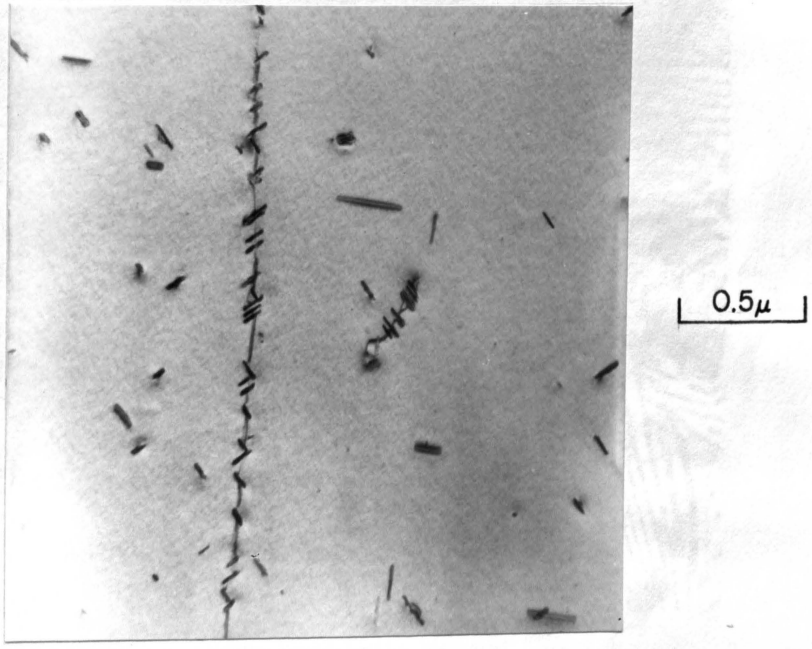

Figure 21. Cu-9.5at.%In, solution treated 5 minutes at 625°C water quenched and aged 1 minute at 322°C. General precipitate nucleating on dislocations. X32,500

Figure 22. Cu-9.5at.%In, solution treated 5 minutes at 625°C, water quenched and aged 15 minutes at 428°C. Cellular precipitate. X14,400

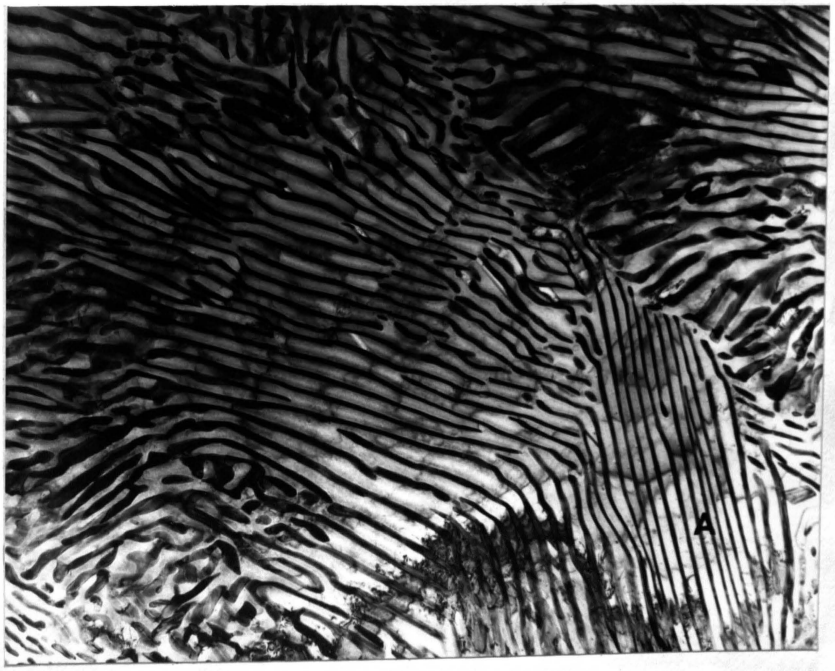

Figure 23. Cu-9.5at.%In, solution treated 5 minutes at 625°C, isothermally aged 2 hours at 366°C. Cellular colony. X13,000

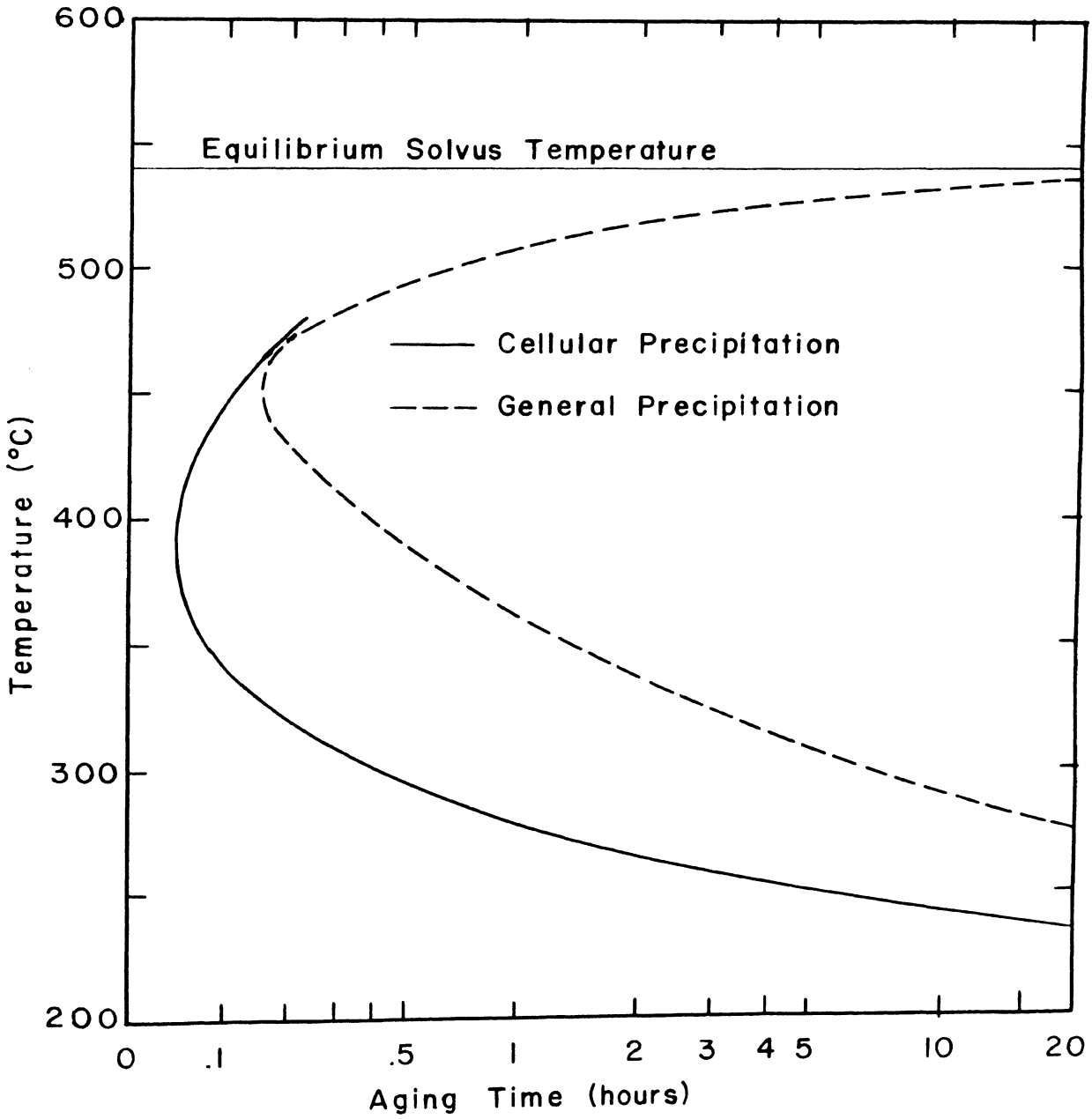

Figure 24. Time-Temperature-Transformation diagram for the start of cellular and general precipitation for quench and age heat treatments.

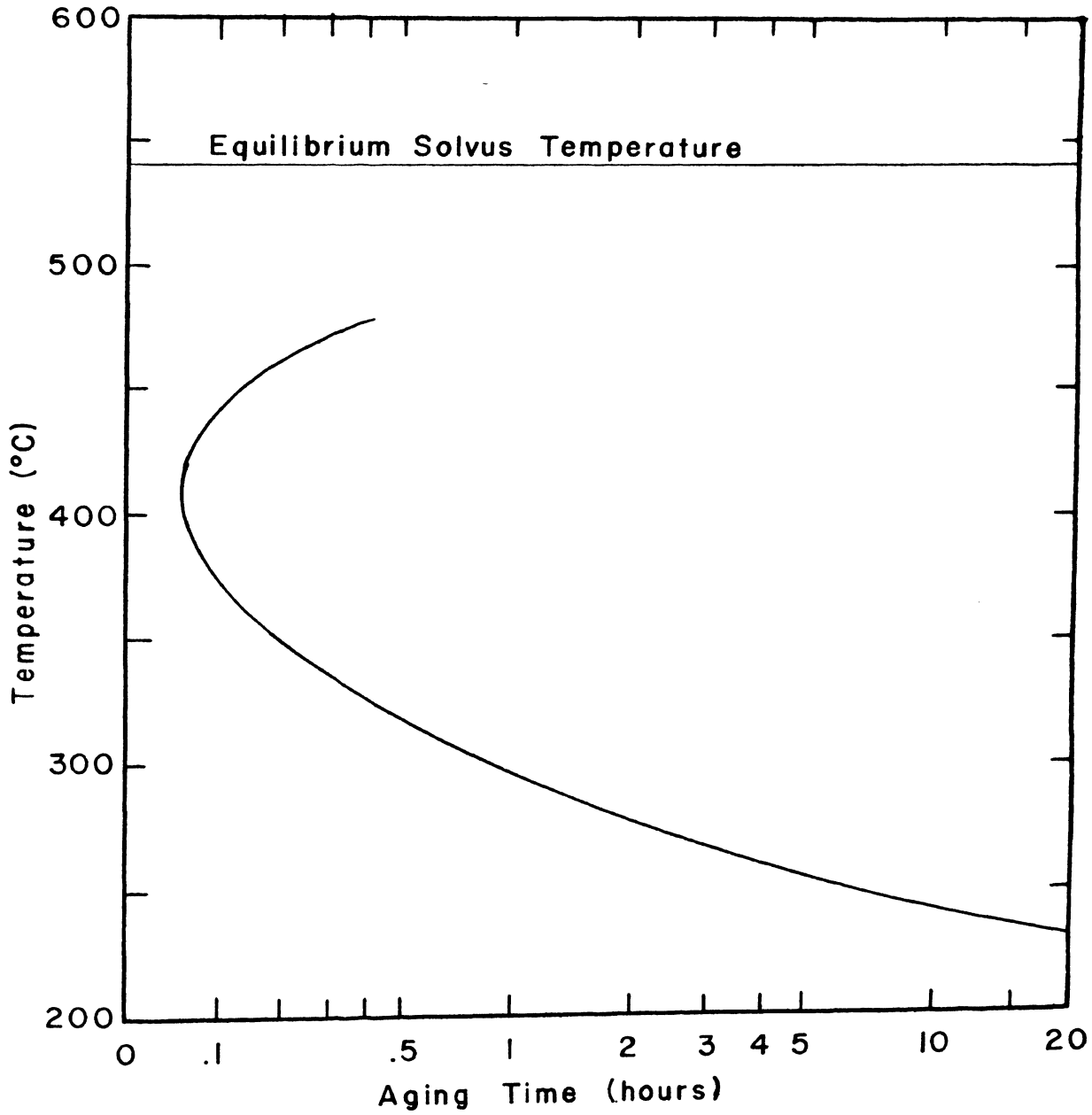

Figure 25. Time-Temperature-Transformation diagram for the start of cellular precipitation for isothermal aging heat treatments.

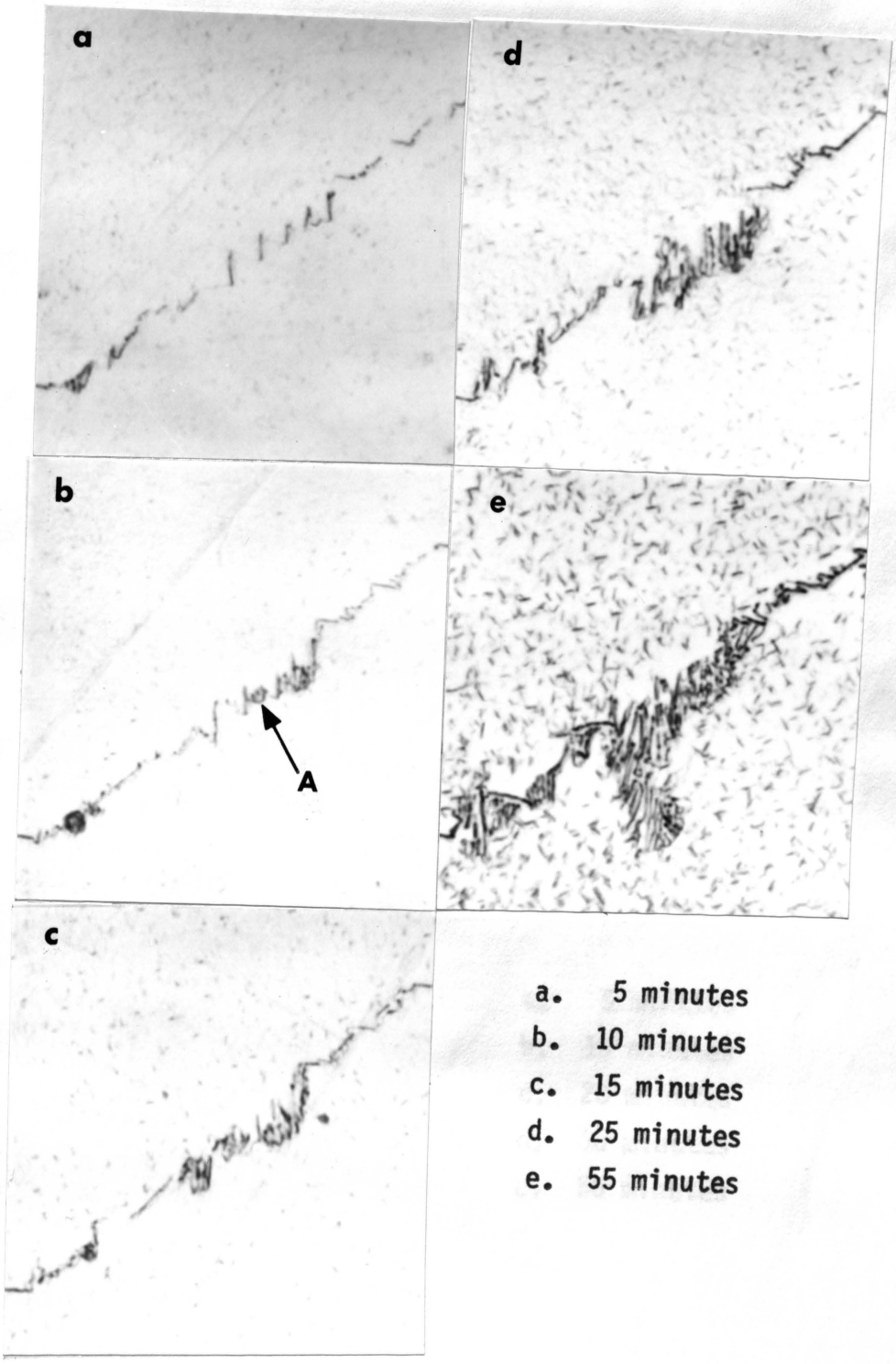

Figure 26. Cu-9.5at.%In, solution treated 2 hours at 625°C, water quenched and aged at 421°C for the times shown above. Sequential development of cellular precipitation in a quenched and aged alloy. X2,000

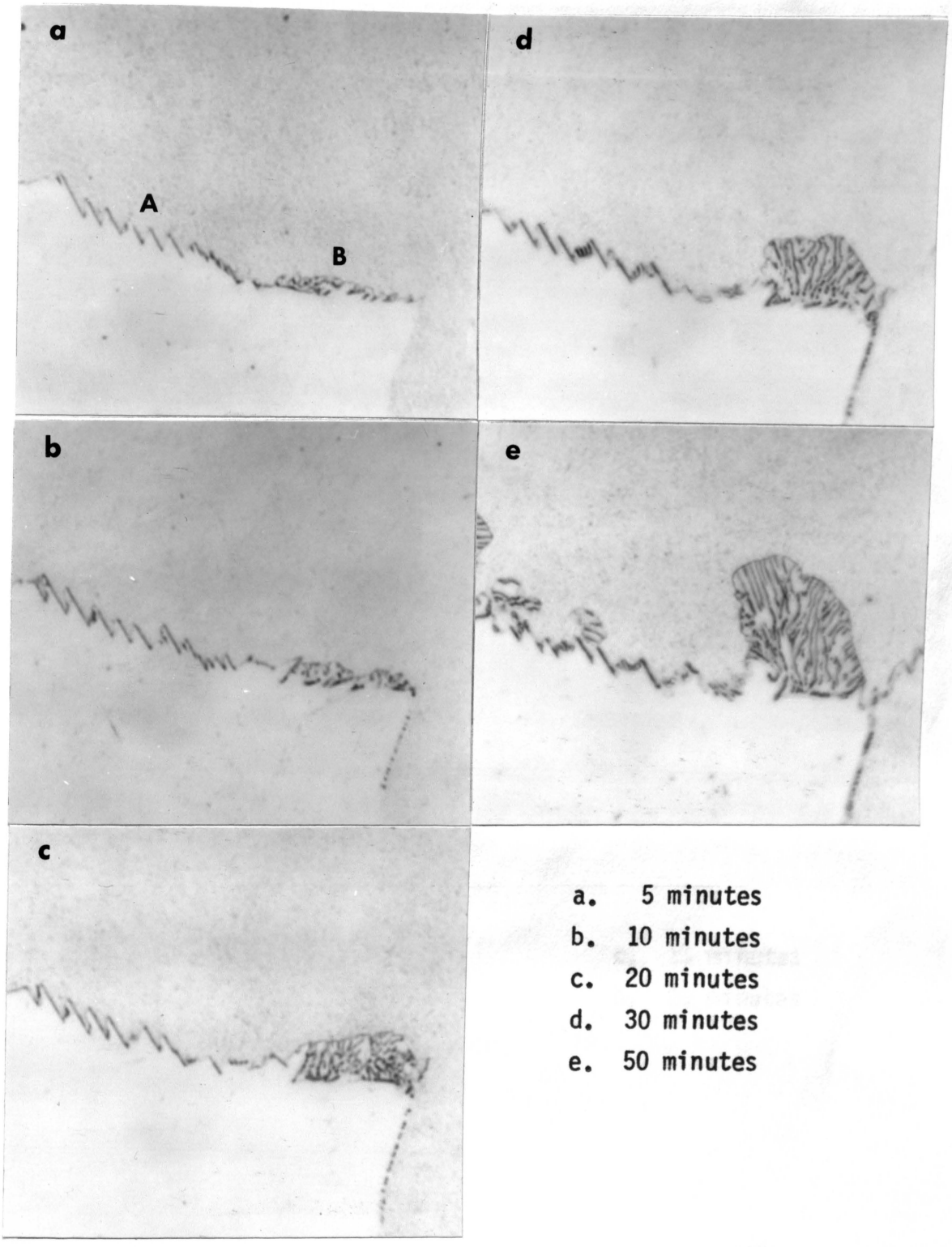

Figure 27. Cu-9.5at.%In, solution treated 2 hours at 625°C, isothermally aged at 425°C for the times shown above. Sequential development of cellular precipitation in an isothermally aged alloy. X2,000

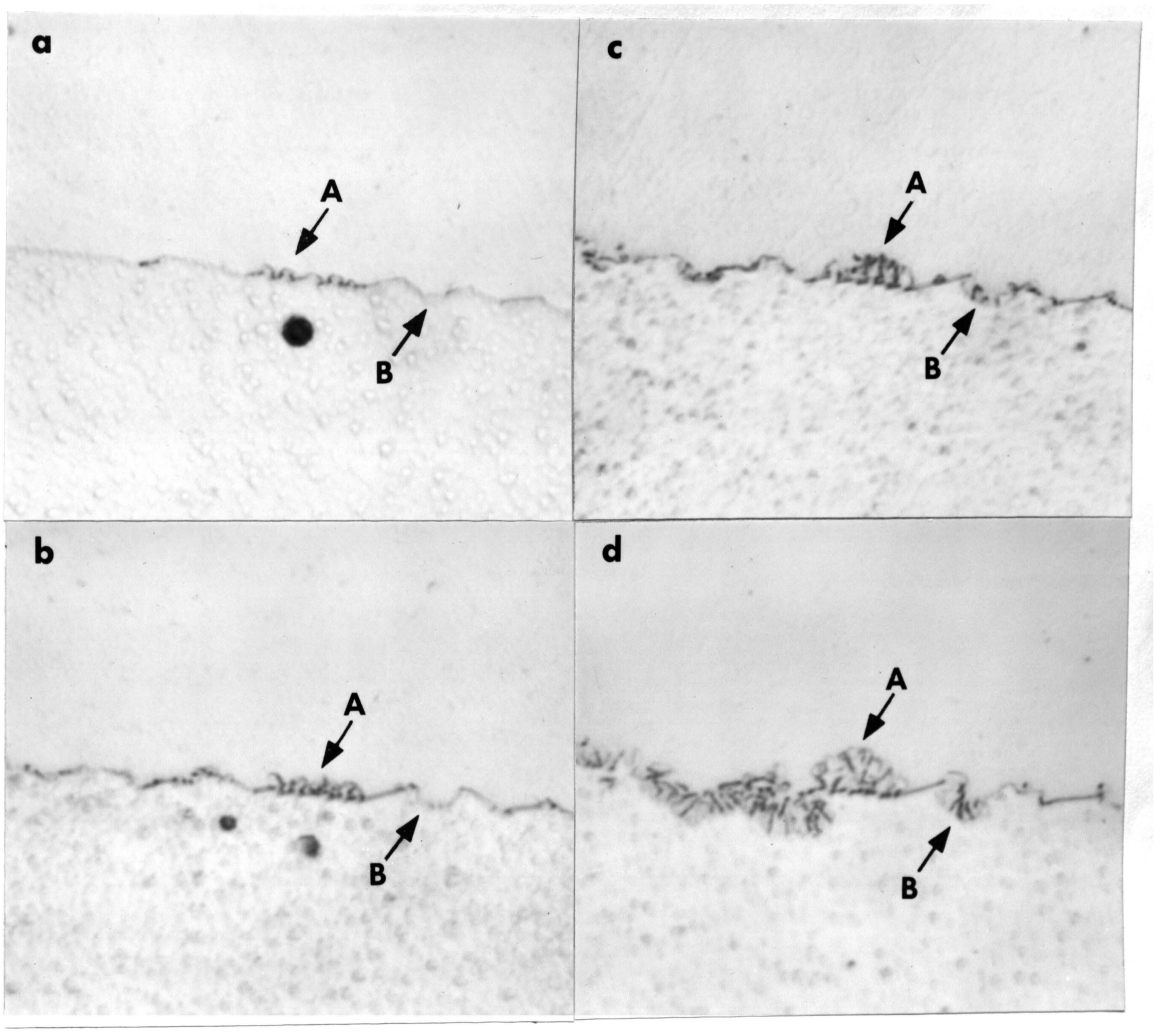

a. 5 minutes
b. 10 minutes
c. 15 minutes
d. 25 minutes

Figure 28. Cu-9.5at.%In, solution treated 2 hours at 625°C, isothermally aged at 425°C for the times shown above. Sequential development of cellular precipitation in an isothermally aged alloy. X2,000

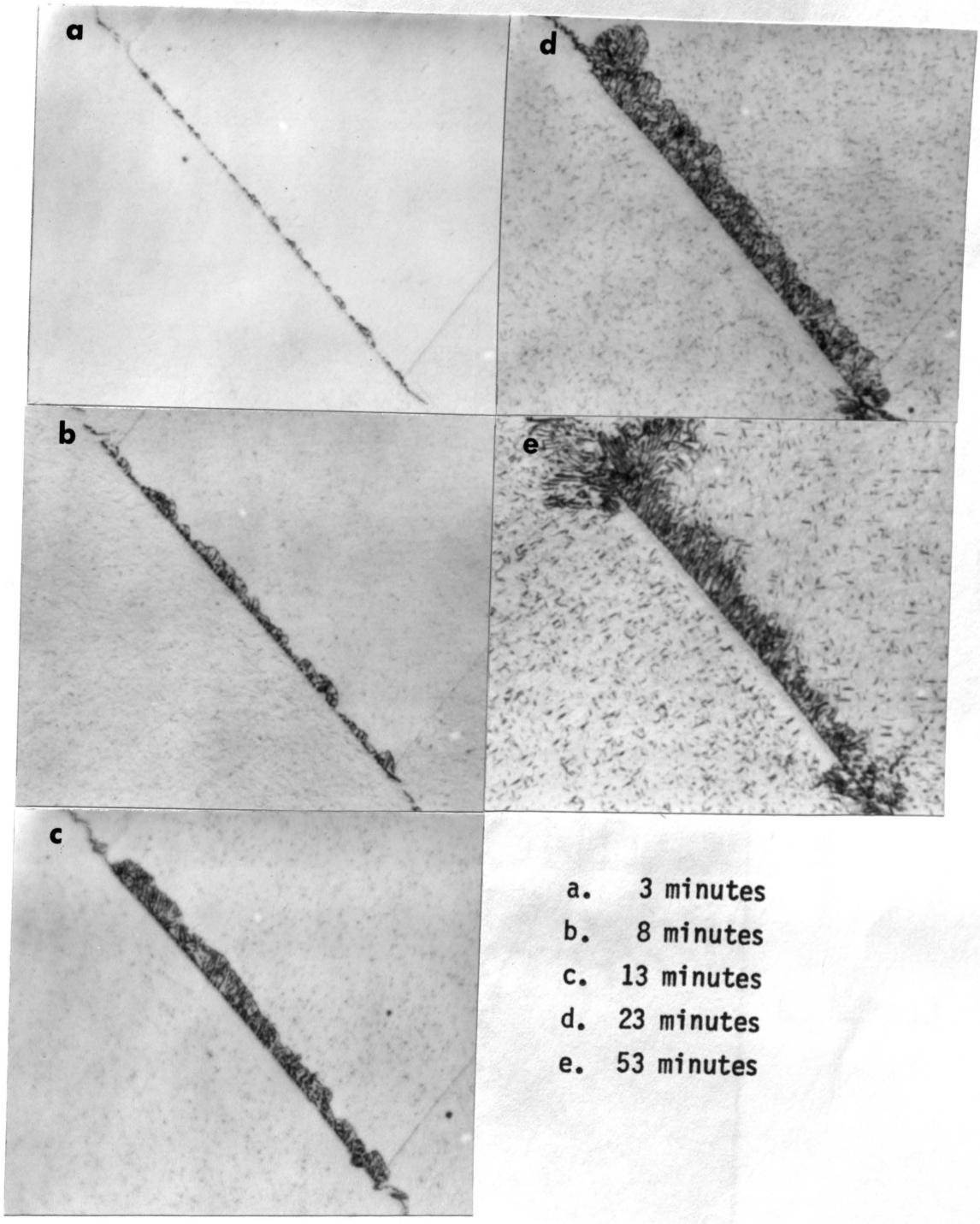

Figure 29. Cu-9.5at.%In, solution treated 2 hours at 625°C, water quenched and aged at 422°C for the times shown above. Sequential development of cellular precipitation in quenched and aged alloy. X1,500

Figure 30. Cu-9.5at.%In, solution treated 5 minutes at 625°C, water quenched and aged 1 minute at 365°C. Grain boundary starting to bow between simultaneously forming grain boundary allotriomorphs at A. X30,000

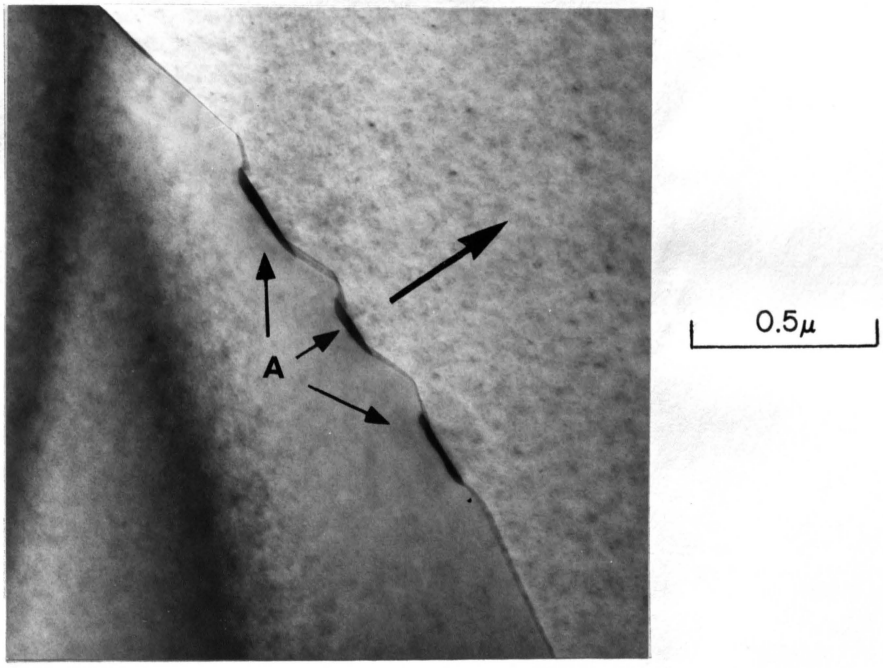

Figure 31. Cu-9.5at.%In, solution treated 5 minutes at 625°C, water quenched and aged 1 minute at 365°C. Grain boundary starting to bow between simultaneously forming grain boundary allotriomorphs at A. X46,800

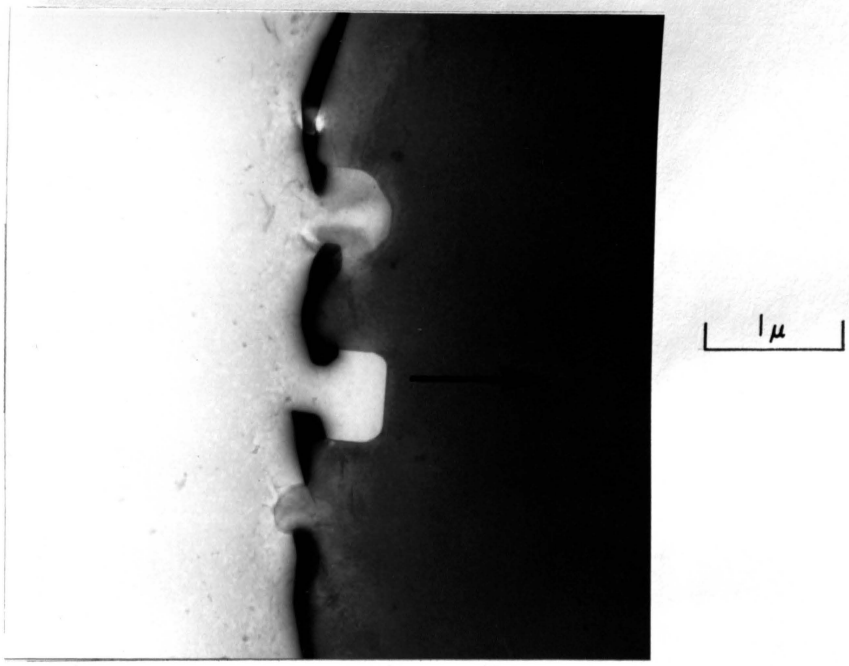

Figure 32. Cu-9.5at.%In, solution treated 5 minutes at 625°C, isothermally aged 15 minutes at 420°C. Grain boundary bowing between allotriomorphs. X17,500

Figure 33. Cu-9.5at.%In, solution treated 5 minutes at 625°C, isothermally aged 15 minutes at 420°C. Grain boundary bowing between allotriomorphs. X12,000

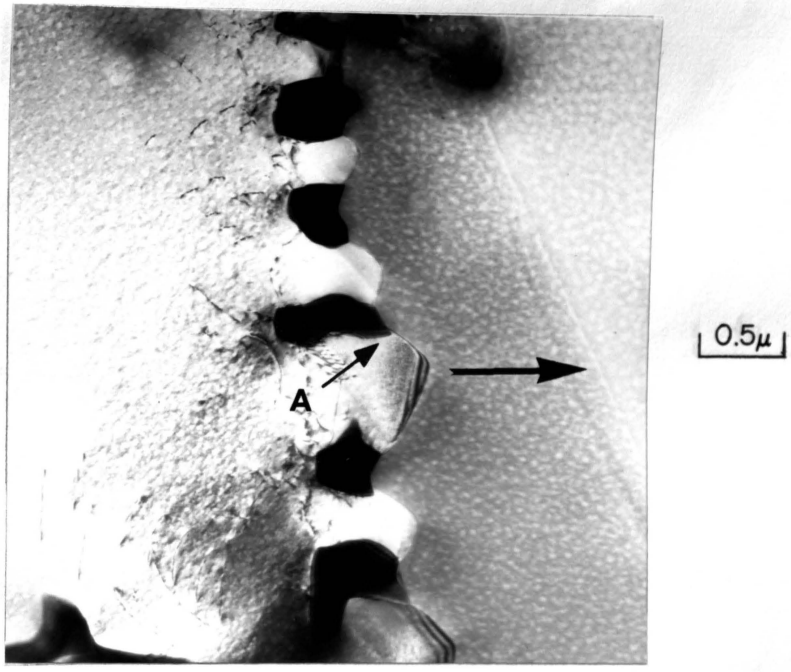

Figure 34. Cu-9.5at.%In, solution treated 5 minutes at 625°C, water quenched and aged 15 minutes at 420°C. Grain boundary bowing between allotriomorphs and trailing precipitate at A. X21,000

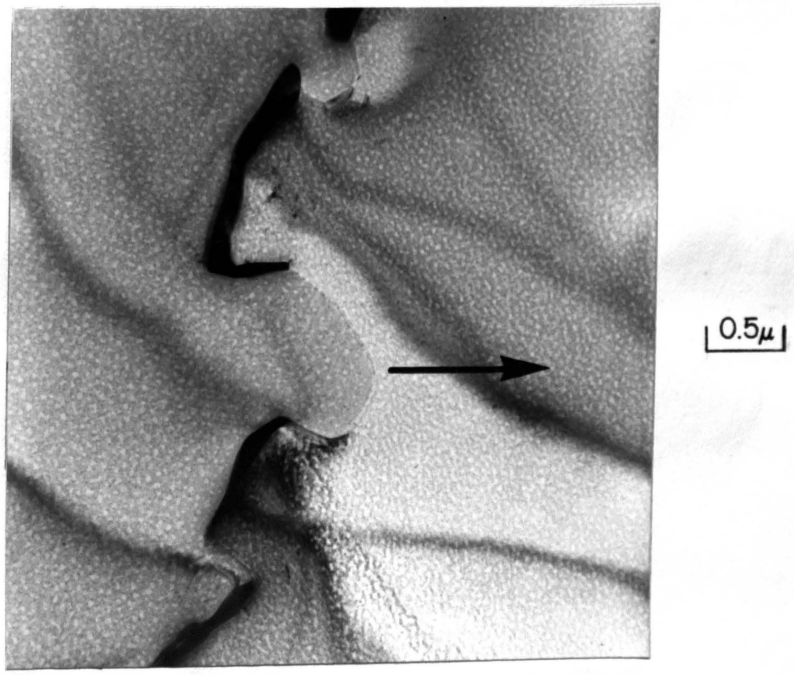

Figure 35. Cu-9.5at.%In, solution treated 5 minutes at 625°C, water quenched and aged 15 minutes at 420°C. Precipitate trailing behind a bowing boundary and forming "L" shaped allotriomorphs. X19,200

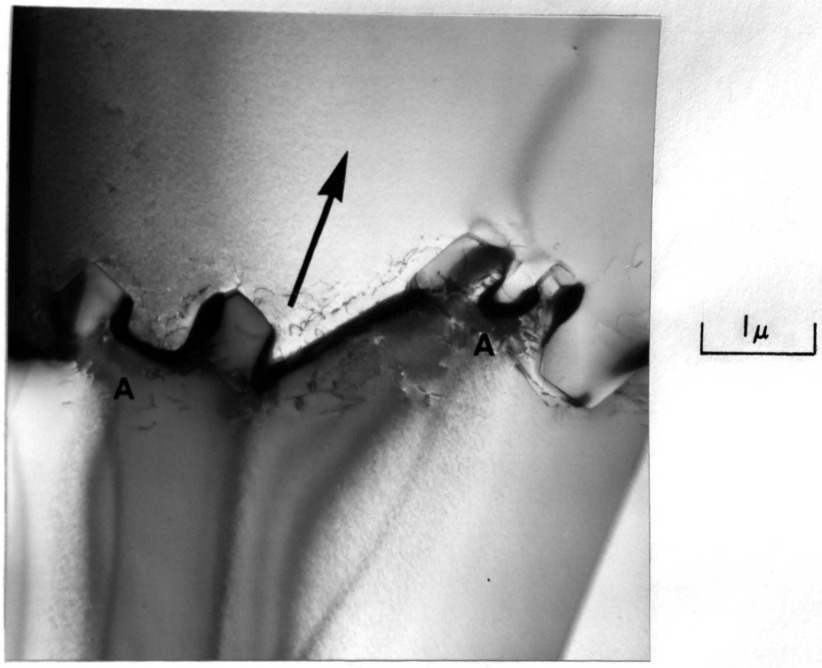

Figure 36. Cu-9.5at.%In, solution treated 5 minutes at 625°C, water quenched and aged 15 minutes at 428°C. Precipitate trailing behind a bowing boundary and forming "U" shaped allotriomorphs. X14,000

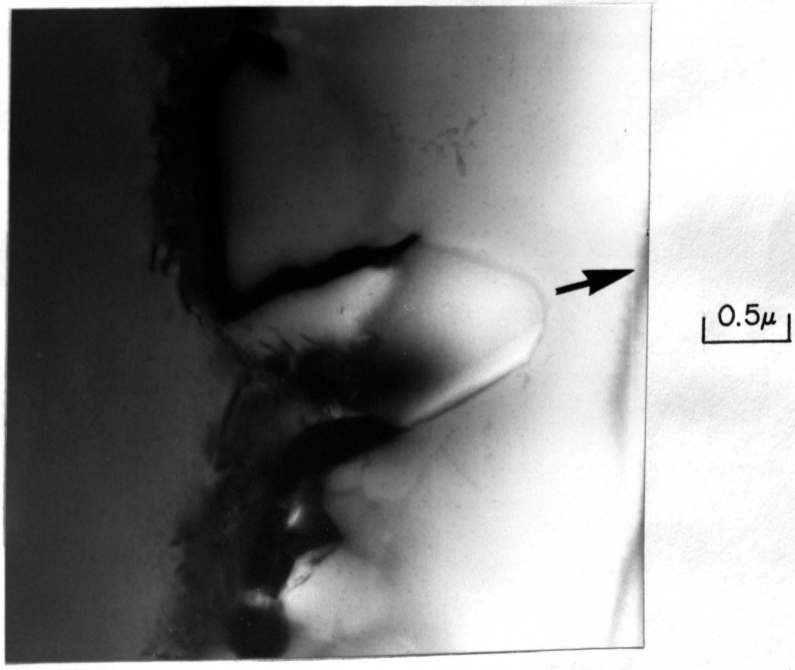

Figure 37. Cu-9.5at.%In, solution treated 5 minutes at 625°C, water quenched and aged 15 minutes at 420°C. Precipitate trailing behind a bowing boundary and forming "L" shaped allotriomorphs. X22,500

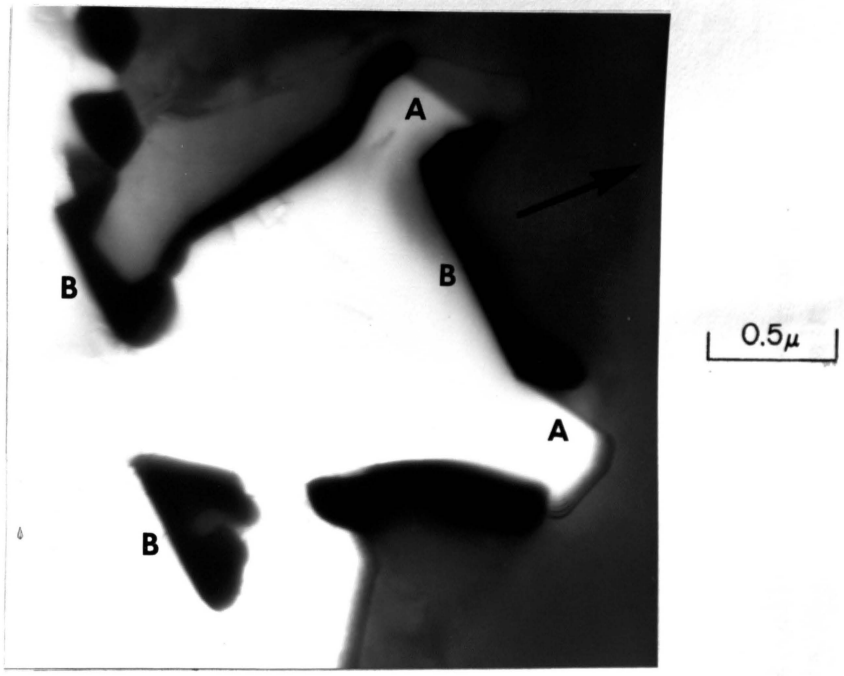

Figure 38. Cu-9.5at.%In, solution treated 5 minutes at 625°C, water quenched and aged 15 minutes at 428°C. Formation of twins and new precipitate at the advancing boundary. X32,500

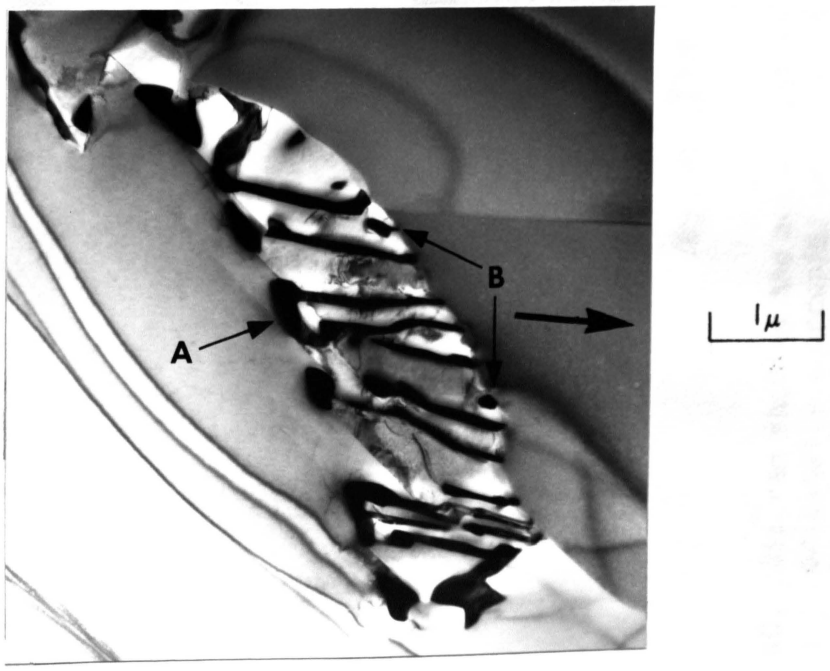

Figure 39. Cu-9.5at.%In, solution treated 5 minutes at 625°C, isothermally aged 15 minutes at 404°C. Early stage of cellular precipitation showing development of lamellae from a "U" shaped allotriomorph at A and the nucleation of new precipitate at B. X14,000

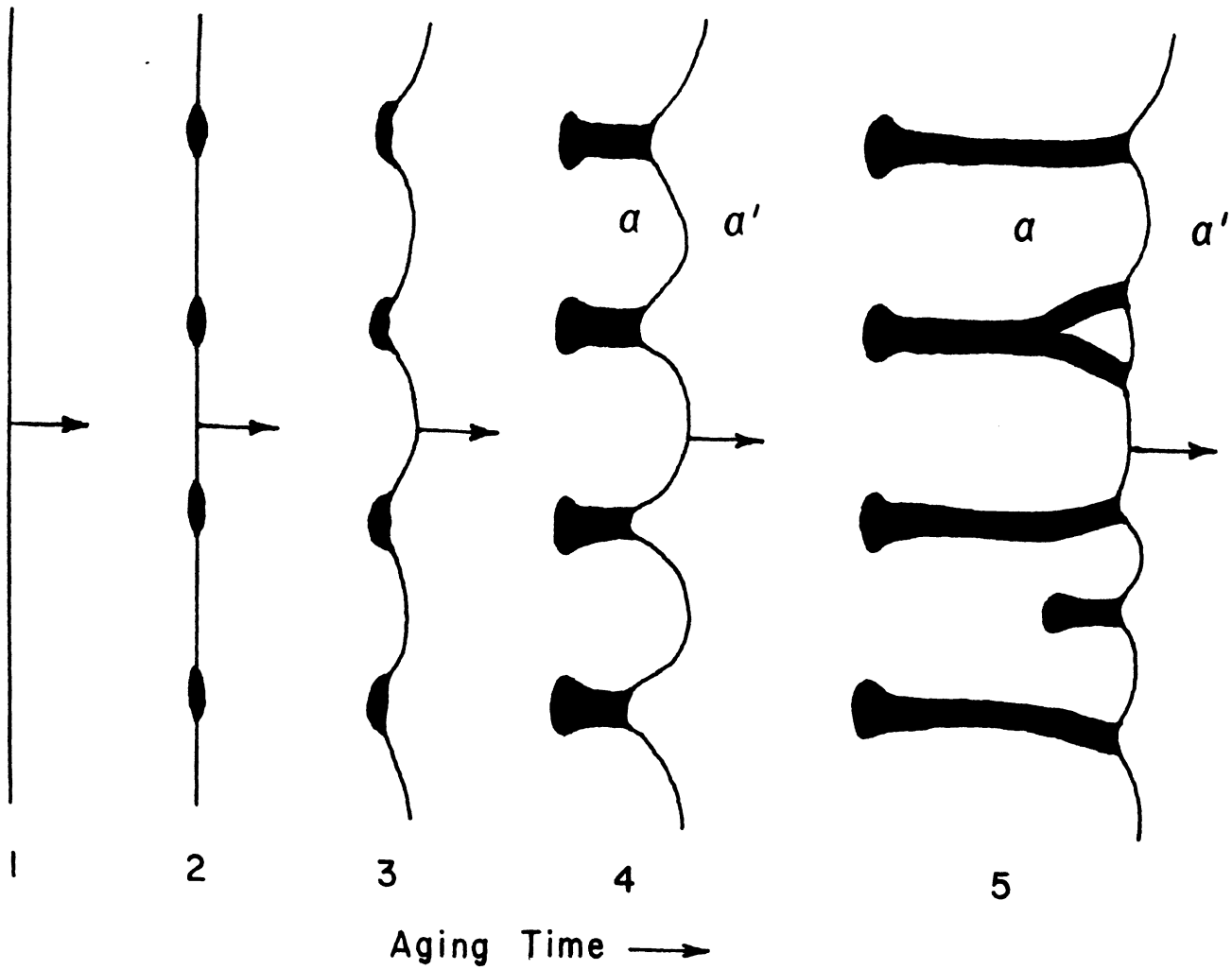

Figure 40. Diagram showing the morphological development of cellular structure from an originally unoccupied grain boundary where the initially formed grain boundary allotriomorphs are small.

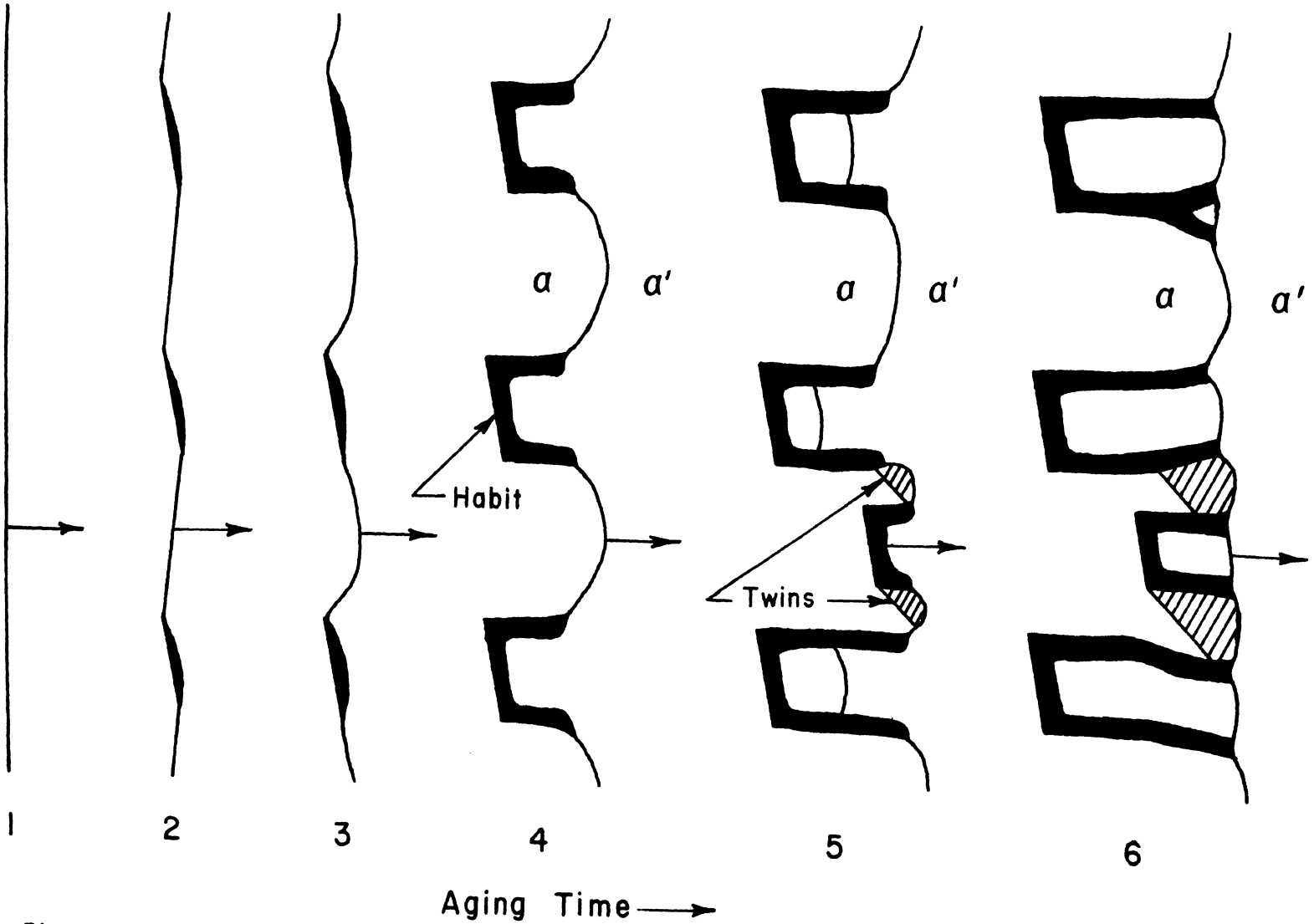

Figure 41. Diagram showing the morphological development of cellular structure from an initially unoccupied grain boundary where the initially formed grain boundary allotriomorphs are large.

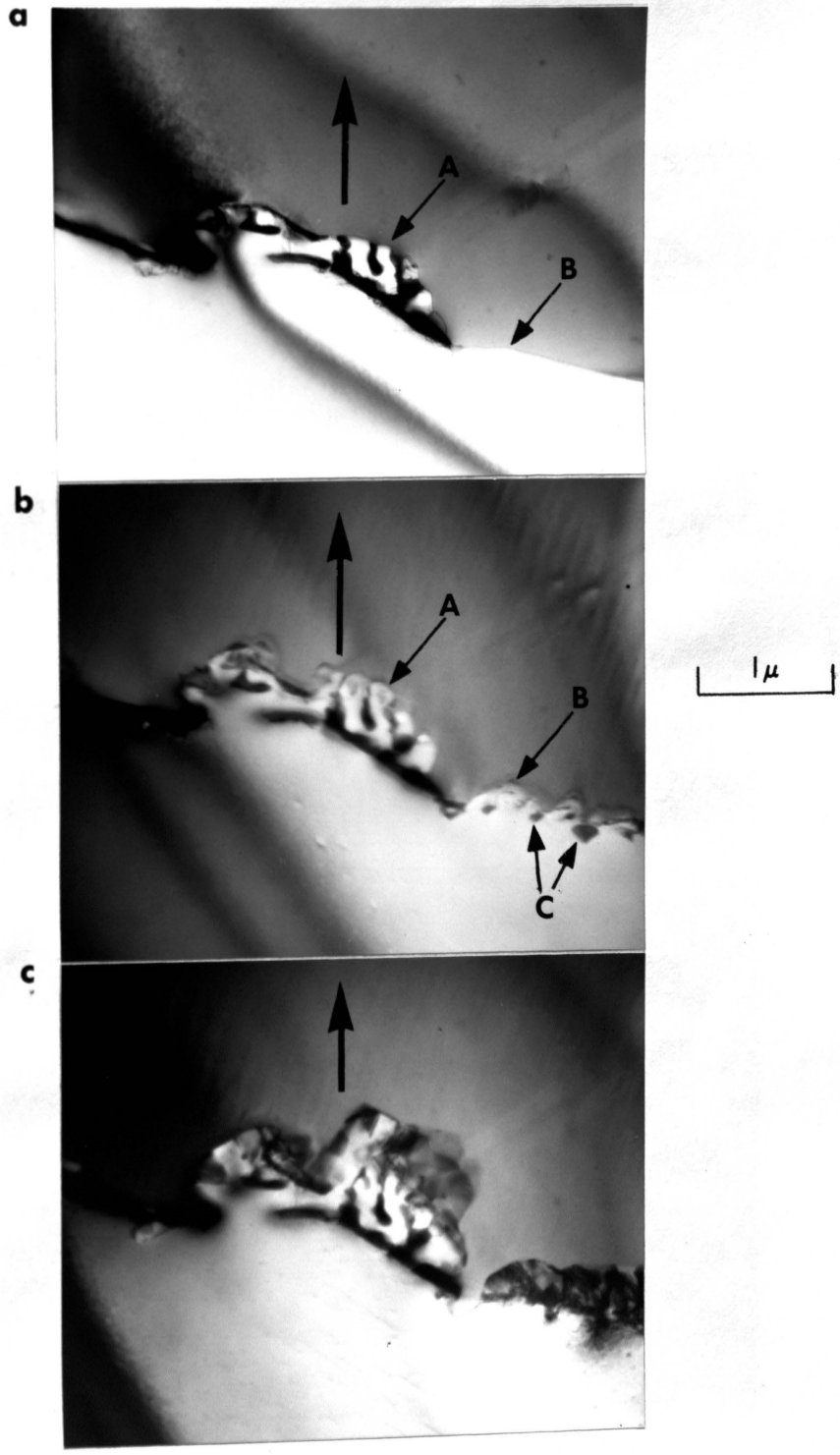

Figure 42. Cu-9.5at.%In, solution treated 5 minutes at 625°C and (a) isothermally aged 15 minutes at 366°C, (b) aged an additional 14 minutes in the electron microscope hot stage at about 350°C and (c) aged an additional 4 minutes in the hot stage. X17,500

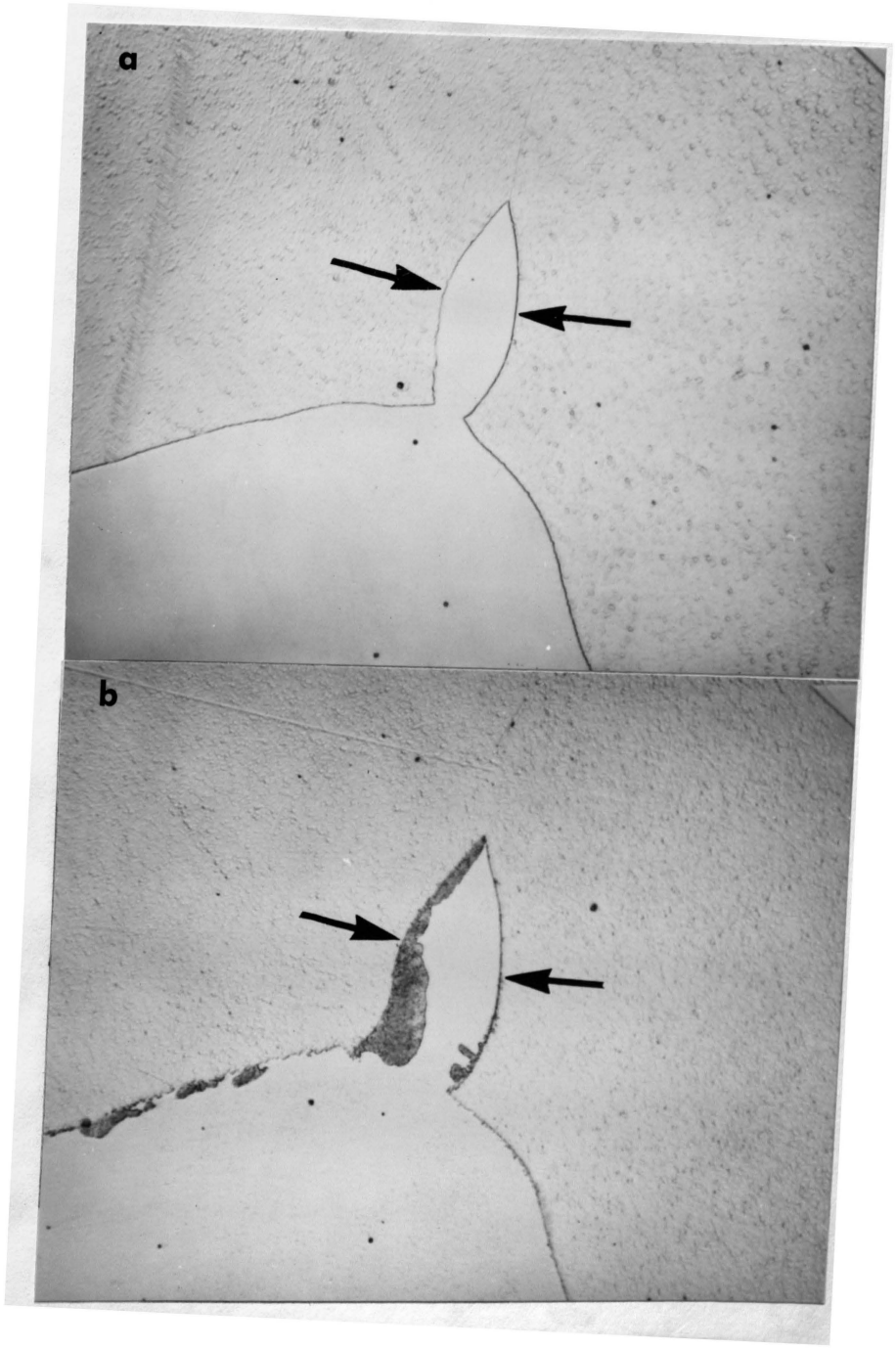

Figure 43. Cu-9.5at.%In, (a) solution treated 2 hours at 625°C and water quenched and (b) aged 15 minutes at 400°C. Cellular growth toward the center of curvature of a small appendage on a large grain. X500

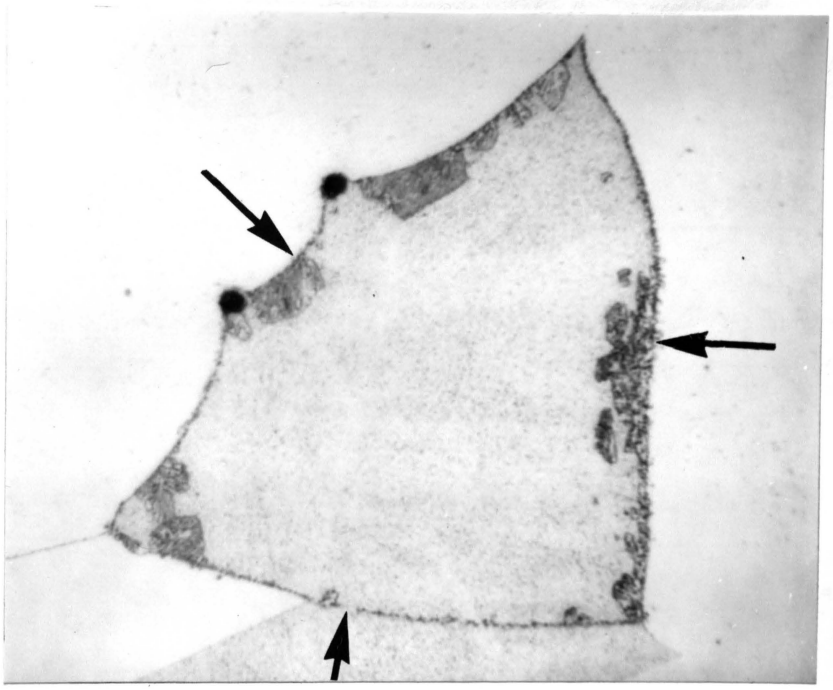

Figure 44. Cu-9.5at.%In, solution treated 2 hours at 625°C, water quenched and aged 15 minutes at 400°C. Cellular growth toward the center of a small grain. X1,000

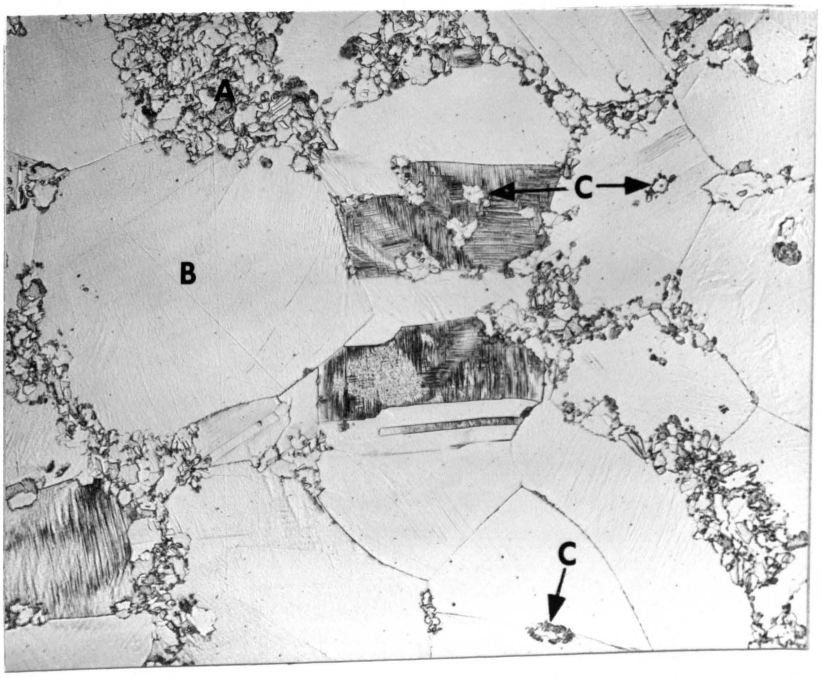

Figure 45. Cu-9.5at.%In, solution treated and water quenched, cold rolled 27%, solution treated 10 seconds at 625°C, isothermally aged 15 minutes at 420°C. A partially recrystallized and aged structure. X75

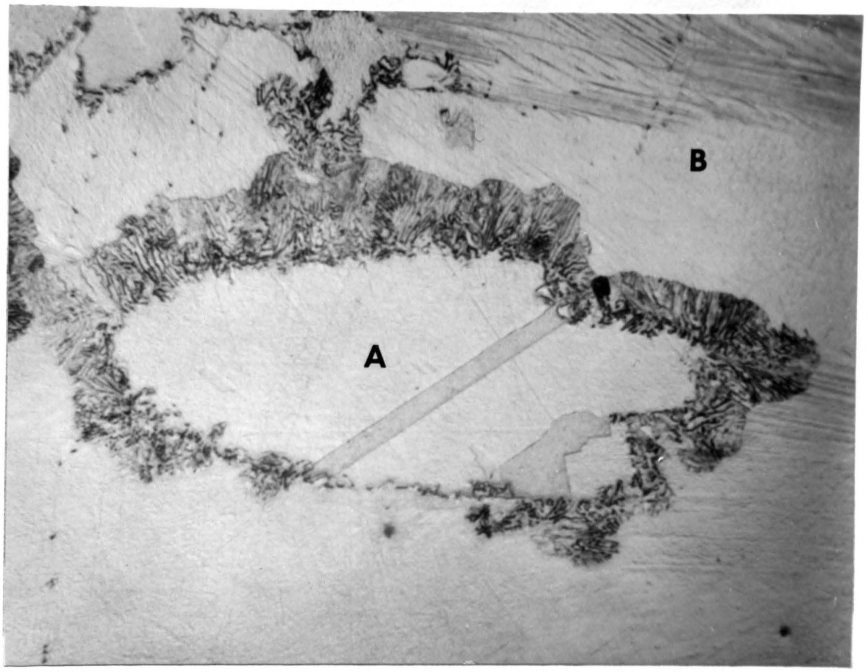

Figure 46. Cu-9.5at.%In, solution treated and water quenched, cold rolled 27%, solution treated 10 seconds at 625°C, isothermally aged 15 minutes at 420°C. Cellular growth on a small recrystallized grain in cold worked matrix. X1,000

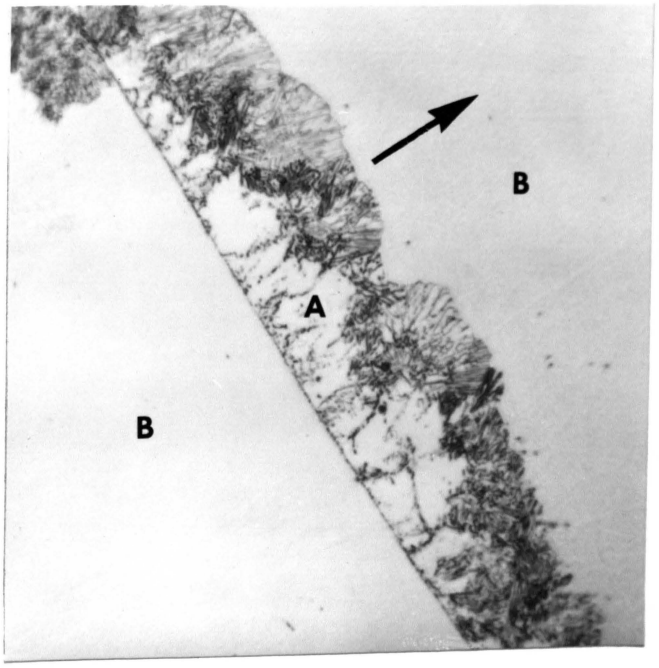

Figure 47. Cu-9.5at.%In, solution treated and water quenched, cold rolled 26%, solution treated 5 seconds at 625°C, isothermally aged 15 minutes at 420°C. Cellular growth after strain induced boundary migration had occurred during recrystallization. X1,000

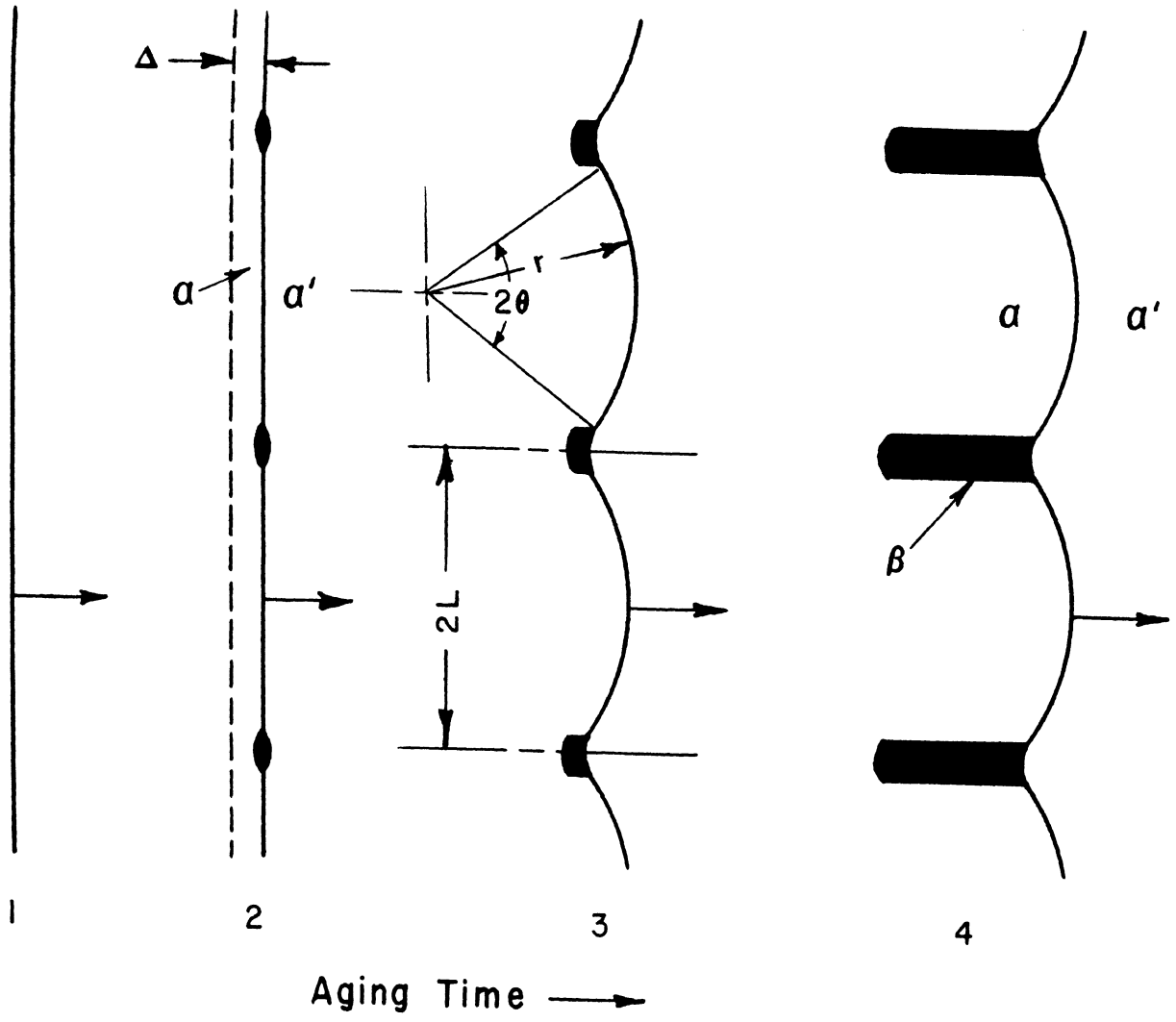

Figure 48. Schematic diagram showing the development of cellular structure from an initially unoccupied grain boundary.

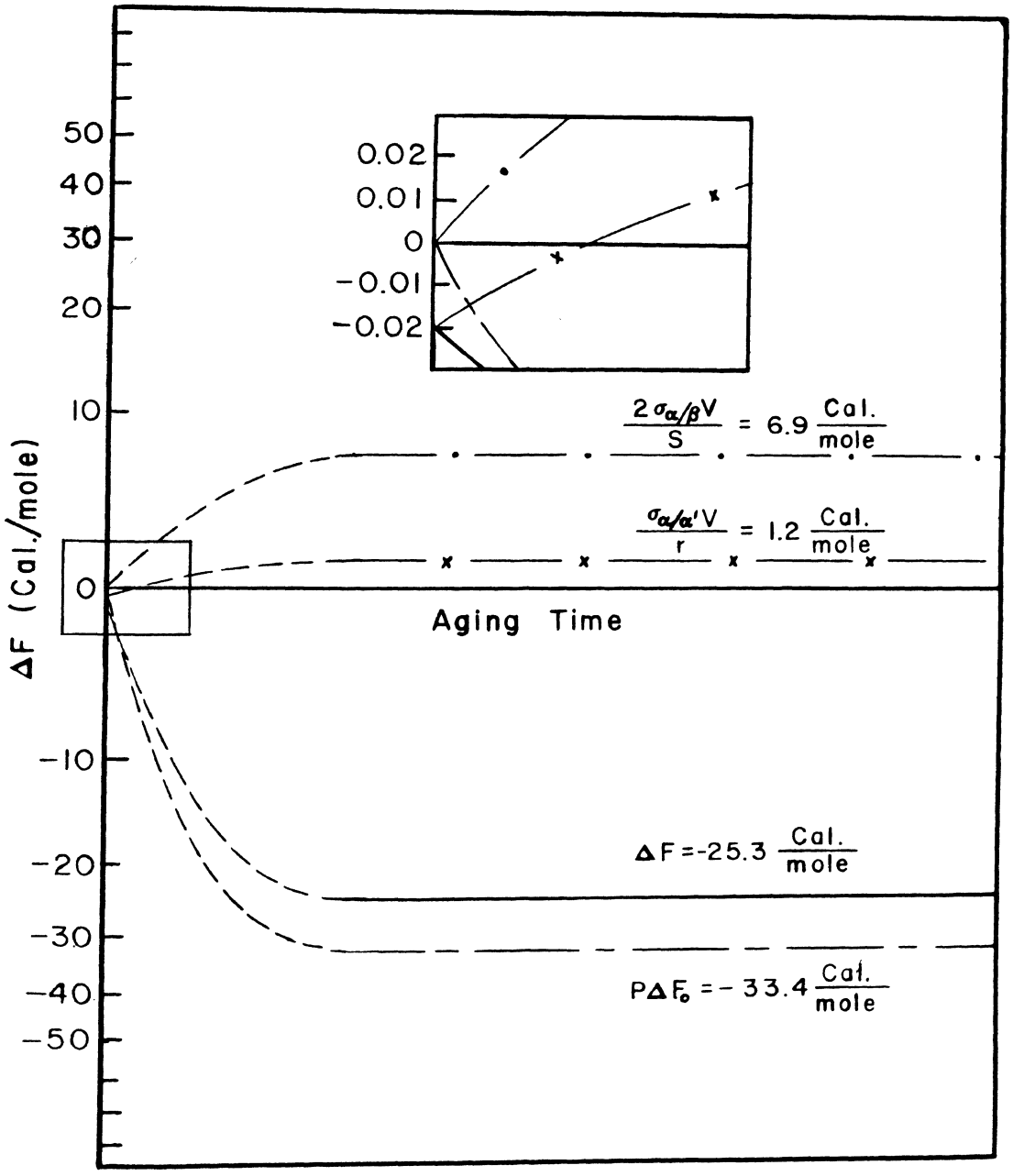

Figure 49. Net free energy change accompanying the migration of an initially unoccupied grain boundary and the formation of cellular structure in an undeformed matrix phase.

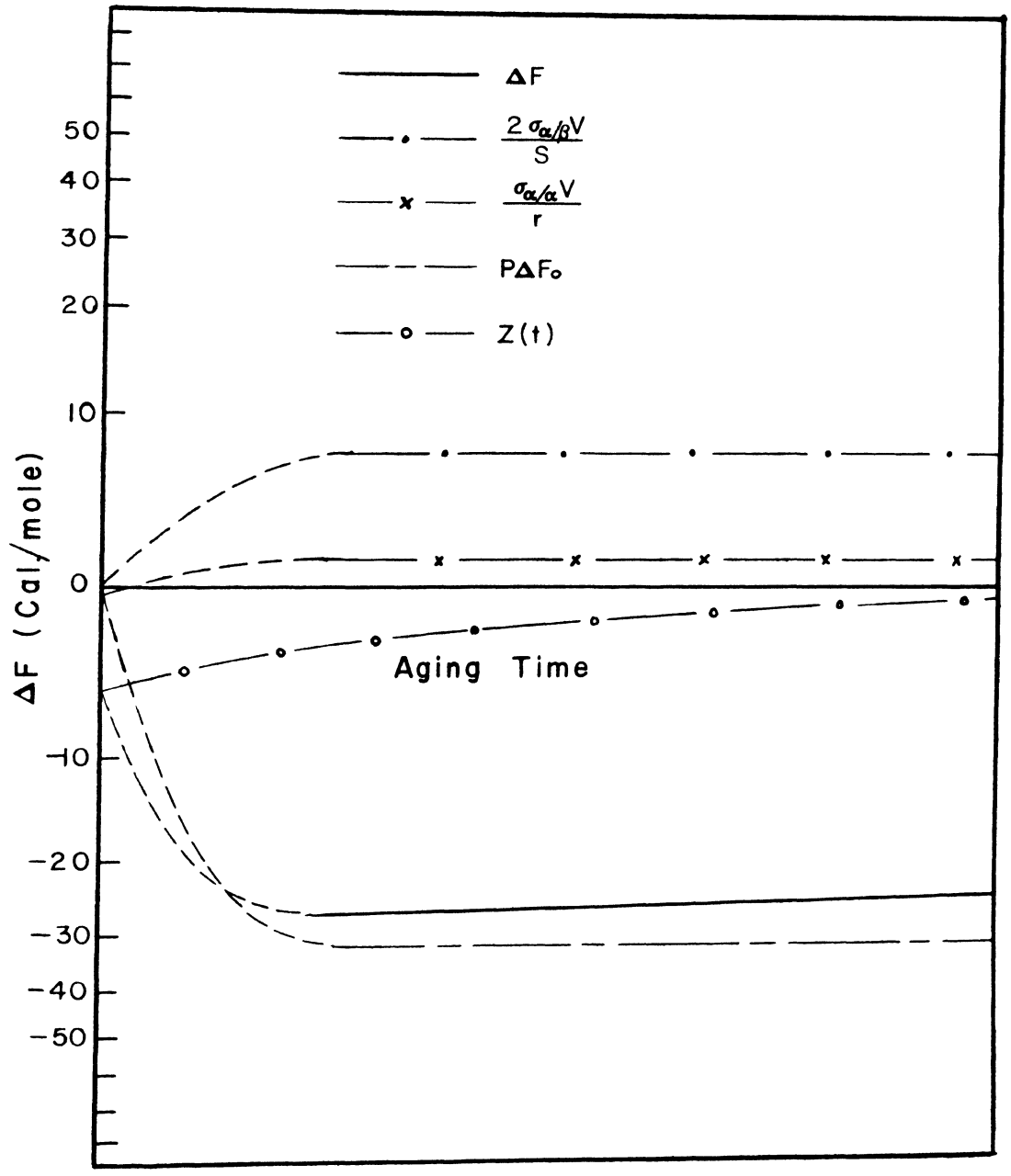

Figure 50. Net free energy change accompanying the migration of an initially unoccupied grain boundary and the formation of cellular structure in a deformed matrix phase.

VI. SUMMARY AND CONCLUSIONS

A. Morphology and General Characteristics

Cellular and general precipitation are observed to occur simultaneously at all aging temperatures up to 0.9 of the absolute solvus temperature in a quenched and aged Cu-9.5at.%In alloy; whereas, only cellular precipitation is observed to form during isothermal aging. At those temperatures at which cellular and general precipitation occur in quenched and aged alloys, general precipitation competes with cellular precipitation for solute in the supersaturated α' solid solution during aging, with the general eventually stopping the cellular reaction by depleting the grain interiors of their solute supersaturation. This effect is more prominent at the higher aging temperatures, where the growth of general is favored by high volume diffusivity, while cellular precipitation is favored at the lower aging temperatures.

Although general precipitation competes with cellular precipitation in quenched and aged alloys, the presence of precipitate free zones in the vicinity of grain boundaries precludes the interference of general precipitation with the early development of cellular precipitation in these alloys. Consequently, the early stage cellular morphologies are identical for both quenched and aged and isothermally aged alloys. Accordingly, for both types of heat treatment, cellular nodules are found to develop from original grain boundary allotriomorphs whose "spacing" is larger than the steady state lamellar spacing characteristic of the aging temperature. Parallel, steady state δ lamellae of identical crystallographic orientation have no

definite habit plane in and no orientation relationship with the continuous, depleted α lamellae; and they appear to develop by branching from a single source. New precipitate lamellae are also observed to nucleate at the advancing interface.

B. The Genesis and Cause of Cellular Precipitation

Cellular precipitation is observed to develop from an initially unoccupied grain boundary by migration of the boundary from one grain into another. As the boundary migrates, it interacts locally with simultaneously forming grain boundary allotriomorphs to eventually form a steady state lamellar growth structure. The details of this boundary migration, the grain boundary-grain boundary allotriomorph interaction, and the formation of a steady state lamellar structure are described below with reference to Figures 40, 41 and 48.

Initially, at the start of aging, grain boundaries migrate under the influence of boundary migration forces as if they were in a single phase alloy and as shown at (1) in the above figures. As they migrate they deplete the area behind them of solute; and, after migrating a short distance, Δ, allotriomorphs begin to form, as shown at (2), pinning the boundary. A thermodynamic driving force develops from the solute depletion of the region behind the boundary; and, thus, the boundary continues to migrate in its original direction of migration and bows out between the pinning allotriomorphs, as shown at (3). As the boundary bows it continues to deplete the region behind it of solute by solute partitioning in what now is an advancing α/α' interface. The solute segregating in the advancing interface now starts to accumulate on the initial allotriomorphs to eventually form trailing

precipitates behind the advancing α/α' boundary, as shown at (4). These trailing precipitates then branch or new precipitates nucleate in the advancing interface to form the final steady state lamellar structure, as shown at (5) in Figure 40 and (5) and (6) in Figure 41.

The driving force for the genesis of cellular precipitation according to this mechanism is given by

$$\Delta F = a\Delta F_o + b\sigma_{\alpha/\beta} + \frac{\sigma_{\alpha/\alpha'}V}{r} , \tag{30}$$

for the growth of cellular structure into an undeformed matrix, and by

$$\Delta F = a\Delta F_o + b\sigma_{\alpha/\beta} + \frac{\sigma_{\alpha/\alpha'}V}{r} + Z(t) , \tag{29}$$

for the growth of cellular structure into a deformed matrix.

For the development of cellular precipitation in an undeformed alloy, the net free energy change transforms from an initial value of

$$\Delta F = \frac{\sigma_{\alpha/\alpha'}V}{r} \tag{31}$$

at $t = 0$ to a value of

$$\Delta F = P\Delta F_o + \frac{2\sigma_{\alpha/\beta}V}{S} + \frac{\sigma_{\alpha/\alpha'}V}{r} \tag{32}$$

after a steady state obtains.

For the development of cellular precipitation in a deformed alloy, the driving force transforms from an initial value of

$$\Delta F = \frac{\sigma_{\alpha/\alpha'}V}{r} + Z_o \tag{35}$$

at $t = 0$ to a value of

$$\Delta F = P\Delta F_o + \frac{2\sigma_{\alpha/\beta}V}{S} + \frac{\sigma_{\alpha/\alpha'}V}{r} + Z(t) \tag{34}$$

after a quasi steady state is attained.

The exact path by which the driving force, ΔF, transforms from its initial value to its final value is uncertain and no attempt is made to describe it in this investigation.

Assuming that the ability of the boundary to bow between pinning allotriomorphs is the critical step in the development of a cell, the following criterion for the occurrence of cellular precipitation was established.

$$-\frac{P\Delta F_o L}{V\sigma_{\alpha/\alpha'}} > 2 \qquad (41)$$

Here P is the fraction of the chemical free energy, ΔF_o, released during the bowing of the boundary, 2L is the distance between initial allotriomorphs, V is the molar volume and $\sigma_{\alpha/\alpha'}$ is the surface energy of the α/α' boundary. Unfortunately, insufficient thermodynamic and surface energy data are available to test the criterion for its validity.

BIBLIOGRAPHY

1. Aaronson, H. I. and Clark, J. B. "Influence of Continuous Precipitation upon the Growth Kinetics of the Cellular Reaction in an Al-Ag Alloy," Acta Metallurgica, 16, 845 (1968).

2. Aaronson, H. I. and Liu, Y. C. "On the Turnbull and the Cahn Theories of the Cellular Reaction," Scripta Metallurgica, 2, 1 (1968).

3. Bailey, J. E. "Electron Microscope Observations on the Annealing Processes Occurring in Cold-Worked Silver," Philosophical Magazine, 5, 833 (1960).

4. Beck, P. A. and Sperry, P. R. "Strain Induced Grain Boundary Migration in High Purity Aluminum," Journal of Applied Physics, 21, 151 (1950).

5. Böhm, H. "Die diskontinuierliche Ausscheidung," Metall, 13, 929 (1959).

6. Böhm, H. "Die diskontinuierliche Ausscheidung in Kupfer-Indium-Legierungen," Zeitschrift für Metallkunde, 50, 87 (1959).

7. Böhm, H. "Über das Ausscheidungsverhalten der Binären Kupferlegierungen und seine Beeinflussung durch Zusätze," Zeitschrift für Metallkunde, 52, 564 (1961).

8. Böhm, H. "Über die Ursachen des Auftretens der diskontinuierlichen Ausscheidung," Zeitschrift für Metallkunde, 52, 518 (1961).

9. Böhm, H. "Untersuchungen zur Aushärtung bei der diskontinuierlichen Ausscheidung," Zeitschrift für Metallkunde, 52, 512 (1961).

10. Böhm, H. "Verformung und diskontinuierliche Ausscheidung," Zeitschrift für Metallkunde, 54, 142 (1963).

11. Cahn, J. W. "The Dependence of Grainboundary Precipitation on the Orientation of Adjoining Grains," Acta Metallurgica, 4, 217 (1956).

12. Cahn, J. W. "The Kinetics of Cellular Segregation Reactions," Acta Metallurgica, 7, 18 (1959).

13. Clark, J. B. "Age Hardening in a Mg-9wt.%Al Alloy," Acta Metallurgica, 16, 141 (1968).

14. Corderoy, D. J. H. and Honeycombe, R. W. K. "Age-Hardening in Copper-Base Indium Alloys," Journal of the Institute of Metals, 92, 65 (1963-64).

15. Entwisle, A. R. and Wynn, J. K. "Precipitation in Commercial Copper-Beryllium Alloys," Journal of the Institute of Metals, 89, 29 (1960-61).

16. Fisher, J. C. "Eutectoid Decompositions," Thermodynamics in Physical Metallurgy, American Society for Metals, 201 (1950).

17. Fountain, R. W. and Forgeng, W. D. "Phase Relations and Precipitation in Cobalt-Titanium Alloys," Transactions of the Metallurgical Society of A.I.M.E., 215, 998 (1959).

18. Gjostein, N. A. and Rhines, F. N. "Absolute Interfacial Energies of [001] Tilt and Twist Grain Boundaries in Copper," Acta Metallurgica, 7, 319 (1959).

19. Geisler, A. H. "Precipitation from Solid Solutions of Metals," Phase Transformations in Solids, John Wiley & Sons, Inc., New York, 432 (1951).

20. Gleiter, H. "The Mechanism of Grain Boundary Migration," Acta Metallurgica, 17, 565 (1969).

21. Gleiter, H., "Theory of Grain Boundary Migration Rate," Acta Metallurgica, 17, 853 (1969).

22. Gruhl, W. and Ammann, D. "Uber die Abhängigkeit der Korngrenzen Ausscheidung von der Orientierung der benachbarten Kristalle," Acta Metallurgica, 3, 347 (1955).

23. Gruhl, W. and Kramer, H. "Über das Wesen der diskontinuierlichen Ausscheidung," Metall, 12, 707 (1958).

24. Hansen, M. and Anderko, K. Constitution of Binary Alloys, McGraw-Hill, New York, 590 (1958).

25. Hellner, E. and Laves, F. "Kristallchemie des In und Ga in Legierungen mit einigen Übergangselementen (Ni, Pd, Pt, Cu, Ag und Au)," Zeitschrift für Naturforschung, 2A, 177 (1947).

26. Hillert, M. "The Role of Interfaces in Phase Transformations," The Mechanism of Phase Transformations in Crystalline Solids, The Institute of Metals, London, 231 (1969).

27. Hillert, M. "The Formation of Pearlite," Decomposition of Austenite by Diffusional Processes, Interscience, 197 (1962).

28. Hirsch, P. B., Howie, A., Nicholson, R. B., Pashley, D. W.; and Whelan, M. J. Electron Microscopy of Thin Crystals, Butterworths, London, 26 (1965).

29. Hirschhorn, J. S. and Gregg, R. A. "Cellular Precipitation in Niobium-Chromium Alloys," Journal of Less Common Metals, 6, 333 (1964).

30. Hopkins, R. H. and Kossowsky, R. "The Crystallography of Phase Interfaces in the Ni-Cr Alloy System," Acta Metallurgica, 19, 203 (1971).

31. Hornbogen, E. "Two Types of Discontinuous Precipitation in Alpha Iron Solid Solutions," Transactions of the Metallurgical Society of A.I.M.E., 227, 1411 (1963).

32. Jones, B. L. "Cellular Precipitation in an Undercooled Ni-Sn Alloy," Journal of the Institute of Metals, 99, 27 (1971).

33. Korchynsky, M. and Fountain, R. W. "Precipitation Phenomena in Cobalt-Tantalum Alloys," Transactions of the Metallurgical Society of A.I.M.E., 215, 1033 (1959).

34. Li, J. C. M. "Recovery Processes in Metals," Recrystallization, Grain Growth and Textures, American Society for Metals, 45 (1965).

35. Liu, Y. C. and Aaronson, H. I. "Kinetics of the Cellular Reaction in Oriented Bicrystals of Pb-7at.%Sn," Acta Metallurgica, 16, 1343 (1968).

36. Lücke, K. "Korngrenzenstrucktur und Rekristallization," Zeitschrift für Metallkunde, 52, 1 (1961).

37. Mack, D. J. "The Isothermal Transformation of a Eutectoid Aluminum Bronz," Transactions of the A.I.M.E., 175, 246 (1948).

38. Mäder, K. and Hornbogen, E. "Beeinflussung der dis kontinuierlichen Ausscheidung in Blei-Natrium-Mischkristallen durch Dotieren mit Silber," Zeitschrift für Metallkunde, 60, 475 (1969).

39. Margolin, H. and Hibbard, W. R. "Effect of Ternary Additions on the Age-Hardening of a Copper-Silver Alloy," Transactions of the A.I.M.E., 191, 174 (1951).

40. Milalisin, J. R. and Decker, R. F. "Phase Transformations in Nickel Rich Nickel-Titanium-Aluminum Alloys," Transactions of the Metallurgical Society of A.I.M.E., 218, 507 (1960).

41. Moisio, T. and Mannerkoski, M. "Modes of Precipitation of Cu_2Mg from Solid Solutions of Magnesium in Copper," Journal of the Institute of Metals, 95, 268 (1967).

42. Nielsen, J. P. "Grain Coalescence Theory," Recrystallization, Grain Growth and Textures, American Society for Metals, 141 (1965).

43. Petermann, J. and Hornbogen, E. "Drei Mechanismen der Auscheidung in Blei-Natrium-Mischkristallen," Zeitschrift für Metallkunde, 59, 814 (1968).

44. Phillips, V. A. "Electron-Microscopy Observations on Precipitation in a Cu-3.1wt.Pct Co Alloy," Transactions of the Metallurgical Society of A.I.M.E., 230, 967 (1964).

45. Piearcey, B. J., Jackson, R., and Argent, B. B. "The Mechanical Properties and Structure of Cobalt-Nickel-Niobium Alloys," Journal of the Institute of Metals, 91, 257 (1962-63).

46. Predel, B. and Ruge, H. "Untersuchung der Kinetic der diskontinuierlichen Entmischung übersättigter Silber Mischkristalle," Zeitschrift für Metallkunde, 59, 777 (1968).

47. Rao, K. K., Katz, L. E. and Herman, H. "Decomposition of Quenched Al-29at.%Zn," Materials Science and Engineering, 1, 263 (1966-67).

48. Reynolds, J. Wiseman, W. A., and Hume-Rothery, W. "The Equilibrium Diagram of the System Copper-Indium in the Region 25-35At.-% Indium," Journal of the Institute of Metals, 80, 637 (1951-52).

49. Rose, R. G. "The Precipitation of Copper from a Silver-5.5% Copper Solid Solution at 220°C," Acta Metallurgica, 5, 404 (1957).

50. Shapiro, J. M. and Kirkaldy, J. S. "The Kinetics of Discontinuous Precipitation in Copper-Indium Alloys," Acta Metallurgica, 16, 1239 (1968).

51. Shapiro, J. M. and Kirkaldy, J. S. "Theory of Decomposition of Eutectoids Assuming Local Equilibrium and Phase Boundary Diffusion," Acta Metallurgica, 16, 579 (1968).

52. Shapiro, J. M. "The Kinetics of Discontinuous Precipitation in Copper-Indium Alloys," Ph.D. Thesis, McMaster University, 1966.

53. Smart, R. F. and Haynes, F. G. "Some Observations on the Chromium-Nickel System," Journal of the Institute of Metals, 91, 153 (1962-63).

54. Smith, C. S. "Microstructure," Transactions of American Society for Metals, 45, 533 (1953).

55. Speich, G. R. "Cellular Precipitation in an Austenitic Fe-30Ni-6Ti Alloy," Transactions of the Metallurgical Society of A.I.M.E., 227, 754 (1962).

56. Speich, G. R. "Cellular Precipitation in Fe-Zn Alloys," Transactions of the Metallurgical Society of A.I.M.E., 242, 1359 (1968).

57. Spencer, C. W. and Mack, D. J. "Decomposition of the Beta Phase in a Copper-Gallium Eutectoid Alloy," Journal of the Institute of Metals, 84, 461 (1955-56).

58. Straumanis, M. E. and Yu, L. S. "Lattice Parameters, Densities, Expansion Coefficients and Perfection of Structure of Cu and Cu-InαPhase," Acta Crystallographica, A25, 676 (1969).

59. Sulonen, M. "Discontinuous Precipitation from Solid Solutions of Cadmium in Copper," Annales Academie Scientiarum Fennice, 4, Series A, 1 (1957).

60. Sulonen, M. S. "Contributions to the Theory of Discontinuous Precipitation," Acta Polytechnica Scandinavica, Ch28, 1 (1964).

61. Sulonen, M. S. "On the driving force of discontinuous precipitation and dissolution," Acta Metallurgica, 12, 749 (1969).

62. Tiedema, T. J., Bouman, J. and Burgers, W. G. "Precipitation in Gold-Platinum Alloys," Acta Metallurgica, 5, 310 (1957).

63. Tu, K. N. and Turnbull, D. "Analysis of Kinetics of Boundary Diffusion Limited Cellular Precipitation," Scripta Metallurgica, 1, 173 (1967).

64. Tu, K. N. and Turnbull, D. "Morphology of Cellular Precipitation of Tin from Lead-Tin Bicrystals," Acta Metallurgica, 15, 369 (1967).

65. Tu, K. N. and Turnbull, D. "Morphology of Cellular Precipitation of Tin from Lead-Tin Bicrystals - II," Acta Metallurgica, 15, 1317 (1967).

66. Tu, K. N. and Turnbull, D. "Morphology and Structure of Tin Lamellae Formed by Cellular Precipitation," Acta Metallurgica, 17, 1263 (1969).

67. Turnbull, D. "Diffusion Short Circuits and their Role in Precipitation," Defects in Crystalline Solids, The Physical Society, 203 (1954).

68. Turnbull, D. and Treaftis, H. N. "Kinetics of Precipitation of Tin from Lead-Tin Solid Solutions," Acta Metallurgica, 3, 43 (1955).

69. Turnbull, D. "Theory of Cellular Precipitation," Acta Metallurgica, 3, 55 (1955).

70. Turnbull, D. and Tu, K. N. "The Cellular and Pearlitic Reactions," Phase Transformations, American Society for Metals, 487 (1968).

71. Unwin, P. N. T., Lorimer, G. W. and Nicholson, R. B. "The Origin of the Grain Boundary Precipitate Free Zone," Acta Metallurgica, 17, 1363 (1969).

72. Watanabe, R. and Koda, S. "The Grain Boundary Reaction of a Copper-1.85% Beryllium Alloy," Journal of Hokkaido Gakugei University, 11, 38 (1960).

73. Watanabe, R. and Koda, S. "A Kinetic Investigation of Grain Boundary Reaction Type Precipitation," Transactions of National Research Institute for Metals (Japan), 7, 13 (1965).

74. Watanabe, R. "The Cracked Film and the Grain Boundary Reaction Type Precipitation in Zinc Alloy Containing 2st.% Copper," Transactions of National Research Institute for Metals, 10, 201 (1968).

75. Weibke, F. and Eggers, H. "Das Zustands-diagram des Systems Kupfer-Indium," Zeitschrift für anorganische und allgemeine Chemie, 220, 273 (1934).

76. Zener, C. "Kinetics of the Decomposition of Austenite," Transactions of the A.I.M.E., 167, 550 (1946).

VITA

Raymond Albert Fournelle was born on December 9, 1941 in St. Louis, Missouri. He completed his primary and secondary education in St. Louis, Missouri and entered the University of Missouri, School of Mines and Metallurgy in January, 1960. He was graduated with honors from the University of Missouri, School of Mines and Metallurgy in January, 1964, receiving a Bachelor of Science Degree in Metallurgical Engineering. From February, 1964 to September 1966 the author was employed as a research engineer by Shell Oil Company at their Wood River Research Laboratory in Wood River, Illinois. During this period the author was granted a military leave by the company and served as a lieutenant in the U.S. Army from April 1964 to March 1966.

Since September, 1966 Mr. Fournelle has been a graduate student at the University of Missouri-Rolla. In June, 1968 he received a Master of Science Degree in Metallurgical Engineering from the university.

APPENDIX A

CRYSTAL STRUCTURE OF THE $\delta(Cu_9In_4)$ PRECIPITATE

A. General

According to Figure 12, the copper-indium phase diagram, a Cu-9.5at.%In alloy held below the $\alpha/\alpha+\delta$ solvus should segregate into α of equilibrium solvus composition and δ of composition, Cu-28.9at.%-In. A phase diagram study of the 25-35at.%In region of the copper-indium system by Reynolds, Wiseman and Hume-Rothery[48] describes the $\delta(Cu_9In_4)$ phase to be a tetragonal distortion of the cubic γ brass type of structure with a = 8.97kX, c = 9.14kX and c/a = 1.020, and to have composition limits of 28.9 and 30.6at.%In at room temperature. Hellner and Laves[25] describe this phase as a superlattice of the NiAs type. Both of the above references describe the δ phase as forming from a high temperature γ phase having a cubic γ brass type of structure, and Reynolds et al.[48] found that this transformation could not be suppressed. Corderoy and Honeycomb,[14] in a study of age hardening in copper base copper-indium alloys, found evidence for both a tetragonally distorted unit cell and a superlattice structure from selected area electron diffraction patterns of carbon extracted platelets of general δ precipitate. In the present study selected area diffraction patterns of parallel α and δ lamellae in the cellular precipitate exhibited zero order Laue zones of the δ phase which could not be indexed satisfactorily with the tetragonally distorted γ brass structure proposed by Reynolds et al. Because a knowledge of the crystal structure of the precipitate is necessary for precipitate-

matrix orientation studies, an investigation of the structure of the δ lamellae in the cellular nodules was performed.

The structure of the δ lamellae was established by combining the results of Debye-Scherrer x-ray diffraction studies of pure δ phase (Cu_9In_4) and a completely transformed Cu-9.5at.%In alloy with electron diffraction studies of parallel α and δ lamellae in cellular nodules.

B. Experimental Procedure

A Cu-29.6at.%In alloy (δ phase) was prepared from the same copper and indium described in Section IV. B. 1. by melting appropriate quantities of the components in an evacuated Vycor capsule. Prior to encapsulation the Cu and In were cleaned in dilute nitric acid and washed with water and methanol. After encapsulation, any remaining oxygen or hydrogen were removed from the capsule by an 87.5Zr-12.5Ti getter, sealed in a separate compartment of the capsule. Following this, the compartment was removed and the components were melted in a resistance furnace set at 750°C. At this temperature the indium melted first and dissolved the copper. Once the alloy was completely molten the capsule was removed from the furnace and shaken to insure mixing. The capsule was then returned to the furnace for about 10 minutes after which it was removed and water quenched. The resulting alloy ingot was then weighed to establish if any material had been lost during melting. A weight loss of about 0.1% of the weight of the original components was noted. The alloy was then cleaned by belt sanding, encapsulated in Pyrex tubing under an argon atmosphere and annealed for 24 hours at 550°C in a salt bath. Several grams of this alloy were analyzed for nominal composition and impurity level by

Industrial Testing Laboratories, St. Louis, Missouri. The Cu-9.5at.%In alloy used in this study was the same 0.007 inch thick foil described in Section IV. B. 3.

To insure consistency both the Cu-9.5at.%In alloy and the Cu-29.6at.%In alloy were given the same aging treatment. Both were solution treated for 5 minutes at 625°C in a salt bath and then isothermally aged for 4 hours at 420°C in another salt bath. The Cu-29.6at.%In alloy was encapsulated under argon for this heat treatment but the Cu-9.5at.%In foil was not. Photomicrographs of the two aged alloys were obtained by methods described in Section IV. D. 1.

Powder x-ray diffraction samples of the Cu-29.6at.%In alloy were prepared by grinding the alloy in an agate mortar and screening it through a 400 mesh screen. Some -600 mesh material was also obtained. This -400 mesh material was then mounted on a glass fiber, coated with petroleum jelly. X-ray samples of the Cu-9.5at.%In alloy were prepared by cutting a sliver of material from a foil that had been electrolytically thinned by the method described in Section IV. D. 2.

Powder x-ray diffraction patterns of these samples were obtained in 155 millimeter asymmetrically loaded Debye-Scherrer cameras using nickel filtered copper radiation with exposures of 8 and 12 hours. In addition to the above diffraction patterns, a pattern of a Cu-9.5at.%In alloy, solution treated 5 minutes at 625°C and water quenched was obtained. The x-ray specimen was prepared in the same way as that of the aged Cu-9.5at.%In alloy.

Transmission electron micrographs and selected area diffraction patterns were obtained from areas of parallel cellular lamellae such as shown at A in Figure 23.

In addition to the x-ray diffraction and electron diffraction data the density of the Cu-29.6at.%In alloy at room temperature was also determined. It was established by noting the difference between the weight of a bulk sample in air and in xylene. Both the density of air and that of xylene were corrected for temperature and atmospheric pressure.

C. Experimental Results and Discussion

1. Metallography

Figure 51 shows the structure of the Cu-29.6at.%In alloy to be single phase substance with a relatively large grain size. No second phase segregation is noted at the grain boundaries. Figure 52 shows the structure of the Cu-9.5at.%In alloy, isothermally aged for four hours at 420°C, to be that of an alloy completely transformed to α and δ lamellae by cellular precipitation.

2. X-ray Diffraction

Figure 53 shows the front reflection region of diffraction patterns from the solution treated and water quenched alloy, the isothermally transformed alloy, and the Cu-29.6at.%In Alloy, and the correlation between these patterns. Figures 53a and 53b show the correlation between the reflections from the single phase supersaturated α' solid solution and the depleted α lamellae in the transformed alloy. Figures 53b and 53c show the correlation between the strong lines in the pure δ phase and in the δ lamellae in the overaged alloy. These strong lines are indexed according to the tetragonal structure

proposed by Reynolds et al. The correspondence of the strong δ lines with the strong precipitate lines shows that the precipitate structure is, indeed, similar to that of the pure δ phase. The "d" values of the first 26 lines from the x-ray pattern in Figure 53c are listed in Table V.

3. Electron Microscopy and Selected Area Diffraction

Figures 54a and 54b show a transmission electron micrograph of cellular lamellae and the selected area diffraction pattern from this area. Figure 54c is a diagram of the diffraction pattern and shows the zero order Laue zones of the α matrix phase and the δ precipitate phase. The α matrix has a [011] zone axis and the δ precipitate has a [001] zone axis. Figure 54c shows a more detailed analysis of the zero order Laue zone of the precipitate. This precipitate zone is indexed using the structure proposed by Reynolds et al. and shows the four fold symmetry expected of the [001] zone of a tetragonal structure.

Figures 55a and 55b show another electron micrograph and selected area diffraction pair. However, if Figure 55b is analyzed as Figure 54b was, it is found that the zero order Laue zone of the δ precipitate cannot be accounted for by a tetragonal structure with lattice parameters of a = 8.99Å and c = 9.16Å. However, if the lattice parameters are increased by a factor of 4 to a = 35.95Å and c = 36.63Å, Figure 55d can be indexed as shown. In all, seven selected area diffraction patterns of lamellae were analyzed. Three of the zero order Laue zones of the δ precipitate could be accounted for by the structure of Reynolds et al., but the remaining four precipitate

patterns could be indexed only by using a tetragonal unit cell with $a = 35.95\text{Å}$ and $c = 36.63\text{Å}$. Some of the larger "d" values obtained from spots in these selected area diffraction patterns are given in Table V.

Table V shows experimental "d" values obtained from both x-ray and electron diffraction patterns of the δ phase and the δ precipitate respectively. It can be seen from the table that all but three of the x-ray lines can be accounted for by the presently accepted tetragonal structure; however, a tetragonal unit cell with $a = 35.95\text{Å}$ and $c = 36.63\text{Å}$ is required to account for all of the "d" values from both electron and x-ray diffraction patterns.

4. Density of the Cu-29.6at.%In Alloy

The density of the δ phase is found to be 8.93 grams/cm.^{3}. With this density, the tetragonal unit cell of Reynolds et al. would contain about 50 atoms, which is in agreement with the phase being of the γ brass type. A tetragonal unit cell with $a = 35.95\text{Å}$ and $c = 36.63\text{Å}$ would contain 3200 atoms.

D. Conclusions

X-ray diffraction studies show that the δ lamellae have a tetragonal structure related to that of the pure δ phase. Electron diffraction studies show that the precipitate contains a superlattice which can be accounted for by a tetragonal unit cell with $a = 35.95\text{Å}$ and $c = 36.63\text{Å}$. The three lines in the δ phase x-ray patterns that could not be accounted for indicate that the pure δ phase may also have a superlattice. This, however, was not investigated.

The density of the δ phase has been found to be 8.93 grams/cm.^{3} With this density the above unit cell would contain 3200 atoms.

TABLE IV

Analysis of the Cu-29.5at.%In Alloy

1. Chemical Analysis (wt.%)

Copper	56.78
Indium	43.16

2. Semiquantitative Spectrographic Analysis (wt.%)

Lead	0.003-0.03
Iron	0.003-0.03
Nickel	0.001-0.01
Silver	0.001-0.01
Aluminum	0.001-0.01
Silicon	0.001-0.01
Magnesium	0.001-0.01
Cadmium	0.001-0.01
Zinc	<0.001
Sodium	<0.001
Molybdenum	<0.001
Tin	<0.001

TABLE V

"d" Values for the δ Precipitate Phase

Experimental Values		Calculated Values for a=8.99Å and c=9.16Å			Calculated Values† for a=35.95Å and c=36.63Å		
d(Å)	Relative Intensity	hkl	d(Å)	% Deviation	hkl	d(Å)	% Deviation
9.50*	--	--	--	--	321	9.62	-1.25
8.63*	--	--	--	--	114	8.61	+0.23
6.24	weak	--	--	--	441	6.26	-0.32
5.60*	--	--	--	--	260	5.68	-1.41
5.37*	--	--	--	--	262	5.43	-1.10
4.80*,4.77	weak	--	--	--	624	4.83	+1.14
4.50*	--	--	--	--	181	4.43	+1.58
4.17*,4.11	weak	012	4.08	+0.73	048	4.08	+2.20
3.76*,3.69	medium	112	3.71	-0.54	448	3.71	+1.35
3.61*	--	--	--	--	2,2,10	3.52	+2.56
3.24	weak	022	3.21	+0.93			
3.03	strong	003,122	3.05,3.02	-0.66			
2.74	weak	113	2.75	-0.36			

TABLE V - (continued)

2.70	weak	311	2.71	-0.37
2.60	strong	222	2.61	-0.38
2.49	medium	320	2.99	0.00
2.43	weak	123	2.43	0.00
2.32	weak	004	2.29	+1.31
2.26	weak	400	2.25	+0.44
2.25	weak			
2.22	medium	014	2.22	0.00
2.19	weak	322	2.19	0.00
2.16	very strong	033,114	2.14,2.15	+0.93
2.13	very strong	330,411	2.12	+0.49
2.08	weak	133	2.08	0.00
2.05	medium	024	2.04	+0.47
2.01	weak	420	2.01	0.00
1.97	weak	412	1.97	0.00
1.95	weak	421	1.96	-0.51
1.93	weak	233	1.93	0.00
1.91	medium	332	1.92	-0.52
1.86	weak	224	1.86	0.00
1.84	weak	422	1.84	0.00

*These values were obtained from selected area electron diffraction patterns. All other values were obtained by x-ray diffraction.

†Values smaller than 3.61Å are not listed as they are the same as those for the cell with a=8.99Å and c=9.16Å with the indicies increased by a factor of 4.

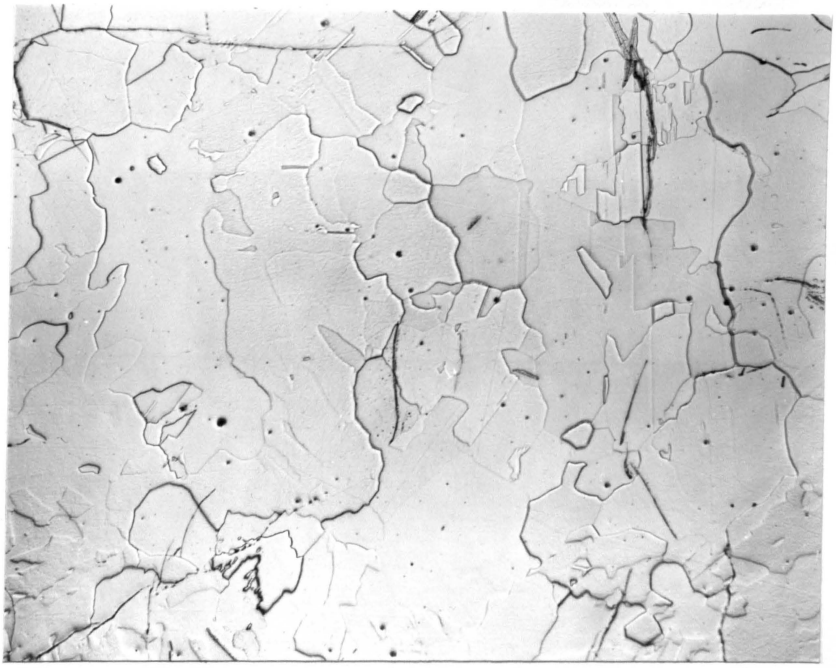

Figure 51. Cu-29.6at%In, annealed 5 minutes at 625°C and 4 hours at 420°C. X250

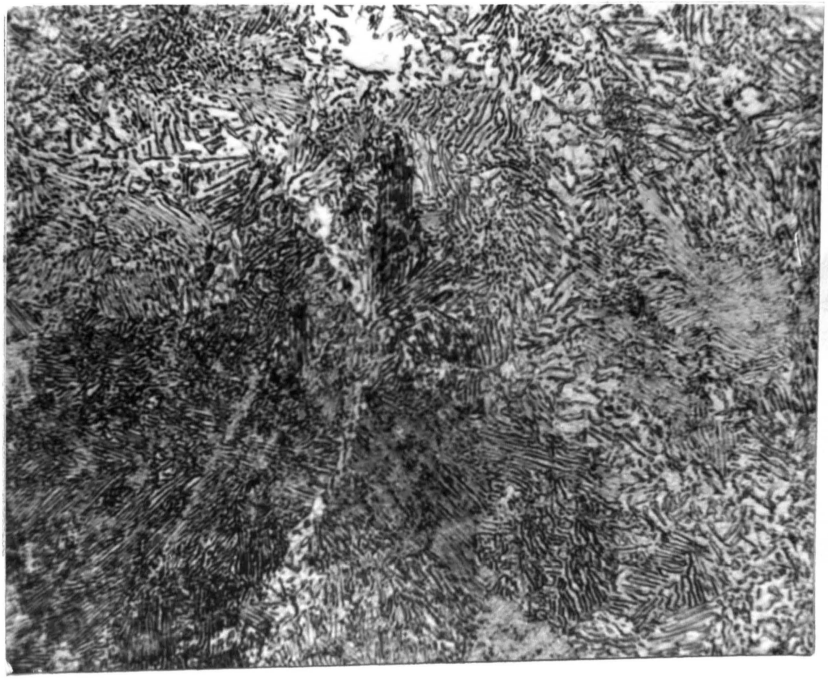

Figure 52. Cu-9.5at.%In, solution treated 5 minutes at 625°C, isothermally aged 4 hours at 420°C. X1,000

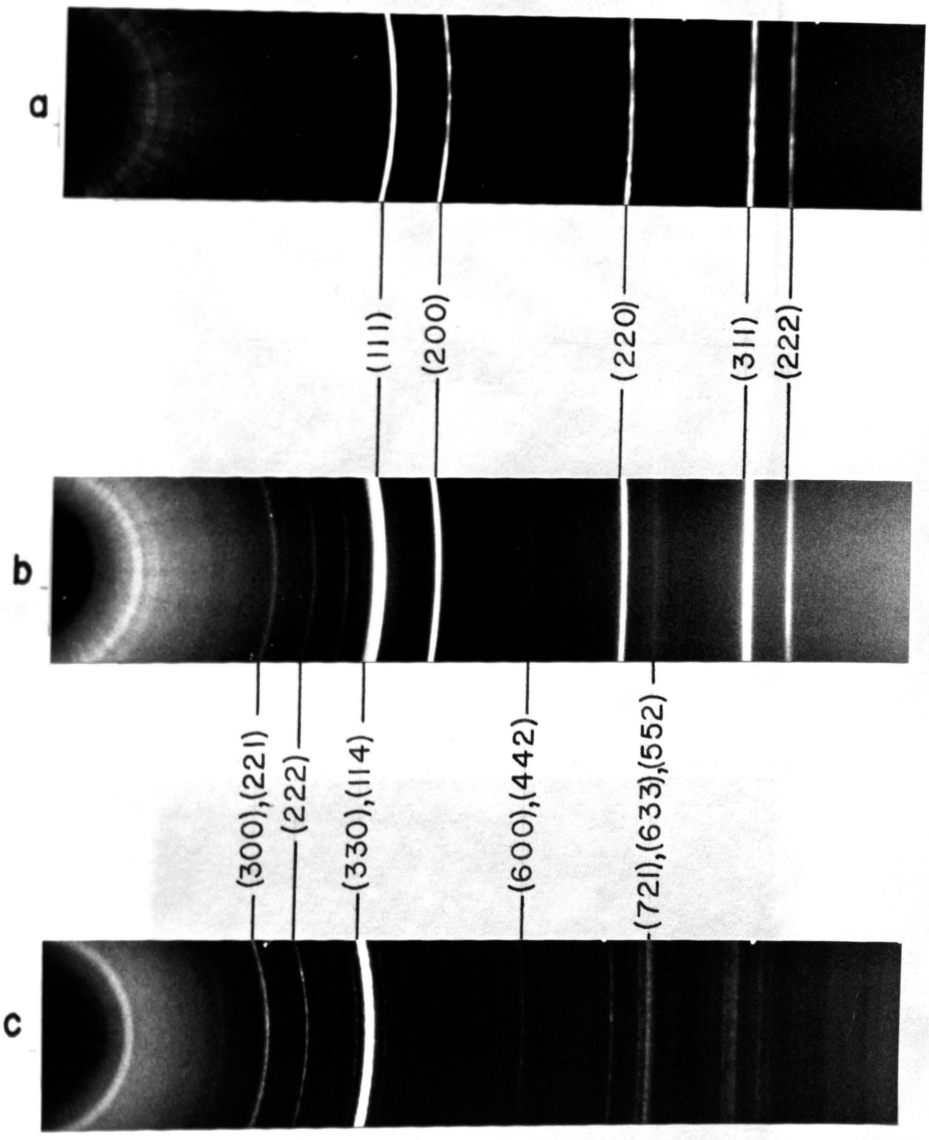

Figure 53. X-ray Diffraction Patterns: (a) Cu-9.5at.%In, solution treated 5 minutes at 625°C, water quenched. (b) Cu-9.5at.%In, solution treated 5 minutes at 625°C, isothermally aged 4 hours at 420°C. (c) Cu-29.6at.%In, annealed 5 minutes at 625°C and 4 hours at 420°C.

Figure 54a. Cu-9.5at.%In, solution treated 5 minutes at 623°C, water quenched, aged 30 minutes at 428°C. Cellular lamellae. X32,500

Figure 54b. Selected area diffraction pattern of the cellular lamellae in Figure 54a. Rotated 44° counterclockwise from Figure 54a. $\lambda l = 3.47 Å cm$.

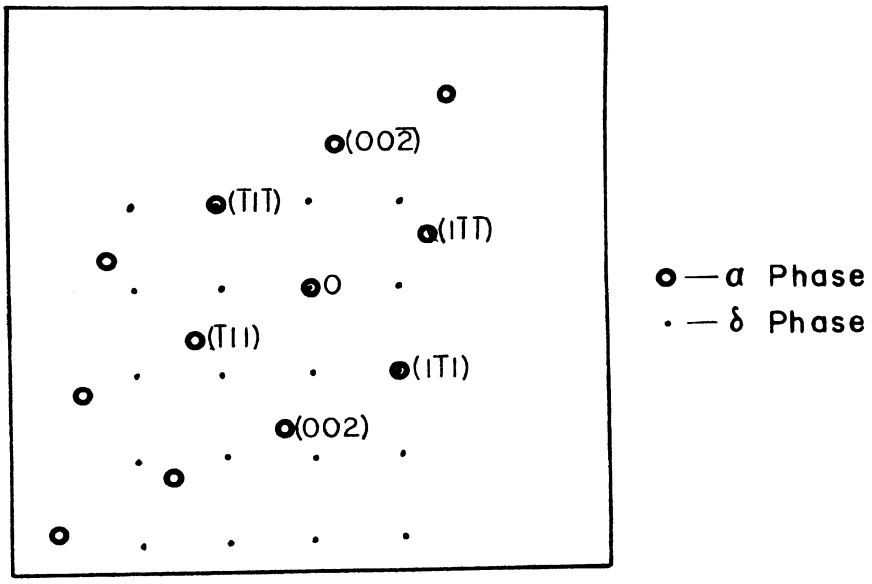

Figure 54c. Diagram of the diffraction pattern in Figure 54b showing the zero order Laue zones from the α and δ lamellae. α phase zone is near [110]

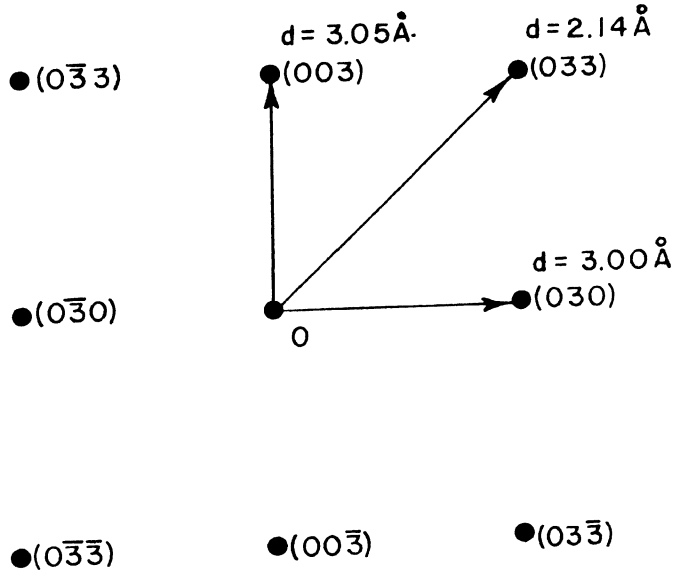

Figure 54d. Diagram of the zero order Laue zone of the δ lamellae shown in Figure 54c. [100] zone of δ.

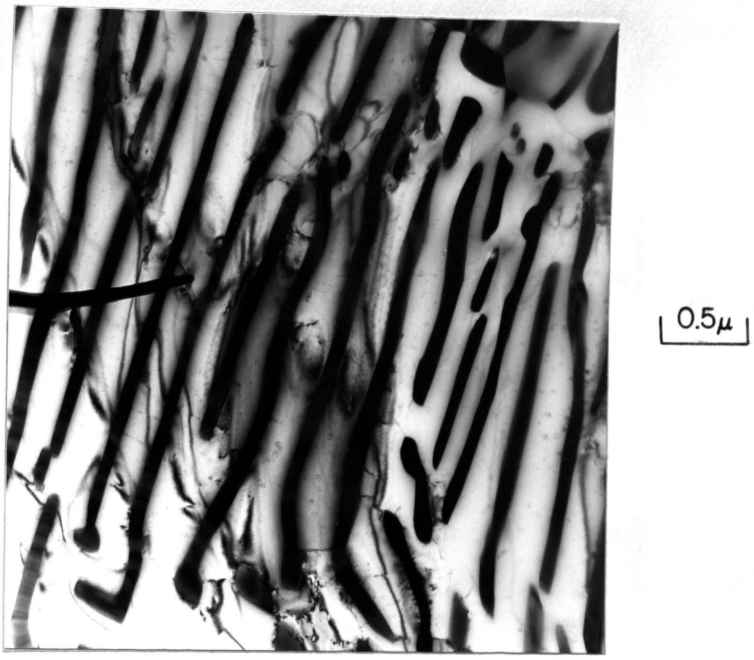

Figure 55a. Cu-9.5at.%In, solution treated 5 minutes at 623°C, isothermally aged 2 hours at 403°C. Cellular lamellae. X22,500

Figure 55b. Selected area diffraction pattern of the cellular lamellae in Figure 55a. Rotated 26° counterclockwise from Figure 55a. $\lambda l = 3.54 Å cm$.

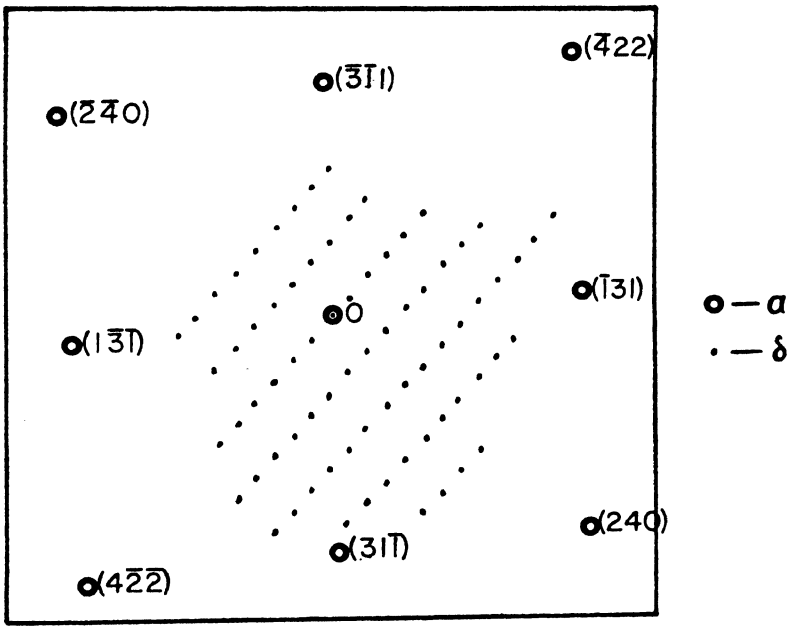

Figure 55c. Diagram of the diffraction pattern in Figure 55b showing the zero order Laue zones from the α and δ lamellae. [2̄15] zone of α.

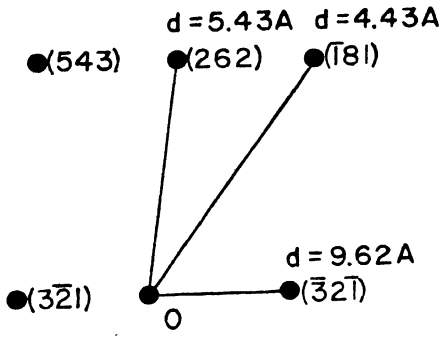

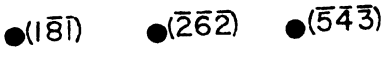

Figure 55d. Diagram of the zero order Laue zone of the δ lamellae shown in Figure 55c. [5̄,2̄,11] zone of δ.

APPENDIX B

CRYSTALLOGRAPHIC NATURE OF GRAIN BOUNDARY PRECIPITATE MORPHOLOGIES

Some of the grain boundary allotriomorphs formed during the aging of Cu-9.5at.%In alloys exhibit flat facets with respect to one of the two adjacent grains as shown at B in Figure 38 and at A in Figure 56. A trace analysis of the poles of the facets in Figure 56 with respect to the lower grain is shown in Figure 58, a standard (110) projection whose orientation was established from Figure 57.

As the allotriomorphs appear to be perpendicular to the surface of the foil, the pole of their habit must lie on the periphery of the projection. Combining this observation with the trace of the habit plane pole results in an unambiguous determination of a (113) habit for the precipitate, in agreement with the earlier observation of a (113) habit for the general precipitate.

A trace of the pole of the twin at B in Figure 56 and the fact that the twin plane also appears perpendicular to the foil surface establishes the twin plane to be a (111) α plane. This is confirmed by the occurrence of a (111) annealing twin at C in the lower grain. The formation of the twin in the bowing boundary can apparently be accounted for only as an accident of growth, and if the twins observed in cellular nodules have a similar origin they can also be expected to result from similar accidents of growth.

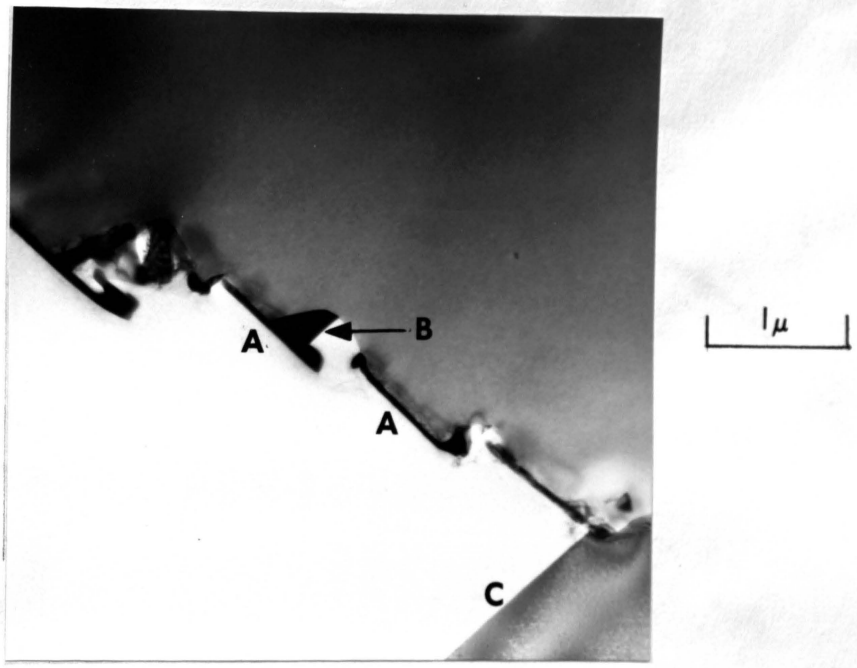

Figure 56. Cu-9.5at.%In, solution treated 5 minutes at 625°C, isothermally aged 15 minutes at 366°C. Grain boundary allotriomorphs having a habit in the lower grain. X17,500

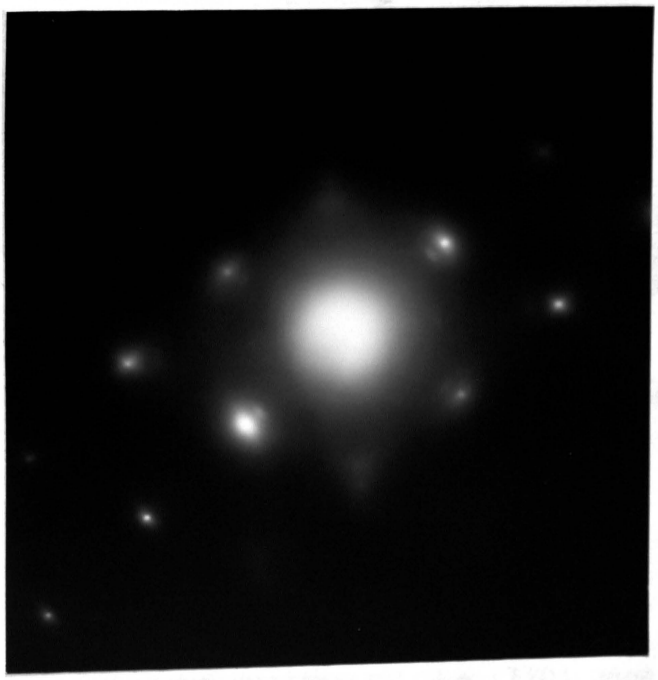

Figure 57. Selected area diffraction pattern of the lower grain in Figure 56. [110] zone of α'_2. Rotated 21° counterclockwise from Figure 56. λl=3.47Åcm.

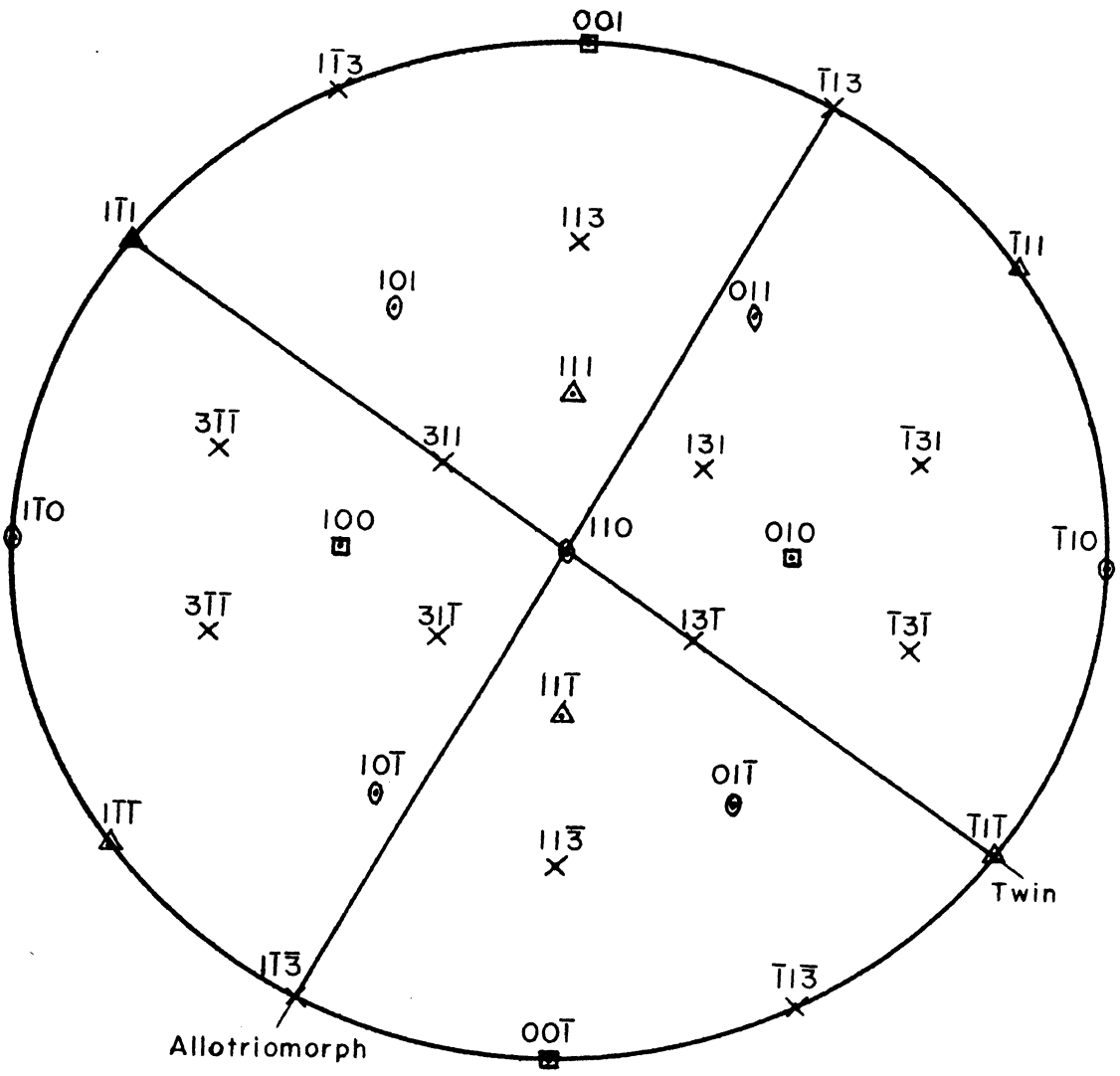

Figure 58. Stereographic projection of the [110] zone shown in Figure 57 showing the traces of the poles of the habit plane of the grain boundary allotriomorphs and twins in Figure 56.